Fall 12-2016

Nanostructured Morphologies in Glassy Polymer Networks

Brian Greenhoe
University of Southern Mississippi

NANOSTRUCTURED MORPHOLOGIES IN GLASSY POLYMER NETWORKS

by

Brian Merle Greenhoe

A Dissertation
Submitted to the Graduate School
and the School of Polymers and High Performance Materials
at The University of Southern Mississippi
in Partial Fulfillment of the Requirements
for the Degree of Doctor of Philosophy

Approved:

_____
Dr. Jeffrey S. Wiggins, Committee Chair
Associate Professor, Polymers and High Performance Materials

_____
Dr. Sarah E. Morgan, Committee Member
Professor, Polymers and High Performance Materials

_____
Dr. Sergei I. Nazarenko, Committee Member
Professor, Polymers and High Performance Materials

_____
Dr. Robson F. Storey, Committee Member
Distinguished Professor, Polymers and High Performance Materials

_____
Dr. Gopinath Subramanian, Committee Member
Assistant Professor, Polymers and High Performance Materials

_____
Dr. Karen S. Coats
Dean of the Graduate School

December 2016

Published by the Graduate School

THE UNIVERSITY OF SOUTHERN MISSISSIPPI®

ABSTRACT

NANOSTRUCTURED MORPHOLOGIES IN GLASSY POLYMER NETWORKS

by Brian Merle Greenhoe

December 2016

The body of this work describes a novel approach for the dispersion of multi-walled carbon nanotubes in a high T_g epoxy prepolymer matrix using a twin screw high-shear continuous reactor. The method demonstrated improves on previous dispersion methods in several ways. It offers increased efficiency through excellent heat transfer, while being solvent-less, scale-able, and tailorable to drive dispersion states to judiciously chosen dispersion states. Furthermore, it was shown that dispersion state and agglomerate morphology can be directed, in several ways, through processing conditions and also by controlling the matrix viscosity profile through cure. Broadband dielectric spectroscopy, optical hot-stage microscopy, transmission electron microscopy, and atomic force microscopy were used to both directly and indirectly monitor agglomerate dispersion state and track secondary agglomeration through to a cured and vitrified material.

ACKNOWLEDGMENTS

First and foremost I would like to thank my advisor, Dr. Jeffrey Wiggins. Through his guidance I was able to pursue my academic and personal interests without interference. The four years of freedom encouraged to me by “Doc” has certainly made me a better scientist, but more importantly a more culturally adept, well-traveled, and cheerful individual; a gift I am grateful for, from a man I will forever be indebted to.

I sincerely thank my committee Dr. Sarah Morgan, Dr. Sergei Nazarenko, Dr. Daniel Savin, Dr. Robson Storey, and Dr. Gopinath Subramanian. I would also like to extend thanks to Dr. Kennith Mauritz and Dr. Mohammad Hassan who have helped shape my writing style and contributed to years of intellectual discussion and discovery.

My list of acknowledgements would be incomplete without thanking Sam Hudson and Butch Sims for the countless hours and miles they have dedicated to involve me in a community well outside polymers, helping me develop a business mindset, and treating me as a member of their families. Thank you.

I must thank Dr. Archana Wadhawan as well as my family for the perpetual and selfless support of myself, my work, my travels, and the life decisions I have made for selfish reasons, which have brought us to where we are today. Thank you.

The 807 crew, specifically, Dr. Jim Goetz, Dr. Brooks “Brooksie” Able, Greg Strange and Kyler Knowles will always hold a special place in my heart. You boys have been great friends outside school and some of the finest problem solvers professionally within. I feel fortunate to have shared a graduate career with you. Lastly, I want to thank members of my group and the community, specifically Dr. Xiole Cheng, Dr. John Misasi, Dr. Jeremy Moskowitz, Ms. Charlene McMillin, Ms. Stephanie Patton, Andy Frazee,

Amit Sharma, Andrew Janisse, Kyle Bentz, Brian Donovan, Mark “Mearly” Early, Hunter Cooke, Bin Yang, Matt Rolland, Jason and Gabi Williamson, Kyle and Denise Joplin, and the WRG processing team who over the years have enriched my life in tangible and intangible ways well beyond my capacity to articulate here. Thank you all.

DEDICATION

I dedicate my dissertation to “the boys” wherever on this planet life has found you. Thinking back to our time together, over the years, I am reminded of a quote:

“I don’t know where I am going but I’m on my way.”

- Carl Sagan

TABLE OF CONTENTS

LIST OF TABLES

LIST OF ILLUSTRATIONS

LIST OF ABBREVIATIONS

1S	One Stage
2S	Two Stage
44DDS	4,4´ Diaminodiphenyl Sulphone
AC	Alternating Current
AFM	Atomic Force Microscopy
BDS	Broadband Dielectric Spectroscopy
C-AFM	Conductive Atomic Force Microscopy
CNT	Carbon Nanotube
D	Dispersion Index Value
DC	Direct Current
DMA	Dynamic Mechanical Analysis
DSC	Differential Scanning Calorimetry
HS	Hot Stage
MWCNT	Multi-walled Carbon Nanotube
OM	Optical Microscopy
RPM	Revolutions per Minute
SEM	Scanning Electron Microscopy
SWCNT	Single-wall Carbon Nanotube
TEM	Transmission Electron Microscope
T_g	Glass Transition Temperature
TGDDM	Tetraglycidyl Diamino Diphenyl Methane
TSE	Twin Screw Extruder

CHAPTER I - INTRODUCTION

The perpetual desire for lighter, stronger, and higher performing materials has propelled materials science through decades of discovery. In this field, nanocomposites undoubtedly represent the contemporary forefront of exploration. Nanocomposites can be described as dispersed nanoparticles stabilized within a matrix, and for this work, the nanoparticles of interest are specifically multi-walled carbon nanotubes (MWCNT) with the matrix being polymeric. Carbon nanotube containing composite materials have found their way into a few interesting high performance applications. For example, they can be found in coatings for low observable military aircraft platforms such as the F-22 Raptor, the F-35 Lightning, and the B-2 Spirit stealth bomber. In non-military applications they are utilized in niche markets, for example high-end bicycle frames. Several issues related to working with or processing of these nanotube-containing composites remain, and have kept them from further utilization and implementation industrially. Those being the

1. arduous task of obtaining maximally dispersed states,
2. challenge in fabricating nanocomposites in high volume,
3. difficulties in managing high CNT loading levels,
4. difficulty in controlling CNT re-agglomeration through cure,
5. and challenges in characterization of composite material.

The current work set out to, in part, resolve these key issues and present a nanotube reinforced composite material with increased utility and application.

Background

Dispersion and stabilization of nanoparticles in epoxy matrices is an area of research that has received considerable attention over the last fifteen years.[1] Over the past decade the mechanical, electrical and thermal properties of carbon nanotubes have spurred intensive investigations aimed at developing nanostructured composites.[2-4] Multiwall carbon nanotubes have the potential to impart desirable value added properties to epoxy materials which include augmented electrical and thermal conductivity as well as increased mechanical performance.

Over the past decade, increased capabilities and efficiencies in the production of MWCNT have made them more conceivable as electrical and thermal modifiers in industrial applications for high performance composite materials. The price of nanotubes has fallen below the cost-prohibitive threshold making them potentially relevant for many commercial applications incentivizing a greater investigation into resolving the five major problems outlined previously. So the reader may better understand the gaps in knowledge, the following section seeks to fill the plenum of understanding surrounding each of these obstacles.

It is known that reduction in size of the dispersed particles towards nanoscale dimensions generally results in an enhancement of the material properties, typically ascribed to the fact that the resulting increase in interfacial area enables a more intimate mutual interaction between the dispersed phase and the polymer matrix components. The pertinent literature demonstrates a dramatic effect of the reduction of the filler size on internal interfacial area. For example, a well dispersed nanocomposite will have an

internal interfacial area six orders of magnitude larger than the same volume fraction microcomposite.[5]

High quality dispersion of CNT is difficult to obtain due to the high amount of energy that is required to overcome the van der Waals interactions and static interactions between neighboring tubes. Several approaches have been developed to promote dispersion and stabilization of CNT. These approaches include mixing techniques such as sonication, calendaring, mechanical stirring and extrusion/melt blending as well as chemical techniques such as CNT surface functionalization and use of dispersive aides or surfactants.

Mixing Techniques for Dispersion

Sonication. The most effective dispersion technique has proven to be ultrasonic mixing, which was first published in 1999 and has been optimized over the years.[6, 7] Sonication is effective at dispersing both SWCNT and MWCNT due to the high shear forces that are generated from shear rates that exceed 107 s-1. The general procedure for this approach begins with a suspension of CNT in a solvent or a solvent-epoxy mixture (usually acetone, ethanol, or DMF) using either bath or tip ultrasonic mixing. Following dispersion, the remaining reactive components are added and subsequently cured. Unfortunately sonication techniques are often limited to lab-scale reactions (500 mL) as larger scale equipment is neither available nor practical due to the large amounts of heat generated by the high localized shear. The high localized shear rates and temperatures have also been shown to reduce nanotube length, thereby decreasing aspect ratio, and degrade polymer components.[8] The degradation of neat epoxy as a result of ultrasonication can be observed visually, as demonstrated in **Error! Reference source**

not found., and worsens with increasing amplitude also known as power or increased sonication time. This effect is observed visually as a color change as the neat epoxy degrades.

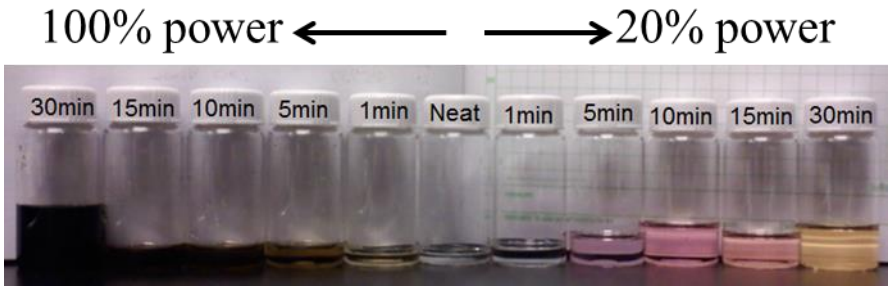

Figure 1. Effect of ultrasonication power and time on neat epoxy monomer

Calendaring. Lower shear techniques such as extrusion and calendaring have proven to be effective techniques for the melt mixing of polymers and CNT as well. Calendaring is a common technique for film formation and processing of thermoplastic materials. It was first used as a dispersion approach for nanocomposites in 2004, and has since been employed by many researchers.[9-13] Calendaring has been shown to yield excellent dispersion yet has limitations when it comes to the high matrix viscosities often associated with high loading levels.

Twin-screw extrusion. Twin-screw extrusion (TSE) is a proven technique for dispersing nanotubes in thermoplastic resins. It has also been investigated as a method for dispersing nano-fillers in epoxies with favorable results.[14, 15] In those studies, the amine curative was mixed with the epoxy-CNT mixture after extrusion. To the best of our knowledge, single-step compounding of epoxy resin, curative, and nanotubes has not yet been investigated.

A continuous high shear reactor presents an interesting and promising approach

for nanocomposite processing. Extrusion technology in thermoplastic compounding and continuous polymerization has evolved over the last several decades. For example, TSE have been reported as continuous reactors[16], bulk polymerization reactors[17], polymer grafting reactors[18], and polymer blend compatibilization reactors[19]. Literature reviews of TSE as polymer reactors have been published by Brown and Orlando[20] and Xanthos[21]. The primary advantages of reaction extrusion compared to other polymerization reactors, such as batch reactors, are lower cost, improved efficiency, and excellent control of processing parameters. The absence of solvent combined with simultaneous transport of low molecular weight monomers and high molecular weight polymers improves energy consumption, making the reactor environmentally favorable. In addition, the twin-screw chemical reactor provides controlled shear energies, excellent heat transfer, precision feeding and mixing, devolatilization, and insensitivity to viscosity changes.[22]

It is well understood that an increase in shear applied to a system translates to an increase in dispersion state. This is due to the relationship, demonstrated in Equation 1, between shear force (τ), matrix viscosity (μ), boundary velocity (u), and distance from shear boundary (y). Shear force scales with viscosity and, thus, it is expected that dispersion states would increase with increasing polymer viscosity. Therefore, it is desirable to develop a dispersion method that is not only capable of handling, but makes use of the high shear forces that arise from high viscosity matrices. Methods of dispersion such as ultrasonication, mechanical mixing, and calendaring require low viscosity media which limit their use, not only in the shear forces they invoke on agglomerates, but also, in the ability to curb re-agglomeration of nanotubes in the highly dynamic and mobile media environment.

$$\tau(y) \propto \mu\frac{\partial u}{\partial y} \quad (1)$$

High-shear continuous reactors, where the reactor is a TSE, offer the capability to handle high viscosity materials and have been the subject of much research as an environmentally-favorable and economic method for industrial scale manufacturing.[23, 24] More specifically, fully intermeshing co-rotating twin screw extruders offer the highest level of mixing, dispersion, and shear control, making them the primary technology used as continuous chemical reactors.[25, 26] Traditionally, extruders have been associated with dispersing nanoparticles within high molecular weight linear thermoplastic polymers. In this process, during melt mixing, the applied shear strength is directly tied to the agglomerate size reduction. Several studies reported that greater dispersion was achieved by using high melt viscosity matrices thereby maximizing the shear environment and shear states applied. [27-34] However, extrusion processes are limited in their ability to disperse nanoparticles into epoxy matrices, since epoxies are generally used or processed in a low viscosity state and therefore result in unfavorable shear environments within the reactor barrel.

We recently reported a novel method for preparing thermoplastic modified epoxy prepolymers based on twin screw extrusion technology.[35] The advancement of epoxy chain extension or conversion was controlled by reaction chemistry, process design, and processing conditions in order to achieve targeted viscosities with tack and drape optimized for prepreg filming applications. The biggest advantages to this continuous reactor design, when compared to the batch process it replaced, is the mitigation of batch-to-batch variation, favorable performance measures relating to processing rate, namely the reduction of space-time and augmentation of space-velocity for the system, and the

abatement of conditions where large volumes of reactive materials are involved in which safety concerns arise.

Intermeshing co-rotating twin screw extruders can be configured with a broad array of screw design elements. These elements are the core technology of the chemical reactor and provide necessary transport, mixing, and shear. Typically, two types of screw elements dominate continuous reactor design: conveying elements and mixing elements. Examples of typical intermeshing co-rotating modular screw elements used in continuous chemical reactors are shown in **Error! Reference source not found.**.

Figure 2. . Extruder reactor elements

Reactor screws are modular and designed for specific functions such as material transport through the reactor, receiving of solid or liquid feed, dispersive or distributive mixing, entrapment or ventilation of volatiles, etc. Reactor screws are precision machined with tolerance to fit within a series of barrel sections that are independently controlled for adjustable heating and cooling. The points where various liquid and solid reactants, catalysts, modifiers, vacuum, etc. are introduced into the continuous reactor are

also spaced along the barrel. **Error! Reference source not found.** shows the processing section of a typical TSE continuous chemical reactor. We have been developing continuous epoxy prepolymer reactors for several years and have obtained excellent results for solubilizing amines and advancing prepolymer molecular weights to well-controlled viscosities and tack for utilization in prepreg film development activities.[35]

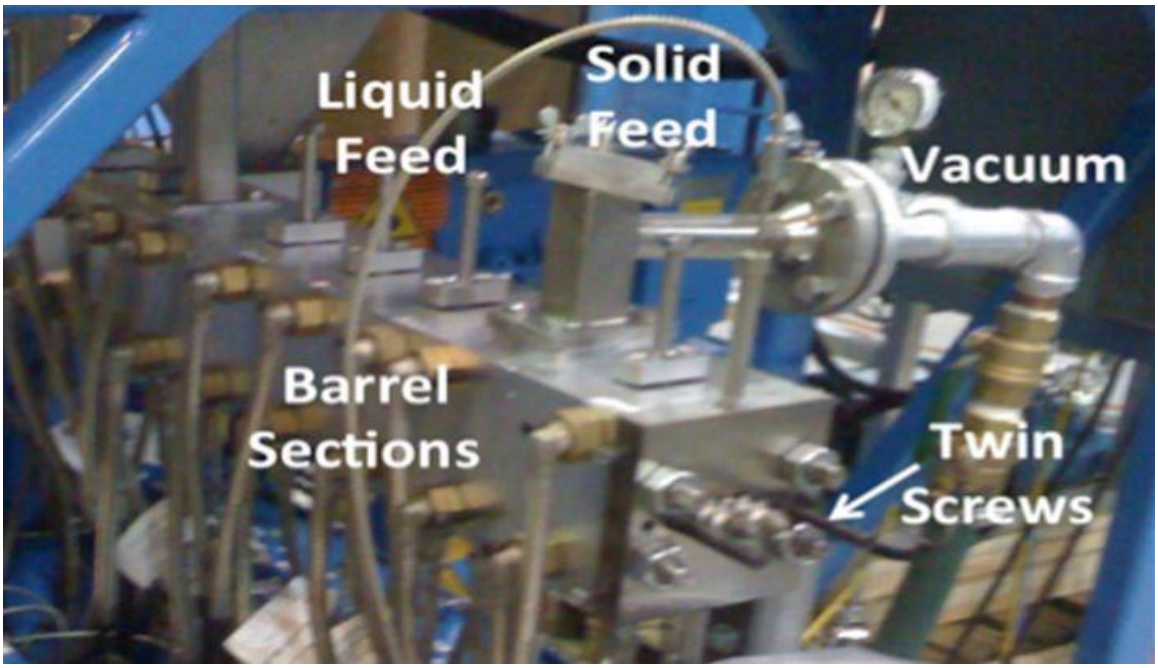

Figure 3. Twin screw chemical reactor

In a co-rotating TSE, mixing is generally categorized as dispersive mixing or distributive mixing. During dispersive mixing, a critical stress is applied to the dispersant through laminar shear fields generated in the extruder. The shear forces overcome cohesive forces in particulates so particle sizes are reduced. High shear rates are a requirement for successful dispersive mixing. In contrast, distributive mixing is more effectively carried out by shear stresses that generate large strains, as there is no critical stress threshold. Distributive mixing is facilitated by splitting and reorienting the flow streams. **Error! Reference source not found.** depicts good and poor dispersive and

distributive mixing in particle/liquid systems. When considering screw element geometries, wide kneading blocks with reverse pitch facilitate dispersive mixing while narrower kneading blocks with forward pitch, gear and tooth elements provide distributive mixing action.[36] This is particularly important in the dispersion of nanotubes as CNT agglomerates are known to be shear sensitive and require both dispersive and distributive mixing to achieve a maximally dispersed state. Continuous reactor modular screws are designed by placing appropriate screw elements in the proper positions according to the type of action favorable to accomplish specific reactions or activities within defined regions of the reactor.

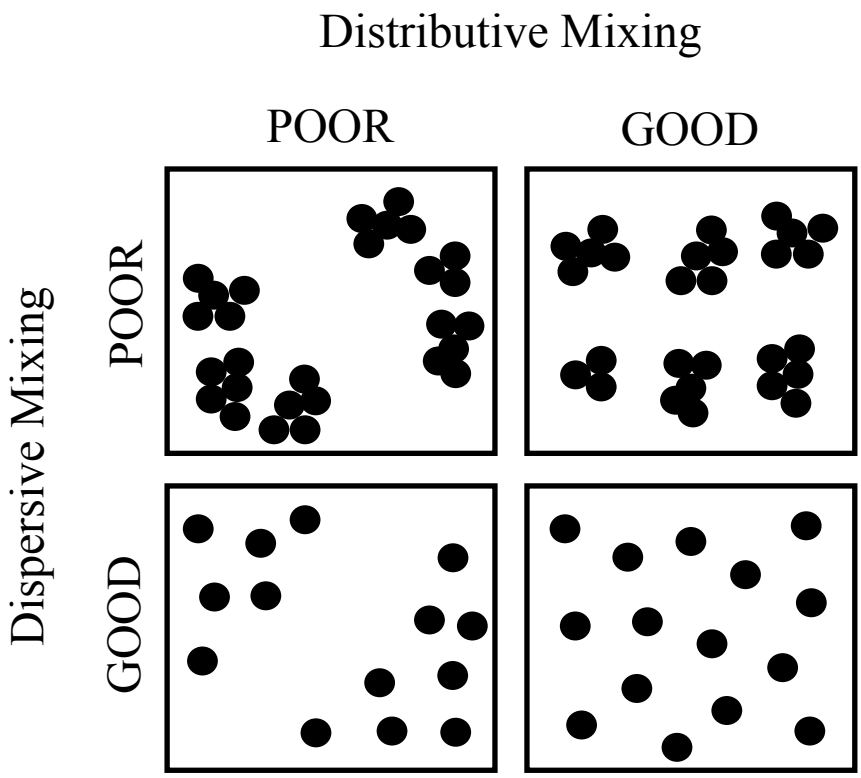

Figure 4. Dispersive and distributive mixing

Numerous examples of dispersion of carbon nanotubes and other nanoparticles using TSE and reaction processes have been reported in the literature.[28, 30, 37] These

reports are typically associated with dispersing nanoparticles within high molecular weight linear thermoplastic polymers. Our research in developing twin-screw extrusion technology to synthesize epoxy prepolymers under continuous reactor conditions is essentially unreported. The research presented in this document represents a non-conventional use of the technology since linear polymers dominate extrusion processing.

Other Techniques for Dispersion

Aided by other various techniques, CNT can be chemically modified to improve dispersion into a polymer matrix. The sidewalls of CNT can be functionalized with reactive groups. Functionalization improves dispersion, first by increasing the solubility of CNT in organic solvents and resins during mixing, then by forming covalent bonds between the CNT and the epoxy network during the cure process. Commonly-used functionalities for epoxy-CNT systems are amino groups[11, 38-40] and acid groups.[41] Nanocomposites with functionalized CNT generally have increased modulus and strength as compared to unfunctionalized CNT. The enhancement in strength is attributed to decreased aggregation and improved load transfer between the matrix and the filler. Although mechanical gains are generally reported with this method electrical properties are hindered due to the disruption of the sp^2 hybridization on the CNT latus structure.

Chemical Dispersion Aids. Dispersion aids have also been used to reduce aggregation of CNT in epoxies. Nonionic surfactants improve the dispersibility of CNT, but they have the potential to reduce material T_g by acting as plasticizers.[42, 43] Block copolymers can produce an even greater enhancement of material properties but again result in the same plastization effects.[44, 45]

Each of the dispersion methods discussed so far presents considerable drawbacks when considering large-scale applications. Solvent processing and sonication are expensive techniques on a large scale. Furthermore it is crucial for epoxy performance that all solvent be completely removed prior to cure, to prevent the development of voids in the cured matrix. As stated previously, surfactants have the potential to plasticize the epoxy networks, negating many of the property improvements gained from CNT dispersion. Therefore solvent-free high-shear mixing processes are an attractive route for dispersion of CNT in epoxies and will be a focus of the proposed research.

Managing Secondary Agglomeration

The tendency for nanotubes to agglomerate due to a drop in viscosity is widely acknowledged and well reported.[46, 47] Controlling this tendency to agglomerate is considered one of the biggest challenges facing CNT nanocomposites today.[48] It has been shown that agglomerate size and morphology can be manipulated by processing conditions in thermoplastic materials, specifically by adjusting shear conditions or annealing temperature.[49-52] In fact, conductivity gains approaching four orders of magnitude were reported by Alig and co-workers, within a single sample, as a percolated network type agglomerate morphology was developed upon annealing well above the melting temperature in a polypropylene/MWCNT composite.[50] Schueler and co-workers extended this work and observed they could control agglomerate morphology in a carbon black/epoxy composite by applying shear forces through mechanical stirring or through increasing the matrix ionic strength by the addition of copper chloride.[53, 54] In these cases the state of dispersion morphology was being investigated specific to its roll and contribution to conductivity within the composite material. This work demonstrates the

need for a method to judiciously dictate agglomerate size and morphology in order to tailor bulk properties for specific material requirements.

Characterization of Nanocomposites

The characterization of CNT containing nanocomposites has proven to be especially challenging. As opposed to layered-silicate polymer composites, which offer the benefit of predictable inter-layer registry and a large electron density differential between filler and matrix making them easily observable or detected by X-ray diffraction and transmission electron microscopy (TEM), quantitative characterization of nanotube dispersions is much more difficult. There are two main approaches to dispersion characterization within these materials those being direct observation and indirect estimative methods of dispersion qualification.

Direct Characterization of Nanocomposites. The first approach to dispersion characterization includes microscopy across many relevant length-scales and includes optical microscopy (OM), scanning electron microscopy (SEM), atomic force microscopy (AFM), and at the smallest scales transmission electron microscopy (TEM). Individually any one of these methods fails to adequately describe the complete dispersion picture. For example, OM is limited in magnification so that the individual nanotubes are not apparent. In this case only macro-scale dispersion is considered with limitations in resolution becoming problematic with increasing loading levels. SEM and AFM are capable of observing dispersion at the micron and into the submicron length-scale but neglect the largest agglomerates which often have the greatest positive or negative impact on materials properties. Along with this, these methods represent only a cross-section of the composite material and may not necessarily be representative of bulk

dispersion. TEM is excellent for the observation of nanotubes and the smallest agglomerates, but this technique has limitations due to the exceptionally small field of view. Further confounding the direct observation of dispersion states is a lack of agreement within the field of how to quantify the observed microscopic results.

Quantification from OM observation is often attempted using one method or another for obtaining a dispersion index. A commonly accepted method for determining this value can be found in Equation 2.[28] There are many issues with applying a simple number to describe a dispersion state. For example, the dispersive versus distributive arrangement is not described, agglomerates smaller than one micron or larger than the field of view are neglected, agglomerate morphology is not described, index value is largely affected by sample preparation, it is limited to loading levels below 0.5 % CNT, and values are not comparable across multiple samples.

$$D = \left(1 - f\frac{A_{CNT}/A_0}{\emptyset_{vol}}\right) \times 100\% \quad (2)$$

Indirect methods to quantify dispersion include, but are not limited to, dynamic rheological measurements,[55] bulk electrical conductivity measurements,[47] and dielectric permittivity.[56] Even changes in mechanical properties[57, 58] are sometimes implemented to draw some amount of conclusive evidence pertaining to the dispersion state of CNT within these materials. The effect on these properties by differing dispersion states will be discussed in great detail later in this document. Overall, these methods are often utilized as a metric for dispersion state. To date, there in not one agreed upon protocol for characterization of these materials. This has made comparison between experiments or from one group to another challenging and often misleading as far as what "good dispersion" actually looks like. Also, the results from indirect dispersion probing are

confounded by many factors which further complicate a real understanding of these CNT nanocomposite materials.

Indirect Characterization of Nanocomposites. Due to the conductive properties of MWCNT in nanocomposites, broadband dielectric spectroscopy (BDS) and bulk conductivity measurements have been utilized as an indirect metric to qualify dispersion within these materials. As mentioned previously the relationship between bulk conductivity and dispersion state within CNT containing nanocomposites is both complicated and confounded. Although the conductivity of nanocomposites as a function of loading level is often reported, and critical for determination of properties such as percolation threshold, the bulk conductivity of a nanocomposite by itself is not sufficient to describe the dispersion state or dispersion through-space morphology that can be observed through an array of various direct observation methods.

Polymeric nanocomposites, specifically epoxy based systems, are dielectric materials meaning they contain components that can be polarized within an electric field. Upon release from a polarization event the rate at which these components or moieties return to their randomly oriented states is strongly dependent upon their local chemical environment. Because of these characteristics dielectric spectroscopy may be useful to probe local chemical environments and hence could be utilized as an indirect method to probe CNT dispersion states.

Broadband Dielectric Spectroscopy

Broadband dielectric spectroscopy was used extensively in this work. As BDS is an under-exploited characterization method for polymeric materials, at least specifically within our department, the following section has been added to better clarify the method.

BDS is sensitive to the relaxations of dipoles, or better stated polarizable moieties, within a material. Dipoles polarized and aligned in an electric field will return to an indiscriminate orientation over a characteristic relaxation time, τ, upon removal of the electric field. The characteristic time-scale of this relaxation is effected by the degrees of freedom of the moiety in question as well as the local chemical environment. In short, measuring τ for the molecular motions within a system can provide meaningful information regarding through-space relationships, orientation, and chemical environment for α, β, and γ transitions.

BDS operates under some very simple rules of electronics. Ohm's law states ($V=I*R$) where V is the voltage measured across a conductor, I is the current in amperes, and R is the resistance in ohms. By invoking a voltage differential across a sample and measuring I, R, and the lag between the wave function of V and I, a value known as phase angle, BDS can generate an enormous amount of information. Using these four measured variables and a few simple relationships one can back out complex values such as modulus (M*), impedance (Z*), admittance (Y*), dielectric constant (ε*), conductivity (σ*) and non-complex components such as tan delta, etc.

Without getting too distracted by the math in this explanation, dielectric materials can be thought of as being composed of two components; a conductive and a non-conductive component. To that, a dielectric material can be represented by a series of resistors and capacitors, as illustrated in **Error! Reference source not found.**, where the capacitors represent the real component and the resistors represent an imaginary component that is lost in vibrational movement of polarizable moieties. In mathematical terms this conductivity is represented as:

$$\sigma^* = \sigma' + \mathbf{i}\,\sigma'',$$

where σ^* is the complex conductivity, σ' is the real part of conductivity or the conductive term, and σ'' is the imaginary part and a capacitive term. Generally however, with regard to BDS these materials are instead viewed in terms of permittivity (ε), which is the measure of resistance that is encountered across a material within an electric field. This regard is mathematically represented as:

$$\varepsilon^* = \varepsilon' + \mathbf{i}\,\varepsilon'',$$

where ε^* is the complex permittivity, ε' is the real part of permittivity or the resistive term, and ε'' is the imaginary part and a capacitive term.

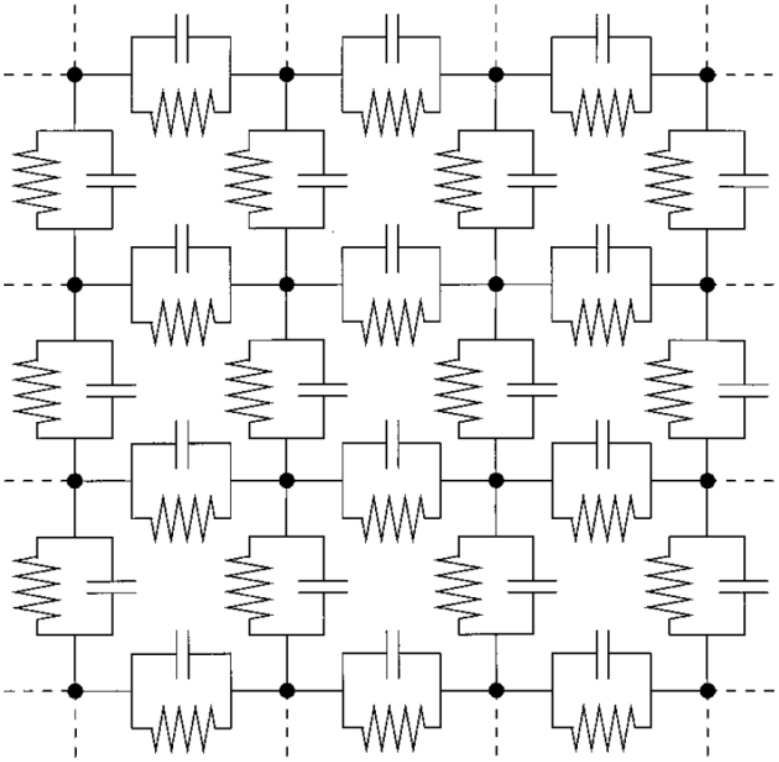

Figure 5. Electrical equivalent representation of a semiconductor material

A basic understanding of how these conductivity and permittivity components relate to dielectric materials will aid the understanding of Maxwell's equation which can be written as:

$$\nabla \cdot \bar{H} = \bar{J}_l + \left[(i\omega\varepsilon_\circ + \sigma_s) + j\omega\varepsilon' \left(1 - i\frac{\varepsilon''}{\varepsilon'}\right)\right] \bar{E} \ ,$$

where $\bar{H}$ is the magnetic field strength, $\bar{J}_l$ is the electric current density, ω is the angular frequency and equal to $2\pi f$ where f is the frequency, $\varepsilon_\circ$ is the permittivity in a vacuum, ε' is the real permittivity, ε'' is the imaginary permittivity (related to energy dispersed by dipoles), σ_s is the static conductivity (DC conductivity), and $\bar{E}$ is the electric field. In this equation, $(i\omega\varepsilon_\circ + \sigma_s)$, describes the conductivity that arises due to the collision of electrons understood commonly as direct current. Alternatively, $j\omega\varepsilon' \left(1 - i\frac{\varepsilon''}{\varepsilon'}\right)$, describes the conductivity lost due to polarization loss or dipole motion understood as an alternating current (AC).

There are two main points to take away from Maxwell's equation. The first is that both the real and imaginary components of a dielectric response are dependent upon the frequency of which they are being measured. This will be discussed further in the following section. The second is that, within the AC component, which contains information regarding the local chemical environment in which it originated, the real and imaginary components are related and inseparable. This second point is important to note because the DC response in a highly conductive material is orders of magnitude larger than the AC response. Because of this relationship, the understanding of dynamic response in highly conductive materials (like the materials being investigated in this

work) is arduously complicated and therefore less understood than, for example, less conductive materials.

To get back to the first point, made in the previous paragraph, ε′ and ε′′ are known to be frequency dependent. For example, the storage component typically decreases with respect to frequency, at a magnitude related to the polarizability of the moiety in question, while the loss component will form a peak across the same frequency range much the same as the storage and loss moduli behave in dynamic mechanical analysis. These transitions will occur and correlate with resonate frequencies of various movements within a material at a given temperature. Remember these responses are measured immediately following a perturbation by an electric field that was acting to align polar moieties in the vector direction of said field. Every molecular movement or vibration will require a particular amount of time to revert back to its original randomly oriented state. This relaxation time, as a reminder, is referred to as τ and is equivalent to $1/(2\pi f_{max})$. Typical behavior of the storage loss components of permittivity are illustrated in **Error! Reference source not found.** with τ labeled in each. With this in mind, it follows with reason that the longest range movements and largest moieties would take the longest amount of time to return to their randomly oriented state. For example, an α transition will take longer to recover from a perturbation than say a β or γ transition at a given temperature. So through observation of dielectric response across a wide frequency range one can probe a large range of relevant length-scales determined by the range of τ for the motions of interest. **Error! Reference source not found.** illustrates the processes that are probed at temperatures near ambient conditions for dielectric or conductive responses.

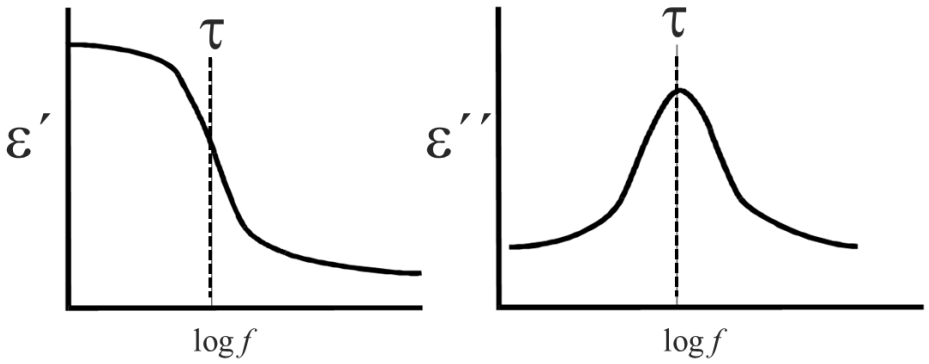

Figure 6. Typical response of storage and loss components of complex dielectric permittivity

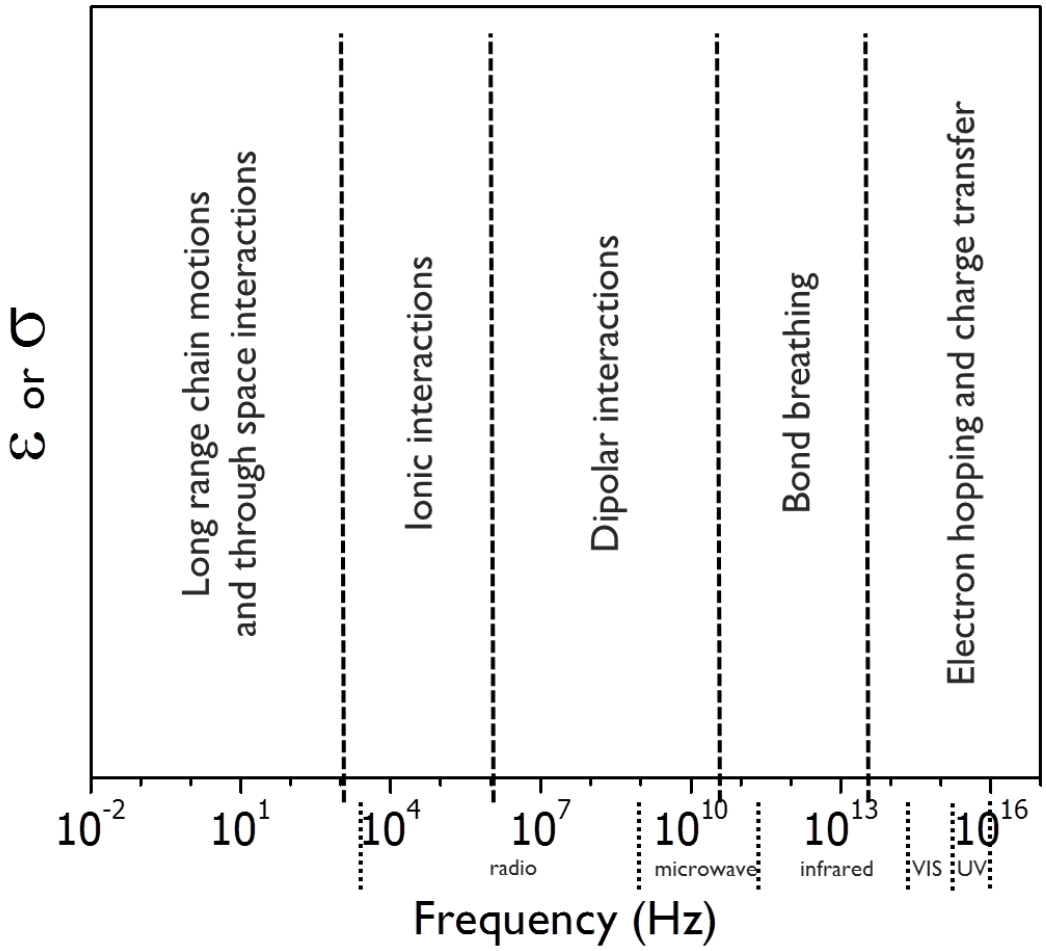

Figure 7. Permittivity or conductivity spectrum showing frequency ranges of molecular and atomic processes

One last representation of dielectric data worth mentioning in a brief overview of BDS is one that is common and most relevant to polymeric thermal characterization. This approach creates a plot similar to a DMA tan delta plot only with the big difference being with BDS the perturbation is electrical as opposed to mechanical in nature as with DMA. This means the lag in response observed in DMA is much less present in BDS. A plot shown in **Error! Reference source not found.** illustrates the result of plotting the dielectric loss tangent ($\varepsilon''/\varepsilon'$) at a single frequency with respect to temperature. In this representative illustration α, β, and γ transitions are visible with real life results having

drastically increased sensitivity to especially the weaker of these responses than that obtainable by DMA.

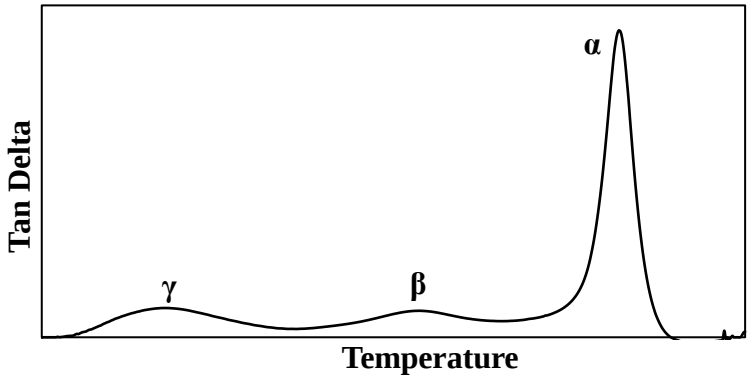

Figure 8. Typical single frequency loss tangent polymeric response in BDS characterization

In highly electrically conductive materials, like those used in the present work, it is often advantageous to consider the conductive nature of the material using BDS. It has been proposed that by probing the low frequency (largest length-scale) limit of dielectric conductivity spectra it may be possible to determine through-space interactions and distances especially in heterogeneous materials where one component is highly conductive and the other is highly insulative. The Mauritz research group was one of the first teams to seek an understanding of these interactions.

Electrical conduction through electrolytes is characterized by log-log plots of σ', the real part of the complex conductivity ($\sigma^* = \sigma' + i\,\sigma''$, where $i = \sqrt{-1}$) vs. frequency (f) like that illustrated in **Error! Reference source not found.**, which shows three distinct regions. In the low f range σ' decreases with decreasing f. This is often attributed to the fluctuation of interfacial polarization at the electrode-sample interface.[59-62] In short, there is layered positive-negative charge separation near the electrode which is primarily capacitive; conductivity is limited in this region owing to the fact that the electric field

therein opposes the applied electric field. At higher *f* there is a plateau of nearly frequency-independent conductivity, which is referred to as the dc conductivity (σ_{dc}) which is described later. The high frequency domain beyond this plateau is the dispersive region characterized by frequency dependent conductivity, which might reflect information on the chemical environment within the material.[63-67] The conductivity proceeding from the plateau region and into this dispersive region can be approximated by the empirical power law first described by Jonscher and referred to as the universal dynamic response as shown below: [64, 67]

$$\sigma_{ac} = A\omega^n \tag{3}$$

where $\omega = 2\pi f$ is the angular frequency of the applied electric field and *A* and *n* are fitting parameters of an empirical nature. *n* is generally seen to fall between zero and unity although this is not a requirement and examples for which $n > 1$ do exist. [68] *n* is also seen to be temperature dependent. Mauritz, based on investigation of ion hopping in hydrated Nafion membranes, suggested that *n* reflects the degree of connectedness of long range charge hopping pathways, or extent of tortuosity for mobile charges.[69]

To date, no rigorous mathematical proof of Equation 3 exists. This universal dynamic response is seen to hold for different types of materials including disordered semiconductors, conducting and semiconducting polymers, conducting polymer composites, ceramics, ion conducting glasses and doped ionic crystals.

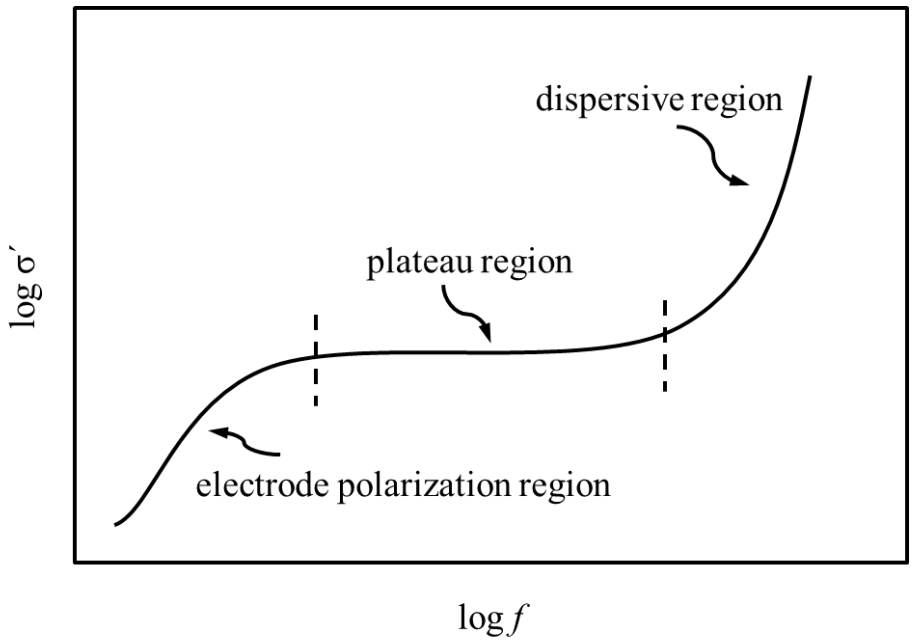

Figure 9. Typical log-log real conductivity σ´ vs. frequency relationship at a given fixed temperature for conductive disordered materials.

It has been considered as to whether there is a link between *A* and *n* and whether these quantities have a mechanistic origin in terms of underlying disordered microscopic structure on a given scale and a particular type of charge hopping mechanism throughout this structure. Models have been proposed including the symmetric hopping model and the macroscopic model, both discussed in a review by Dyre and Schroeder. [68] In general, the two models differ in the length scale of the disorder relevant to conductivity. The details of the mathematical analysis and underlying approximations are too complicated and extensive to summarize here.

The symmetric hopping model assumes disorder of charge transfer to be on a microscopic scale, presumably involving adjacent moieties involved in short ranged hopping of electrons or ions.

The vague macroscopic model assumes length scales on the order of the correlation length of charge transfer moieties. This model considers the distribution in the length of disordered pathways accessible for electric charge flow which involves the concept of percolation. Macroscopic conduction (from one end of the sample to the other) will occur above a charge percolation threshold. The size/shape of a percolation cluster is dependent on morphology and affects nearest neighbor inter- (and intra-, if possible) charge transfer contacts. There will be dead ends on percolation clusters and poorly conducting regions which impede conduction. Classical hopping *over* potential energy barriers is considered, but also quantum mechanical tunneling of delocalized electrons *through* these barriers can occur as is likely the case of arrays of contacting carbon nanotubes as those discussed here. Owing to considerable microstructural heterogeneity present in disordered solid conductors, very broad distributions of jump/tunneling rates and local charge mobility must be the case.

When frequency increases, sub-percolation clusters can become ac-conductive as more rapid charge fluctuations, owing to the shorter period of electric field reversals, can only allow shorter overall charge displacements before the field reverses. At increasingly lower frequencies charge transport extends over longer distances and direct current flow is approximated, accounting for the plateau on the graph in **Error! Reference source not found.**.

Papathanassiou noted a relationship between A and n in that $-\log A/n$ vs. f was independent of disordered material composition at all frequencies up to one terahertz.[70] Furthermore, $-\log A/n$ is nearly constant and consistent between a wide range of materials.[70, 71] This finding contrasted with theories which implied physical meaning

behind these quantities beyond their being empirical fitting parameters. There was a subsequent study of an investigation of power law behavior in a mixed crystal compound in which *A* and *n* were sensitive to structural transitions within the crystal upon increasing temperature. It was found that even through multiple physical transitions the relationship between -log*A*/*n* again remained constant.[72] Interestingly, numerical modeling of this power law suggests that this universal response is just that of a random mixture of conductors and capacitors in an equivalent circuit representation.[73]

To date, there has not been established an interconnection of *A* and *n* with physical meaning at the microscopic level. One component of this work will be to not only test the application of this power law to the curing of glassy epoxy/nanotube nanocomposites but also to consider possible meaning that the relationship between *A* and *n* may have with respect to microscopic level disorder of charge motions in this particular system.

CHAPTER II - EXPERIMENTAL

General Materials

The chemicals used herein were purchased from Fischer Scientific, Royce, Southwest Nanotechnologies, or Bayer chemical companies and were used as received without further purification unless otherwise stated.

There were three benchmark nano-particles selected for the purpose of this research. They were Baytubes ® C 150 P supplied by Bayer AG, Leverkusen, Germany as well as SMW200 and SMW210 supplied by Southwest Nanotechnologies. In general the Baytubes were used to screen processing conditions while the Southwest varieties were chosen specifically for their augmented electrical performance. MWCNT were dispersed into the base epoxide and epoxy prepolymers through a variety of processing conditions utilizing sonication and co-rotating twin-screw extrusion. To preclude any risk to the health and well-being of researchers involved in the handling and processing of these materials, tolerance limits for the research environment were ensured to provide efficient exhaust ventilation and fresh air in the research laboratories in accordance with the Bayer Safety Data Sheet.[74] Micrographs displaying MWCNT morphology for the tubes used in this study are shown in **Error! Reference source not found.** for Baytubes and **Error! Reference source not found.** for Southwest. Typical property values for each are provided in **Error! Reference source not found.** and **Error! Reference source not found.** respectively.[75]

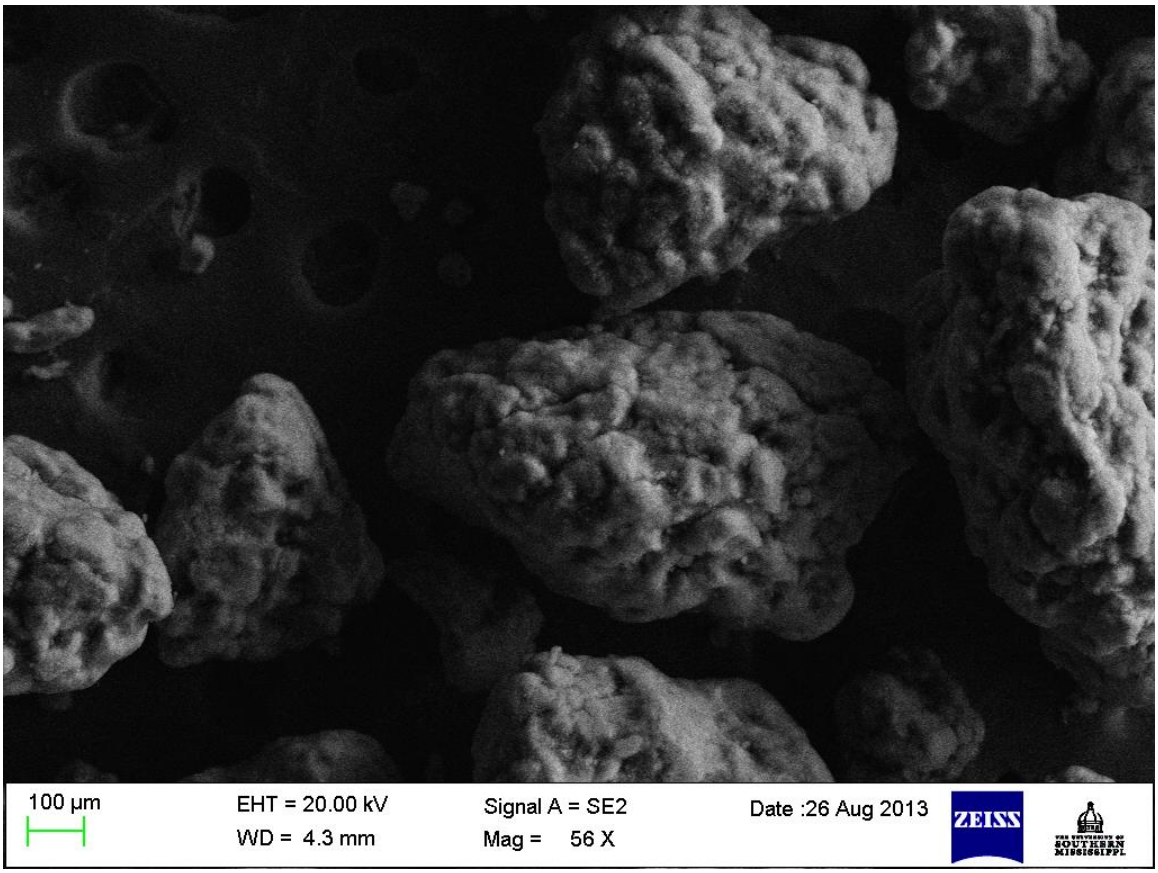

Figure 10. Micrograph of Baytube® C150P agglomerates

Table 1

Baytubes® C 150 P typical properties

Property	**Value**	**Unit**	**Method**
C-Purity	>95%	wt%	ashing
Free Amorphous Carbon	Not Detectable	wt%	TEM
Outer Mean Diameter	~13	nm	TEM
Inner Mean Diameter	~4	nm	TEM
Length	>1	µm	SEM
Bulk Density	130-150	kg/m^3	EN ISO 60
Agglomerate Size	0.1 - 1	mm	PSD

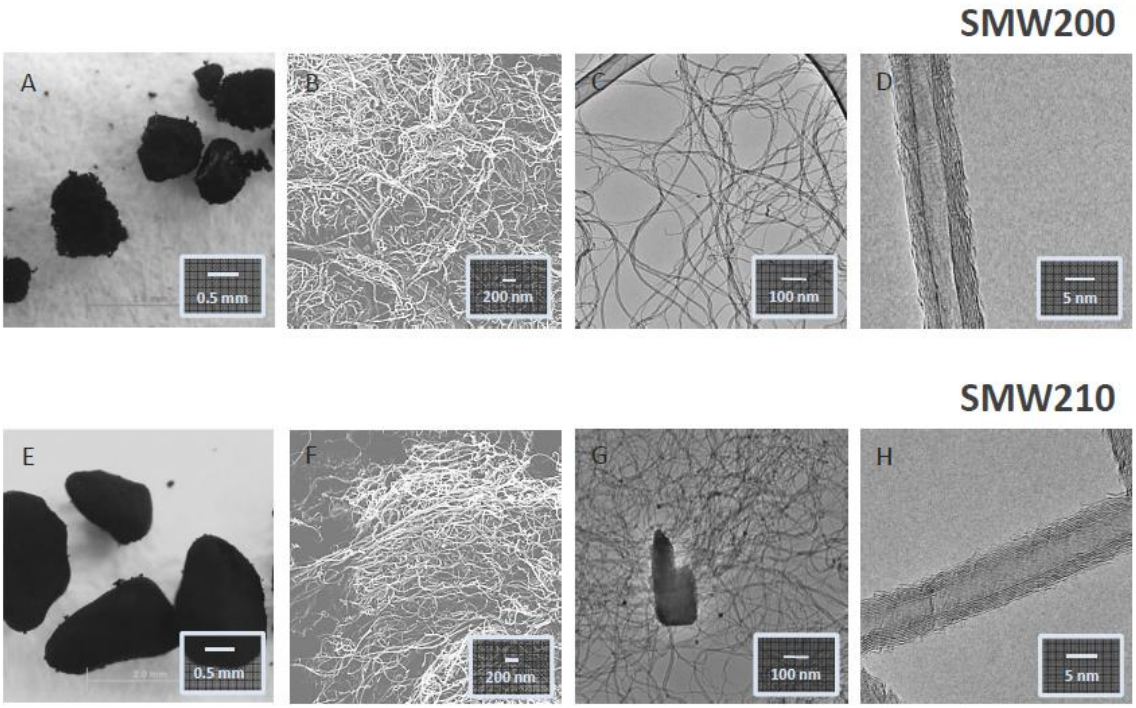

Figure 11. Optical images and micrographs of SMW 200 and SMW 210 nanotubes

Table 2

SMW 200 and SMW 210 typical properties

Property	**SMW 200**	**SMW210**	**Unit**	**Method**
C-Purity	99	84	wt%	TGA
Non-Carbon Content	1	16	wt%	TGA
Median Outer Diameter	10	10	nm	TEM
Median Inner Diameter	4.5	4.5	nm	TEM
Median Tube Length	3.0	3.0	μm	AFM
Median Aspect Ratio	300	300		TEM
Moisture Content	2	1	Wt%	TGA
Bulk Density	100	70	kg m^{-3}	ASTM D7481
Specific Surface Area	350	350	m^2g^{-1}	BET
Agglomerate Size	0.5-1.5	2.0-4.0	mm	SEM

General Nanocomposite Preparation

Prepolymer matrices were produced using the continuous high shear reactor method.[76-78] The reactor used in this work was a 26mm twin screw, co-rotating, fully intermeshing, Coperion Megacompounder equipped with a solid feeding side stuffer, calibrated loss-in-mass controlled solid feeder system, volumetrically controlled liquid feed system, and melt pump all controlled by a touch screen controller. The reactor and its components are illustrated in **Error! Reference source not found.**. Additionally the barrel was divided into ten zones that could be independently electrically heated and liquid cooled. Screw profiles were custom designed to balance throughput, conversion, dispersive and distributive mixing through the utilization of conveying, kneading, feed, and ZME screw elements. Typical processing parameters included a screw speed (200-600 RPM), a throughput (9.8 lbs/hr), and a barrel thermal profile ranging between 40-220°C. All samples were formulated at 1:1 stoichiometric equivalents of epoxide to active amine hydrogen by setting the feeding rate of TGDDM at 6.3 lbs/hr and 44DDS at 3.5 lbs/hr.

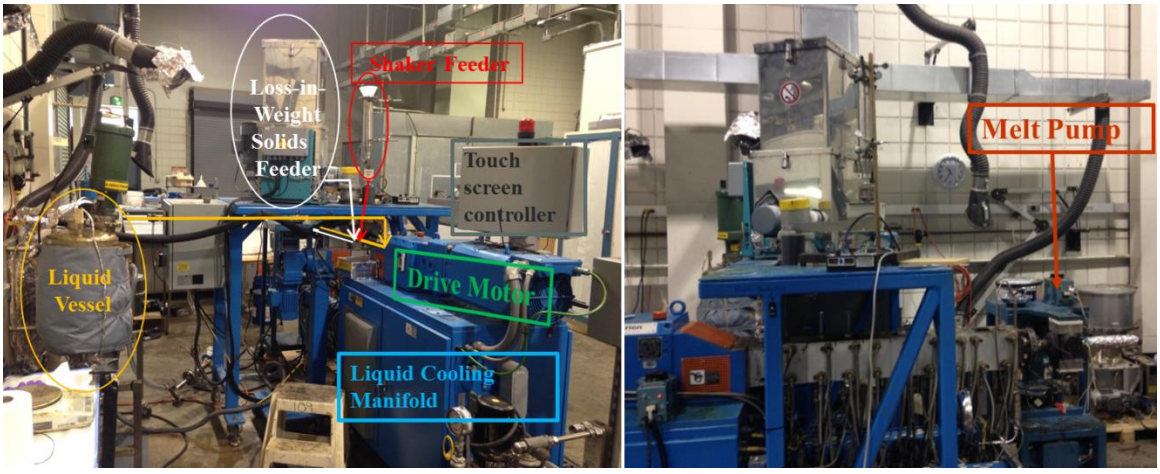

Figure 12. Megacompounder setup

A novel temperature profile was demonstrated by this work that includes two distinct zones. These include a “hot” zone and a “cold” zone. Reactor hot zone temperature was varied between 40 and 220 °C with the cold zone temperature varied from 40 to 100 °C. **Error! Reference source not found.** illustrates a typical hot and cold zone setup where the hot zone appears in red and the cold zone is seen boxed in blue. All experimental samples collected from the reactor were immediately stored in a freezer at 0 °C to arrest continued reactions and reduce post-processing agglomeration until characterization could be conducted.

Figure 13. TSE screw design demonstrating hot and cold zones

General Nanocomposite Cure

The dispersion state of a nanocomposite and the properties derived from it, in the cured form, is highly dependent on the method by which it was cured. A viscosity trace of a typical high performance epoxy network through cure is illustrated in **Error! Reference source not found.**. The elevated temperature required for complete conversion of high glass transition temperature (T_g) epoxies is known to cause a drop in matrix viscosity prior to a gelation event which creates a trace resembling a hyperbolic

well. Within this low viscosity well nanotubes have the highest mobility and therefore the greatest tendency to agglomerate.

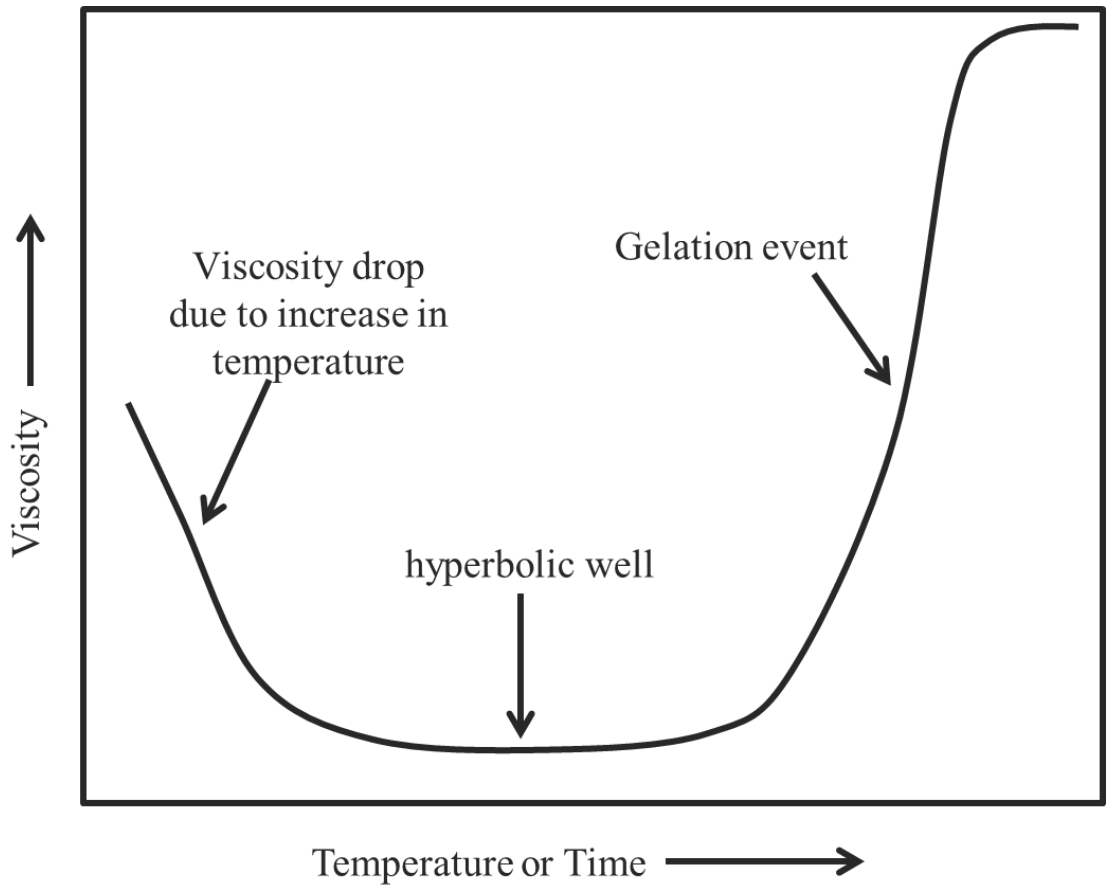

Figure 14. Typical viscosity trace for a curing epoxy/nanocomposite network

Within the scope of this project a great deal of work was directed towards controlling the shape of this viscosity trace. This included augmenting the lower viscosity limit experienced during the cure process and limiting the duration of this well with the goal to drive agglomerate size and morphology to dictate cured material properties.

Chapter III Experimental

Chapter III Materials

The following materials were used as received: 4, 4'-diaminodiphenylsulfone (44DDS) (Royce Chemical Corp, Skippack, PA, USA, M_n = 248.3 g/mol, particle size 4 μm); tetraglycidyl -4, 4'-diaminodiphenylmethane (TGDDM) (Huntsman, Salt Lake City, UT, USA, M_n = 422.5 g/mol). Their chemical structures are shown in **Error! Reference source not found.**. There were three types of MWCNT used in this study. Baytube® C150P, SMW200 purified and SMW210 unpurified MWCNT supplied by SouthWest NanoTechnologies.

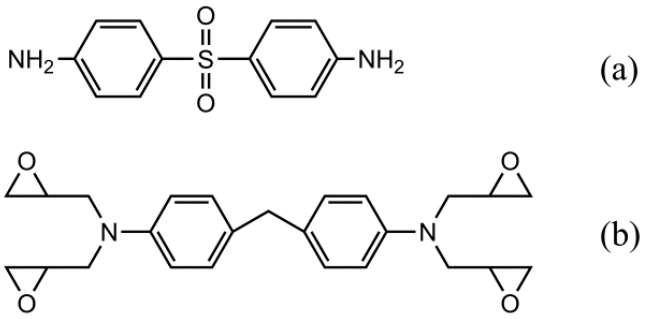

Figure 15. Chemical structure of (a) 44DDS, (b) TGDDM.

Chapter III TGDDM/MWCNT Prepolymers Continuous Reaction

Engineered prepolymers of TGDDM/MWCNT were prepared using a continuous reaction method which was accomplished using a Coperion ZSK 26 mm co-rotating intermeshing twin-screw extruder (L/D = 40). The continuous reactor was modular and specifically designed for the epoxy-amine cure reaction and MWCNT dispersion in a single step process. As illustrated in **Error! Reference source not found.**, the screw profile consists of a liquid feed zone (Zone 1), a solid feed zone (Zone 2), ten electrically

heated and liquid cooled zones (Zone 1-10), and an additional zone to control the thermal profile of the melt pump. The hot zones (Zone 1 to 6) were kept at the same elevated temperature between 160 °C and 200 °C which previous work has shown to be an ideal temperature range for the complete dissolution of 44DDS in TGDDM and the advancement TGDDM prepolymer viscosity without concerns of gelation in the continuous reactor.[79] The cold zones (Zone 7 to 10) also had a static temperature profile that varied from 40 °C to 100 °C. Screw design was configured to balance shear mixing and residence time, which was found to be between one and two minutes, with a combination of various conveying, kneading, gear and reverse elements. The screw design was optimized to incorporate two kneading block sections to provide adequate shear mixing. Gear and reverse elements were incorporated in Zone 8 to optimize the residence time, generate back-pressure and enhance MWCNT dispersive and distributive mixing. A vacuum pump was attached at Zone 9 and was used to remove volatiles, between the melt seals formed at the reverse element in Zone 7 and the melt pump, to reduce trapped air that would otherwise form bubbles during cure.

The benefits of this two-step temperature profile include the ability to control epoxy prepolymer properties such as molecular weight and tack, all the while maximizing MWNCT dispersion and stabilization through to the final cured composite.

For a typical continuous reaction, TGDDM was pre-heated to 80 °C in a 50 L batch reactor and delivered into the continuous reactor through a liquid feed port in Zone 1 at a rate of 47.7 g/min. 44DDS was charged into a gravimetric solids feeder to deliver a rate of 28.0 g/min which gave 1:1 stoichiometric equivalents of epoxy to active amine hydrogen. MWCNT was fed by a laboratory vibratory feeder capable of consistent

feeding rates as low as 0.01 g/min. Both 44DDS and MWCNT were added through a side stuffer at Zone 2. Aliquots of extrudate material were collected just beyond the melt pump and quenched in a freezer for characterization. **Error! Reference source not found.** describes the nomenclature, compositions and processing conditions employed within this work for TGDDM/MWCNT prepolymers.

Table 3

TGDDM/MWCNT prepolymers nomenclature, compositions and processing conditions

Sample No.	MWCNT content (wt %)	Hot zone temperature (°C)	Cold zone temperature (°C)	Screw speed (rpm)
1	1.0	160	60	600
2	1.0	180	60	600
3	1.0	200	60	600
4	1.0	180	40	600
5	1.0	180	80	600
6	1.0	180	100	600
7	1.0	180	60	200
8	1.0	180	60	400
9	1.0	180	60	800

Chapter III Instruments and Characterization

DSC was performed using a TA Instruments DSC Q200 to study the T_g and cure conversion in the epoxy prepolymers at various processing conditions. A heating rate of 5 °C min^{-1} was employed in the temperature range of -20 °C to 300 °C under nitrogen. The T_g for the prepolymers was reported as the peak maximum within the heat capacity trace.

Residual curing enthalpy (ΔH_{res}) was used as an indicator for the degree of cure for the epoxy prepolymers and calculated from the exotherm peak area in the DSC thermogram.

Rheological analysis was conducted on an ATS Rheosystems rheometer with disposable 25 mm parallel plates to measure the complex viscosity (η^*) of epoxy prepolymers and their development during isothermal cure. Experiments were performed within the linear elastic regime at a strain of five percent and a frequency of 1 Hz.

An Olympus GX51 metallurgical microscope with a reflection light source was used to examine the MWCNT dispersed states and their stability in the TGDDM prepolymers. Samples were prepared by sandwiching a thin layer of sample between two pieces of cover glass using one layer of 0.02 mm thick Teflon film to act as a spacer to maintain a uniform sample thickness. The dispersion states of the nanocomposite prepolymers were quantified using an Olympus Stream Image Analysis software package. Dispersion index, *D* which reflects the normalized agglomeration area was calculated according to Equation 2.[52] The area occupied by MWCNT agglomerates A_{CNT} and the total investigated area A_o were obtained from image analysis in which agglomerates with diameters smaller than 1 μm were neglected. $\emptyset_{vol}$ is a term to describe the nanotube volume fraction and *f* is a factor related to the density of CNT agglomerates and was estimated to be 0.25. According to Equation 2, a *D* value of 100 % corresponds to a perfect micro-scaled dispersion in which all the nanotubes are contained within agglomerates less than 1 μm in diameter within the sample. A decreasing dispersion state is reflected in a decreasing *D* value. Average *D* values reported in the current study were determined from optical images taken from five representative locations within each sample.

A Zeiss EM900 transmission electron microscope (TEM) was used to probe the carbon nanotube dispersion at the sub-micron scale with an accelerating voltage of 50 kV. Samples were cut into ultrathin (~100 nm), trapezoidal shaped sections with a Porter-Blum MT-2B microtome using a diamond knife at room temperature. Sections were collected on a 200 mesh copper TEM grid and imaged without staining.

Chapter IV Experimental

Chapter IV Materials

The following materials were used as received: 4, 4'-diaminodiphenylsulfone (44DDS, Royce Chemical Corp, M_n = 248.3g/mol); tetraglycidyl - 4, 4'-diaminodiphenylmethane (TGDDM, Huntsman, M_n = 422.5g/mol); multi-walled carbon nanotube (MWCNT, Bayer C150P Baytubes; length > 1μm, diameter = 4~13nm.) The density of MWCNT after incorporation into epoxy matrices is approximately 1.75g cm^{-3}.[80] The matrices for this work were formulated at 1:1 stoichiometric equivalents of epoxide to active amine hydrogen.

Chapter IV Dispersion and Processing Parameters

The epoxy-amine matrix, TGDDM-44DDS, used in this study was chosen because it is commonly utilized in aerospace grade prepregs. Prepolymers were prepared by using the continuous reaction method outlined in Chapter III.

Chapter IV Rheological Characterization

Variable temperature rheology analyses were obtained through dynamic shear viscosity measurements performed on a Reologica Stresstech Rheometer, using a 25 mm disposable parallel plate assembly. Prepolymer samples, collected from the continuous reactor, were warmed to their lowest workable temperature preventing reagglomeration,

pressed into compression molds, at room temperature, under 1,000 psi, into rheology discs (25 mm in diameter). The plates were preheated for 1 minute with the gap set to 0.5 mm and zeroed at the testing temperature. Testing was conducted at a constant frequency of 1 Hz and a temperature ramp matching that of the cure prescriptions being investigated, those being 60 – 180 °C at a rate of 1 °C/min or a 48h, 80 °C isothermal hold, followed by a 1 °C/min ramp to 180 °C to drive matrix to maximal and equivalent conversion. In this second case, the viscosity profile during the final ramp to 180 °C was used to verify that gelation had been reached during the initial 80 °C isothermal hold. Prior to testing, a frequency sweep method was used to validate that 1 Hz afforded testing within the prepolymer linear viscoelastic regime.

Chapter IV TEM and OM Characterization

Transmission electron microscopy (TEM) was used to characterize dispersion and distribution of dispersion states of the MWCNT TGDDM-44DDS samples at the sub-micron level. For this a Carl Zeiss Inc. 900 TEM was employed and adjusted with an accelerating voltage of 50 kV. Samples were prepared by sectioning into ultrathin (≈100 nm), trapezoidal-shaped sections using a Porter-Blum MT-2B ultramicrotome fitted with a Micro-Star Technologies diamond. The cutting was carried out at room temperature with water to float away the sections. Sections were collected on a Formvar-coated, 300 mesh copper TEM grid and imaged without staining.

A light microscope (OM) in transmission mode outfitted with a Nikon OPTIPHOT2-POL polarizing filter together with a METTLER FP82 HT hot stage (HS) was used to observe agglomeration behavior in the upper micron scale. The experiments were carried out on composites with 0.20wt% MWCNT prepared with a high shear

continuous reactor. OM specimens, approximately 50 microns thick, were compressed between two glass slides and inserted into the HS. The HS was programmed with the one of the two cure cycle used on all the specimens in this study. Those being; 1) a one stage cure (1S) which is a RT - 180 °C ramp at 1 °C /min, followed by a 3 hr isothermal hold at 180 °C or 2) a two stage cure (2S) which is an 80 °C isothermal cure for 48 hrs followed by a 1 °C/min ramp to 180 °C where it soaks isothermally for three hours. An OLYMPUS UC50 color camera recorded the evolution of dispersion states throughout cure, while OLYMPUS Stream Essentials [Version 1.7] image analysis software was used to process the OM images.

Chapter IV Conductivity Measurements

The DC conductivity of nanocomposite samples loaded with between 0.02 and 15wt% MWCNT was investigated using a four-point probe test fixture for strips connected to a Keithley 2400 Sourcemeter. The strips (length 20mm, width 3-4mm, thickness < 500μm) were cut from cured panels ensuing cure. These measurements provided a metric to help indirectly describe the state of agglomerate dispersion, specifically with regards to conductive percolation.[56]

Chapter V Experimental

Chapter V Materials

The materials in this chapter were the same at those indicated in Chapter IV and used without further purification. The epoxy matrix for this work was formulated at 1:1 stoichiometric equivalents of epoxide to active amine hydrogen, and prepared using the TSE method described in Chapter III. [81]

Chapter V Nanocomposite AFM Characterization

Samples were characterized via conductive AFM (C-AFM). C-AFM uses an electrical current to construct the surface profile of the studied sample. The current is flowing through the metal-coated tip of the microscope and the conducting sample. Usual AFM topography, obtained by vibrating the tip, is acquired simultaneously with the current. This enables to correlate a spatial feature on the sample with its conductivity. Several areas of the surface were characterized and scan sizes from 20 μm to 1 μm were collected. It should be noted that C-AFM is a contact mode technique which generally yields poorer morphology images when compared to tapping mode.

Chapter V Nanocomposite Curing and Optical Microscopy Characterization

Optical microscopy in transmission mode was performed using a Nikon OPTIPHOT2-POL polarizing microscope equipped with a METTLER FP82 HT hot stage (HS). OM specimens, approximately 50 microns thick, were compressed between two glass slides and inserted into the HS. The HS was programmed with the same cure cycle that was used on all the specimens in this study (25-180 °C at 1 °C/min, 180 ˚C isothermal hold for 3 hrs). An OLYMPUS UC50 color camera recorded the evolution of nanotube agglomerate dispersion states throughout cure. OLYMPUS Stream Essentials [Version 1.7] image analysis software was used to process the OM images.

Chapter V Conductivity Measurements using a Broadband Dielectric Spectrometer

Complex conductivity vs. *f* data were collected using a Novocontrol GmbH Concept 80 Broadband Dielectric Spectrometer. Frequency sweeps were carried out from 0.01 Hz to 3 MHz over the temperature range of 25 to 180 °C using a nitrogen gas controlled heating system (Quatro Cryosystem Novocontrol). This particular temperature ramp was chosen specifically to mimic the cure program used in collecting the OM

images. Frequency sweeps were carried out when temperature stability of the instrument was within ± 0.2° C. Samples were tested in a custom stainless steel liquid parallel plate sample cell equivalent to the Novocontrol BDS 1308. Samples were sandwiched between stainless steel electrodes of 2 cm diameter with a silica spacer to maintain sample thickness at 0.9 mm.

Chapter VI Experimental

Chapter VI Materials

The materials in this chapter were the same at those indicated in Chapter IV and used without further purification. The epoxy matrix for this work was formulated at 1:1 stoichiometric equivalents of epoxide to active amine hydrogen, and prepared using the TSE method described in Chapter III. [81]

Chapter VI Prepolymer Matrix Preparation

Prepolymer matrices were prepared using the TSE continuous high shear reactor method[76-78] described in Chapter III. The reactor hot zone temperature was varied (60, 120, 180 °C) and the cold zone temperature was unchanged at 60 °C to control the extent of conversion within the prepolymer promote dispersive and distributive mixing. The effect of MWCNT loading level on polymer network development was tested at each processing temperature by comparing loading levels of 0.23, 0.59, and 0.97 wt%. Herein, samples processed at 60 °C are defined as slurries because they contain well mixed and undissolved 44DDS. It should be noted that a neat sample, not containing MWCNT, was collected at each hot zone temperature to serve as a control. Lastly, the experimental samples collected from the reactor were immediately stored in a freezer at 0 °C to arrest continued reactions and reduce post-processing reagglomeration until analyzed.

Chapter VI Rheological Characterization

Dynamic viscosity measurements were performed on a Reologica Stresstech Rheometer, using a 25 mm disposable parallel plate assembly using the same sample preparation method described in Chapter IV.

Chapter VI Nanocomposite Curing and Optical Microscopy Characterization

Variable temperature optical microscopy (OM) in transmission mode was conducted utilizing the method described in Chapter IV. TEM characterization was conducted by the method described in Chapter III.

Chapter VI Thermal Characterization

Dynamic mechanical analysis (DMA) was conducted using a TA Instruments Q800. Prior to testing, prepolymer samples collected from the continuous reactor were warmed to their lowest workable temperature preventing post-processing reagglomeration, cast into silicon DMA molds (35 mm x 5 mm x 2 mm), compressed to 1,000 psi at room temperature, and cured in a laboratory oven using the 1S cure protocol. DMA testing was performed in film tension mode with a strain of 0.05 % and a frequency of 1 Hz. The temperature was ramped from 30 °C to 350 °C at 5 °C/min. Testing was conducted in a nitrogen atmosphere. The T_g values were determined from the peak maximum of the Tanδ plot. Crosslink density (ν) determinations were calculated using Equation 4:

$$\nu = \frac{E'}{3RT}, \tag{4}$$

where E′ is the storage modulus in the rubbery region (T_g + 40 °C); *R* is the gas constant; and *T* is the absolute temperature (T_g + 40 °C). It should be noted that the use of Equation 1 is a qualitative consideration because it is limited to lightly crosslinked systems.

Chapter VI Statistical Analyses

The mean values of the glass transition temperatures and crosslink densities were compared using a one-way ANOVA at a $p < 0.05$ level. This test was performed using MINITAB 17 statistical software.

CHAPTER III – EFFECTIVE DISPERSION

Introduction

Dispersion and stabilization of nanoparticles in epoxy matrices is an area of research that has received considerable attention over the last fifteen years.[1] Over the past decade the mechanical, electrical and thermal properties of carbon nanotubes have spurred intensive investigations aimed at developing nanostructured composites.[2-4] Multiwall carbon nanotubes have the potential to impart desirable properties of epoxies including electrical and thermal conductivity and mechanical performance. However, the experimentally observed properties depend heavily on the dispersion state of the nanotubes. The strong tendency of MWCNT to agglomerate in epoxy matrices often lead to cured networks with diminished material properties.[40, 44, 57, 82-84] Increased capabilities and efficiencies in the production of specifically MWCNT have made them more conceivable as electrical and thermal modifiers in industrial applications for high performance composite materials.

High quality of MWCNT dispersion is difficult to obtain for several reasons. First, there is a large amount of energy required to overcome the van der Waals interactions between neighboring tubes. This causes them to stick together in primary agglomerates and recombine into secondary agglomerates after a dispersion event. Second, determination of nanotube quality is not straight forward and is not always reflected in the comparison of properties listed by manufactures. Differences in nanotube properties make direct comparison of literature studies difficult and can further complicate the already exhaustive process of exceptional nanotube dispersion. Lastly, the quantification of dispersion state is difficult. Despite decades of research, there still does

not exist a single accepted method of dispersion quantification that takes into account the continuum of length-scales relevant to fully describe a dispersed state for nanofillers like MWCNT. Despite these challenges, several approaches have been developed to promote MWCNT dispersion in polymer matrices. These approaches include mixing techniques such as sonication[7], high shear mechanical mixing[6], and calendaring,[85] as well as chemical techniques such as surface functionalization[86] and use of dispersive surfactants.[43, 87] Unfortunately these techniques are often limited to small quantities because of the impractical nature of operation at larger volumes. This is due to the excessive amount of heat generated by the high localized shear and inefficiency associated with these methods.[45]

It is well understood that an increase in shear, applied to a system, translates as an increase in dispersion state. This is due to the relationship between shear force (τ) matrix viscosity (μ), boundary velocity (u), and distance from shear boundary (y) is presented in Equation 5. Shear force scales with viscosity and, thus, it is expected that dispersion states would increase with increasing polymer viscosity. Therefore, it is desirable to develop a dispersion method that is not only capable of handling, but makes use of, the high shear forces that arise from high viscosity matrices. Methods of dispersion such as ultrasonication, mechanical mixing, and calendaring require low viscosity media which limit their use, not only in the shear forces they invoke on agglomerates, but also, in the ability to curb re-agglomeration of nanotubes in the highly dynamic and mobile media environment.

$$\tau(y) \propto \mu\frac{\partial u}{\partial y} \tag{5}$$

High-shear continuous reactors, where the reactor is a twin screw extruder, offer the capability to handle high viscosity materials and has acquired great interest for research as an environmentally-favorable and economic method for industrial scale manufacturing.[23, 24] More specifically, fully intermeshing co-rotating twin screw extruders offer the highest level of mixing, dispersion, and shear control, making them the primary technology used as continuous chemical reactors.[25, 26] Typically this method is associated with dispersing nanoparticles within high molecular weight linear thermoplastic polymers. In this process, during melt mixing, the applied shear strength is directly tied to the agglomerate size reduction. Several studies reported greater dispersion was achieved by using high melt viscosity matrices thereby maximizing the shear environment and shear states applied. [27-34] However, extrusion processes are limited in their ability to disperse nanoparticles into epoxy matrices, since epoxies are generally used or processed in a low viscosity state and therefore result in unfavorable shear environments within the reactor barrel.

We recently reported a novel method for preparing thermoplastic modified epoxy prepolymers based on twin screw extrusion technology.[35] The advancement of epoxy chain extension or conversion was controlled by reaction chemistry, process designs and processing conditions in order to achieve targeted viscosities with tack optimized for prepreg filming applications. The biggest advantages to this continuous reactor design, when compared to the batch process it replaced, was the mitigation of batch-to-batch variation, favorable performance measures relating to processing rate, namely the reduction of space-time and augmentation of space-velocity for the system, and the abatement of conditions where large volumes of reactive materials are involved in which

safety concerns arise. Our intention through the present research was to combine our successful strategies for advancing epoxy chemistries with our approach to achieve high levels of nanotube dispersion using a continuous reactor. We believe MWCNT dispersion and stabilization in epoxy matrix can be drastically improved via a continuous reaction process, as opposed to conventional methods, owing to the unique advantage of controlling prepolymer matrix viscosity. To the best of our knowledge, a single-step approach to formulate epoxy resin, curative, and nano-reinforcement has not yet been reported. The development of an economical process for producing large quantities of epoxy matrix prepolymers modified with carbon nanotubes will have huge value in the aerospace and other composites communities. It is the goal of the present work to highlight the dispersive capabilities of TSE, employed as a continuous reactor, and the benefits there within. Using the reactor setup, as described in the present work, nanocomposites have been successfully dispersed at concentrations from 0.02% to 26.0% by weight into TGDDM based prepolymers.

Results and Discussion

Influence of Hot Zone Temperature

Several key processing parameters are discussed to highlight crucial control variables and benchmark properties of TGDDM/MWCNT prepolymers produced via the continuous reactor. The hot zone was designed to partially cure, or B-stage, the matrix using the barrel temperature to control the extent of reaction between the epoxide resin and amine curative. This aim was demonstrated through the preparation of TGDDM/MWCNT prepolymers with varying hot zone temperatures (160 °C, 180 °C, and 200 °C) with a constant cold zone temperature of 60 °C and their properties were

examined by DSC. A threshold condition of 200 °C was used as the maximum hot zone temperature to avoid system gelation and prevent runaway crosslinking within the barrel of the extruder. This temperature was determined experimentally through isothermal cures of the TGDDM 44DDS matrix system on a parallel plate rheometer to track the time to gelation within the viscoelastic regime. Comparison of this time-to-gel with the known residence time of the continuous reactor afforded the determination of this celling temperature with a factor of safety and confidence built in.

Error! Reference source not found. shows the DSC curves for the TGDDM/MWCNT prepolymers during the heating stage from 0 °C to 300 °C. As expected, all thermograms follow a similar motif, but with T_g and residual heat of cure (ΔH_{res}) which correspond to the extent of B-staging. These values are tabulated in **Error! Reference source not found.**. The T_g increased from 5.1 °C for the 160 °C sample to 8.0 °C for the 200 °C sample while ΔH_{res} reduced from 608.7 J/g to 582.8 J/g, suggesting that the temperature of the hot zone did indeed advance the conversion of the prepolymers significantly. In the continuous reactor, the cure reaction took place immediately after TGDDM and 44DDS mixed in the hot zone. The cure reaction is kinetic-controlled prior to reaching its gel point, with the cure rate being sensitive to cure temperature in an Arrhenius relationship. Thus, increasing the hot zone temperature increases the reaction cure rate, consequently leading to higher glass transition temperatures and cure conversion. An inflated polymer T_g yields an additional increase in viscosity within the cold zone portion of the reactor barrel. This increase in prepolymer viscosity is thought to serve two purposes; first it increases the shear environment the nanotube agglomerates experience within the cold zone of the reactor. Second, it acts to better stabilize, or lock

in, the nanotube dispersion state mitigating secondary agglomeration. The ability to tailor the viscosity of epoxy prepolymers through the control of hot zone conditions confirms the feasibility of using the hot zone to control epoxy prepolymer properties. This is particularly useful for maintaining processability and tack for use in aerospace prepreg filming applications, which is essential for high T_g epoxies.

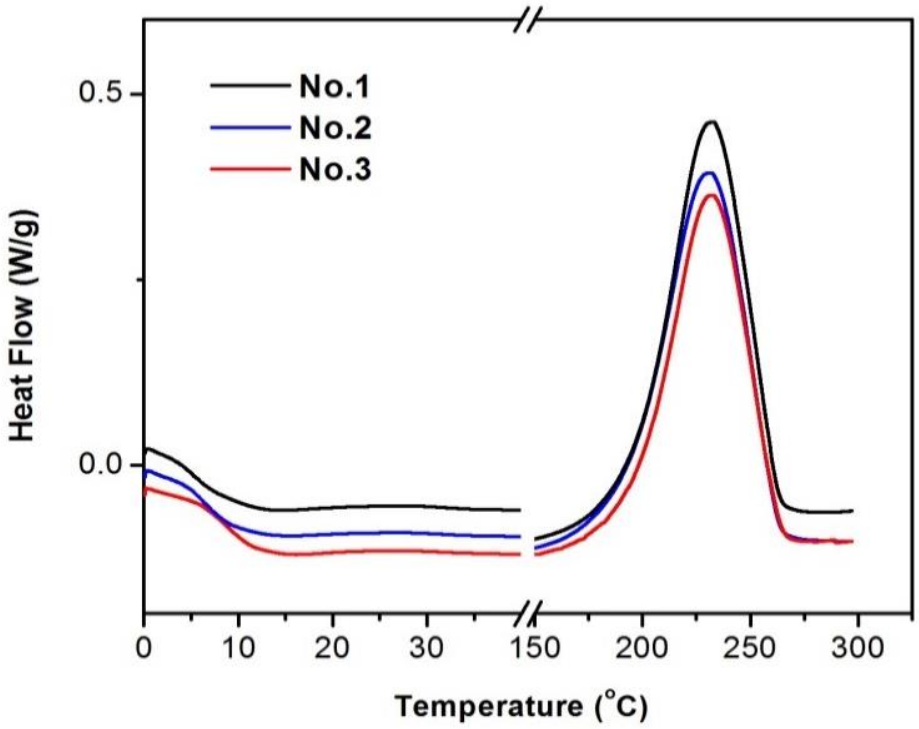

Figure 16. DSC exotherms for prepolymers prepared at different hot zone temperatures.

Table 4

Properties of TGDDM/MWCNT prepolymers at different hot zone temperatures.

Sample No.	Hot zone temperature (°C)	T_g (°C)	ΔH_{res} (J/g)	η (Pa·s)*
1	160	5.1	608.7	1.0
2	180	6.5	597.3	3.7
3	200	8.8	582.8	5.5

* Prepolymer viscosities were measured at 80 °C.

The agglomerate distributions of nanotubes in the TGDDM based prepolymers, prepared at three hot zone temperatures were investigated. Very similar dispersion states were observed for all three conditions. To provide a statistical comparison, their dispersion indices were calculated using Equation 2. *D* value of 97.9%, 98.5%, and 98.3% were obtained for 160 °C, 180 °C, and 200 °C samples respectively. Since their difference in dispersion index fell within the statistical error ranges, the data suggests that changing the hot zone temperature from 160 °C to 200 °C has little influence on MWCNT dispersion, at least prior to cure. To reiterate, it is the purpose of the hot zone to control the epoxy chain extension reaction, which is hypothesized to have an effect on the extent of stabilization of the dispersed state during cure.

Influence of Cold Zone Temperature

Twin screw extruders are not traditionally designed for low viscous epoxy resins since the shear force imposed on the resin between screw flights and the barrel deteriorates rapidly as the viscosity decreases. When this occurs the particle mixing and dispersing event becomes inefficient. While the purpose of applying the hot zones is to advance the resin cure conversion and viscosity helps to mitigate this issue, the cold

zones are designed to further enhance the nanotubes dispersion within the prepolymer matrix. A reduction in cold zone barrel temperature significantly increases the processing viscosity of epoxy resin which aids the carbon nanotube dispersion by augmenting the shear environment.

Samples were prepared at four cold zone temperatures (40 °C, 60 °C, 80 °C, and 100 °C) using a constant hot zone temperature of 180 °C and their dispersion states were examined via optical microscopy. **Error! Reference source not found.** illustrates the MWCNT dispersion states developed in these epoxy prepolymers at the described processing conditions. Comparison of the pristine MWCNT, shown in **Error! Reference source not found.**, to the dispersion obtained through the continuous processing shows a distinct size reduction from around 500 μm to 10 μm that was observed for all cold zone processing conditions, suggesting the excellent dispersive mixing ability of the continuous reactor. Samples prepared at the lowest cold zone temperatures of 40 °C and 60 °C (No.4 and No.2) showed MWCNT agglomerates that were evenly distributed in the prepolymer matrices. Few isolated bundles larger than 1 μm were observed, characteristic of the high dispersion indices observed for these samples. The increase of cold zone temperature up to 100 °C, lead to increases in both the number and size of MWCNT agglomerates. For example, sample No.6, with cold zone temperature of 100 °C, was dominated by the largest agglomerates with diameters of around 20 μm.

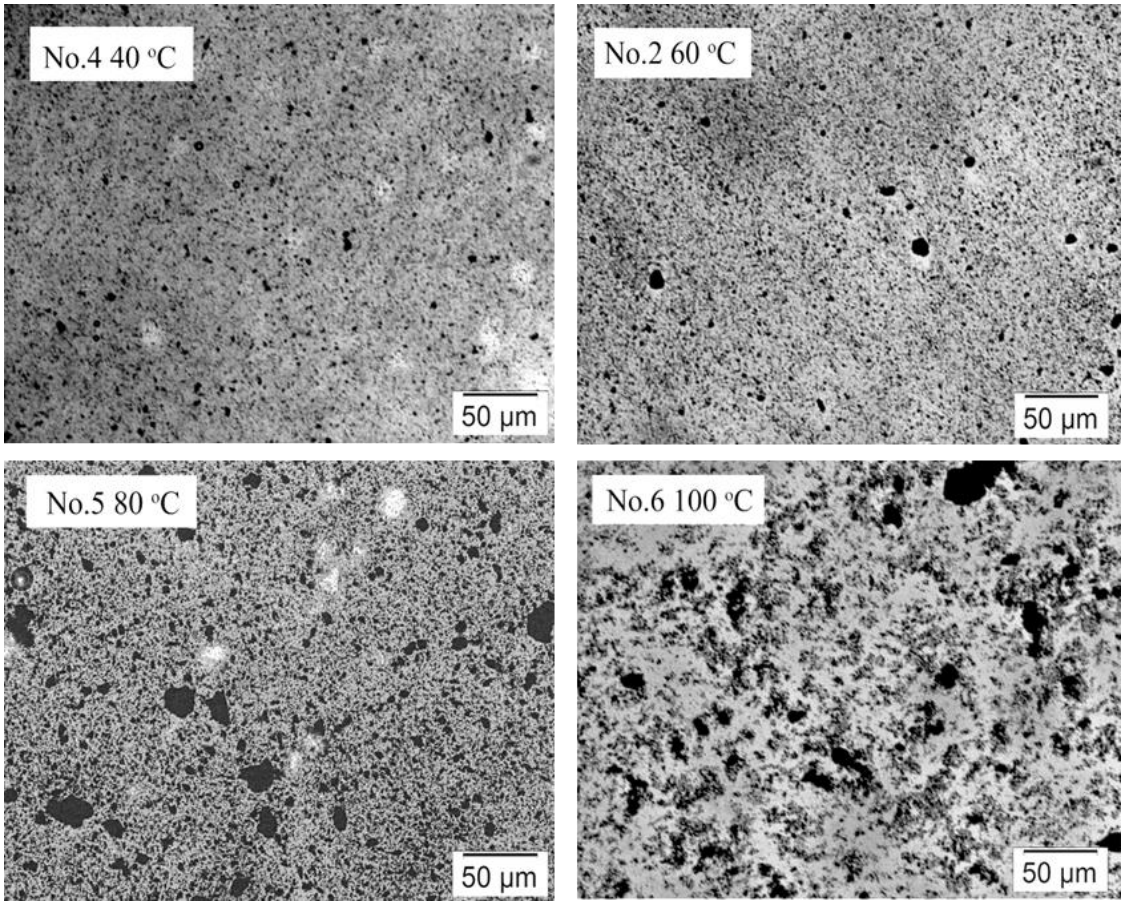

Figure 17. Optical images showing effect cold zone temperature on dispersion.

The effect of nanotube dispersion at varying cold zone temperatures was quantified by the designation of dispersion indices which are tabulated in **Error! Reference source not found.** and clearly reflect the qualitative trends observed in Figure 4. Samples prepared at 40 °C show dispersion index values eclipsing 99%, suggesting nearly homogenous micro-scale dispersion. The value of *D* decreased from 99.2 % to 84.5 % as the cold zone temperature increased from 40 °C to 100 °C. This reflects the reduction in shear environment predicted by Equation 5 with respect to matrix viscosity controlled by cold zone barrel temperature. This shear environment is effective for improving nanotube dispersion in epoxy prepolymer matrices.

Table 5

Dispersion indices and processing viscosities of TGDDM/MWCNT prepolymers at different cold zone temperatures

Sample No.	Cold zone temperature (°C)	*D* (%)	η (Pa·s)*
4	40	99.2	1.3×10^3
2	60	98.5	1.2×10^2
5	80	94.6	0.8×10^1
6	100	84.5	2.7×10^0

*Processing viscosities were measured at the corresponding cold zone temperature after samples were collected.

Although, the shear stress applied on the carbon nanotubes is primarily responsible for the MWCNT agglomerate size reduction, the direct measurement or calculation of shear stresses within the barrel of the TSE is not straight forward. This is due to the dynamic and reactive nature of the epoxy resin, progression of reaction, and the complexity of the screw profile. We can only speculate on these shear states based on the post-processing viscosities of the prepolymers, which are proportional to the shear stress at a constant screw speed.[79] **Error! Reference source not found.** shows the viscosity of each of the nanocomposite samples determined at the cold zone temperature in which they were processed. Decreasing the cold zone temperature from 100 °C to 40 °C increased the viscosity three orders of magnitude from 2.7 E+0 Pa·s to 1.3 E+3 Pa·s which would suggest that the shear environment invoked on the tubes was about three decades higher in the 40 °C samples owing to the increased breakup of the nanotube bundles and improved dispersion observed at the micron scale.

Samples with the best and worst nanotube dispersion state, No.4 and No.6 respectively, were imaged via TEM to better understand the multi-scale dispersion state, and to highlight the influence of cold zone temperature, within these materials. **Error! Reference source not found.** illustrates the sub-micron dispersion for the material prepared at 100 °C. Large unreinforced areas of matrix were observed surrounding localized areas of high nanotube density. Samples prepared at 40 °C showed the highest level of dispersion at the micro-scale and presented a more uniform dispersion at the sub-micron scale and exhibit the smallest diameter agglomerates. The significant improvement in carbon nanotube dispersion at both length-scales demonstrates the importance of cold zone temperature during continuous reaction.

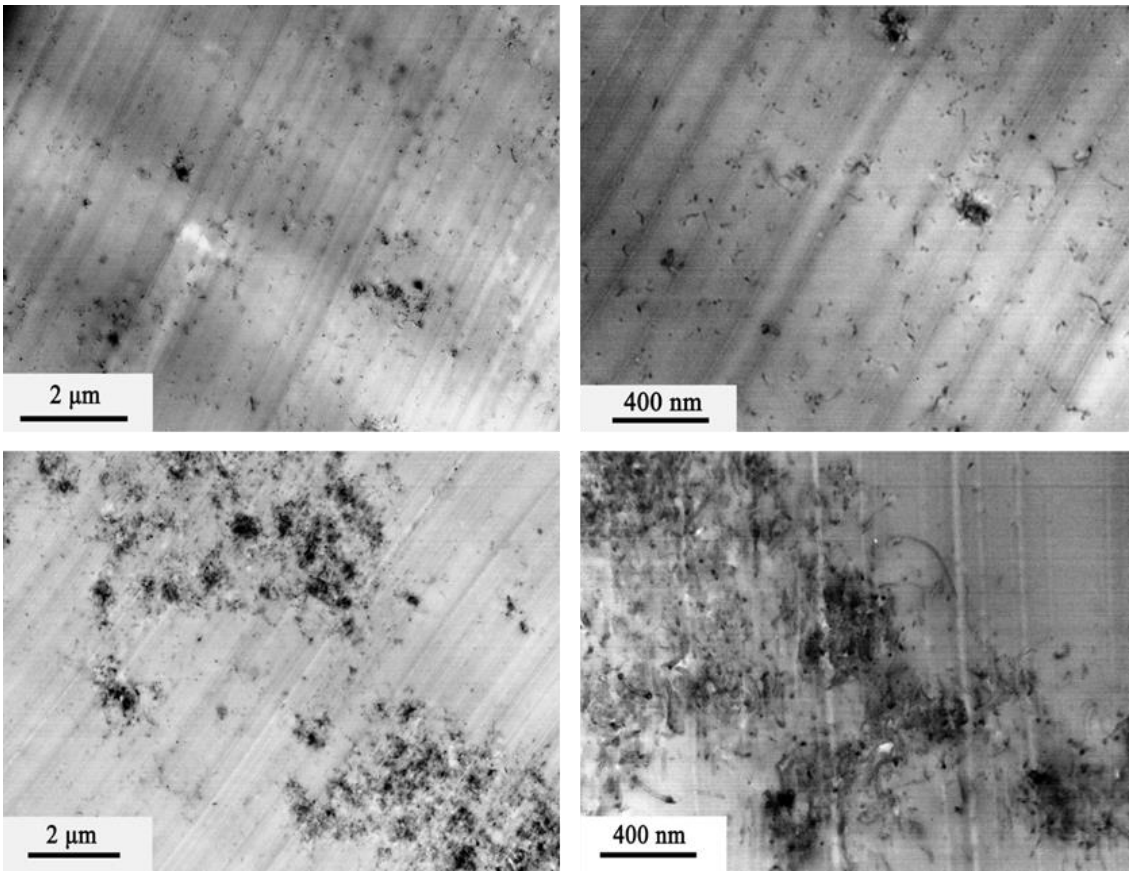

Figure 18. TEM images of samples prepared from different cold zone temperatures. Top images: Sample No.4 processed at 40 °C; bottom images: Sample No.6 processed at 100 °C

At the centers of many of the most densely packed agglomerates, we observe small crystalline impurities that we believe to be residual catalyst left over from the synthesis of the tubes. It is possible that these impurities may be acting as nucleation points for agglomeration resulting in an inferior dispersed state. This result suggests that impurities may be critical to the agglomeration state within these materials.

Unlike thermoplastic polymers, dispersion of MWCNT in epoxy matrices is more complicated as epoxy prepolymers require curing before practical use. When temperature is raised above ambient conditions the viscosity of the resin matrix drops significantly, which affect MWCNT dispersion stability and favors re-agglomeration.[38, 88] Good

nanotube dispersion is often retained in the uncured epoxies but lost in the final cured composites. In this study, however, no apparent change in carbon nanotube agglomerate size was observed at the micron scale comparing prepolymers and cured specimens. This was accomplished by progressing cure beyond the point of gel isothermally at 80 °C over the course of two days and then post curing the samples at 200 °C to further drive conversion. This cure prescription was chosen specifically to minimize the drop in matrix viscosity that would otherwise accelerate nanotube agglomeration in high temperature cure cycles. In this way we could observe dispersion at the sub-micron length-scale using TEM in fully cured nanocomposite materials. It is important to note that the success of this low temperature cure cycle on leaving dispersion state intact is conspicuously bound to the partial curing of epoxies within the hot zone region of the reactor. This finding brings a new approach to the stabilization of carbon nanotube dispersions and subsequent restrictions of re-agglomeration through the partial curing of resin.

Influence of Screw Speed

Screw speeds were also varied to further demonstrate the continuous reactor capabilities in nanoparticle dispersion. The nano-scale dispersion states of MWCNT samples prepared at 200 rpm, 400 rpm, 600 rpm and 800 rpm are shown in **Error! Reference source not found.** with their dispersion indices plotted as a function of screw speed being presented in **Error! Reference source not found.**. The 200 rpm sample showed the lowest level of dispersion among all the samples with a *D* value of 89.8 %. Increasing TSE screw speed led to an improved dispersion state peaking at 600 rpm. Only a small degree of change was observed between 600 rpm and 800 rpm, indicating that there may be a limit to the influence of screw speed on the ability to promote

additional dispersion of MWCNT in epoxy matrices. Similar trends were also described by several authors using alternative polymer systems and explained in terms of shear stress and residence time. [89, 90] Higher screw speed generates higher shear stress during continuous reaction process, facilitating MWCNT agglomerates breakup and enhancing their dispersion in epoxy prepolymer matrices. However, residence times are reduced with increasing screw speed, which leads to the diminishing returns observed. Therefore, the counteracting balance between shear stress and residence time on MWCNT dispersion is observed at around 600 rpm in this study.

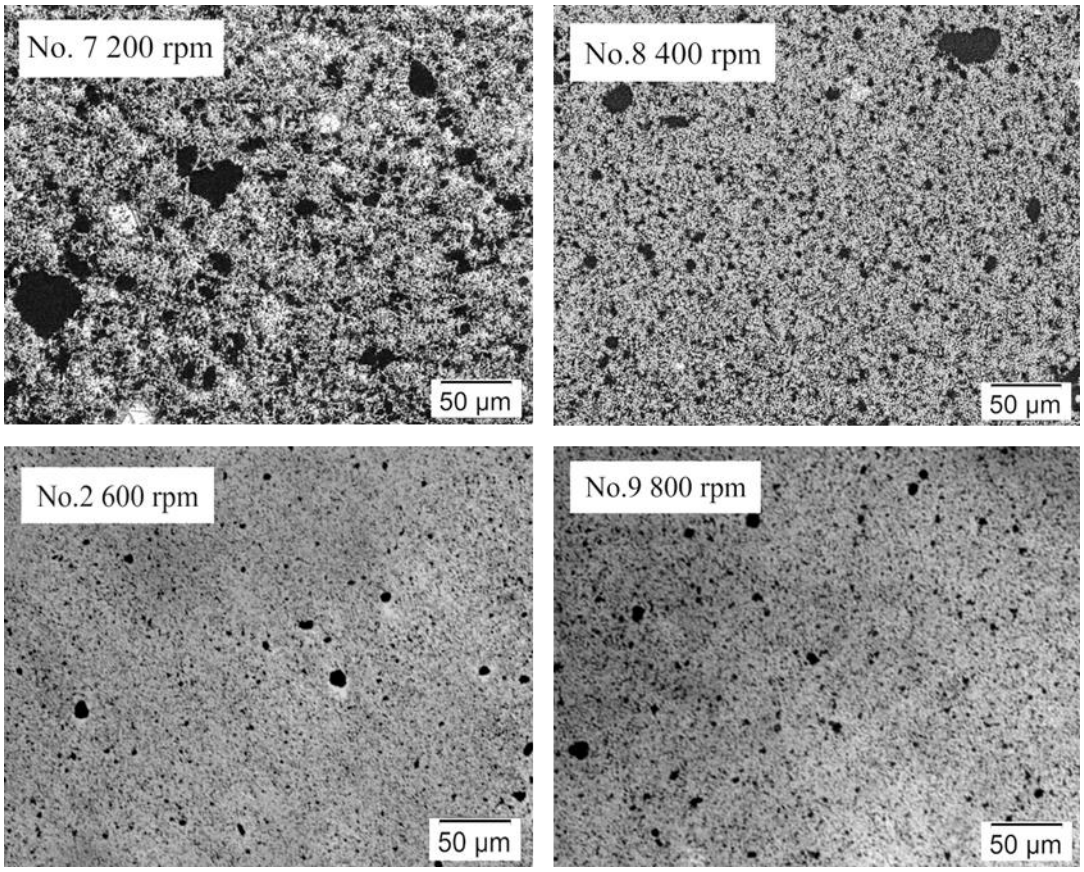

Figure 19. Optical images of TGDDM/MWCNT prepolymers at different screw speeds

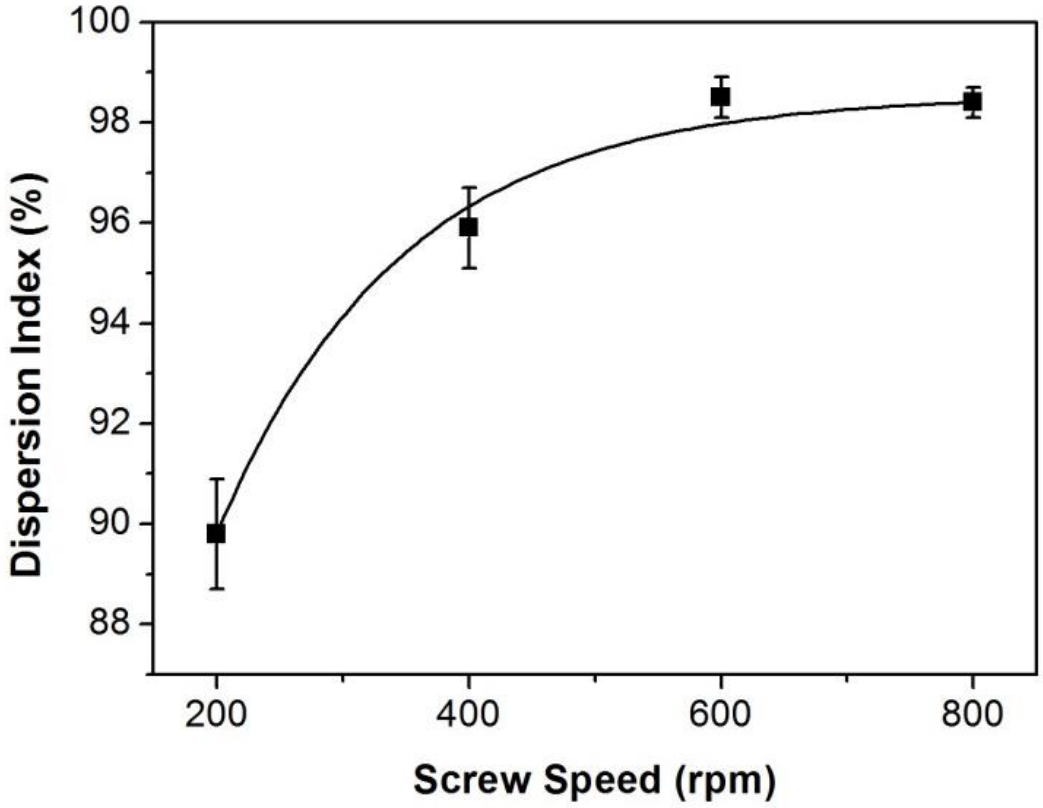

Figure 20. Dispersion indices of TGDDM/MWCNT prepolymers versus screw speed.

The dispersion of Baytubes allowed for the determination of TSE processing conditions that lend themselves most favorable to high quality dispersion of MWCNT in epoxy prepolymers. To better demonstrate the dispersive capacity of this method and better investigate the effect of impurities on the dispersion of the system, the authors would present to you the result of our highest performing processing conditions on dispersing high quality MWCNT where the effect of impurities could be compared directly. This was accomplished through the dispersion of two new types of MWCNT namely SMW200 and SMW210, which are produced by SouthWest Nanotechnologies and are identical in composition with the exception that the SMW200 tubes are the purified version of the 210 type absent of residual catalyst and other impurities.

Nanocomposites of these new tubes were prepared using the optimized conditions determined above, namely hot and cold zone temperatures of 180 °C and 60 °C respectively and a screw speed of 600 rpm. **Error! Reference source not found.** shows TEM images of 2.0wt% loaded composites demonstrating the sub-micron dispersion states realized in the presence and absence of molecular level impurities. The residual impurities, observed as dark black squared off particles, in the unpurified samples again appear to be the nucleus of all of the largest nanotube agglomerates. In contrast, neither the impurities nor the largest agglomerates were observed in the samples made with the purified nanotubes and therefore result in the highest dispersed state.

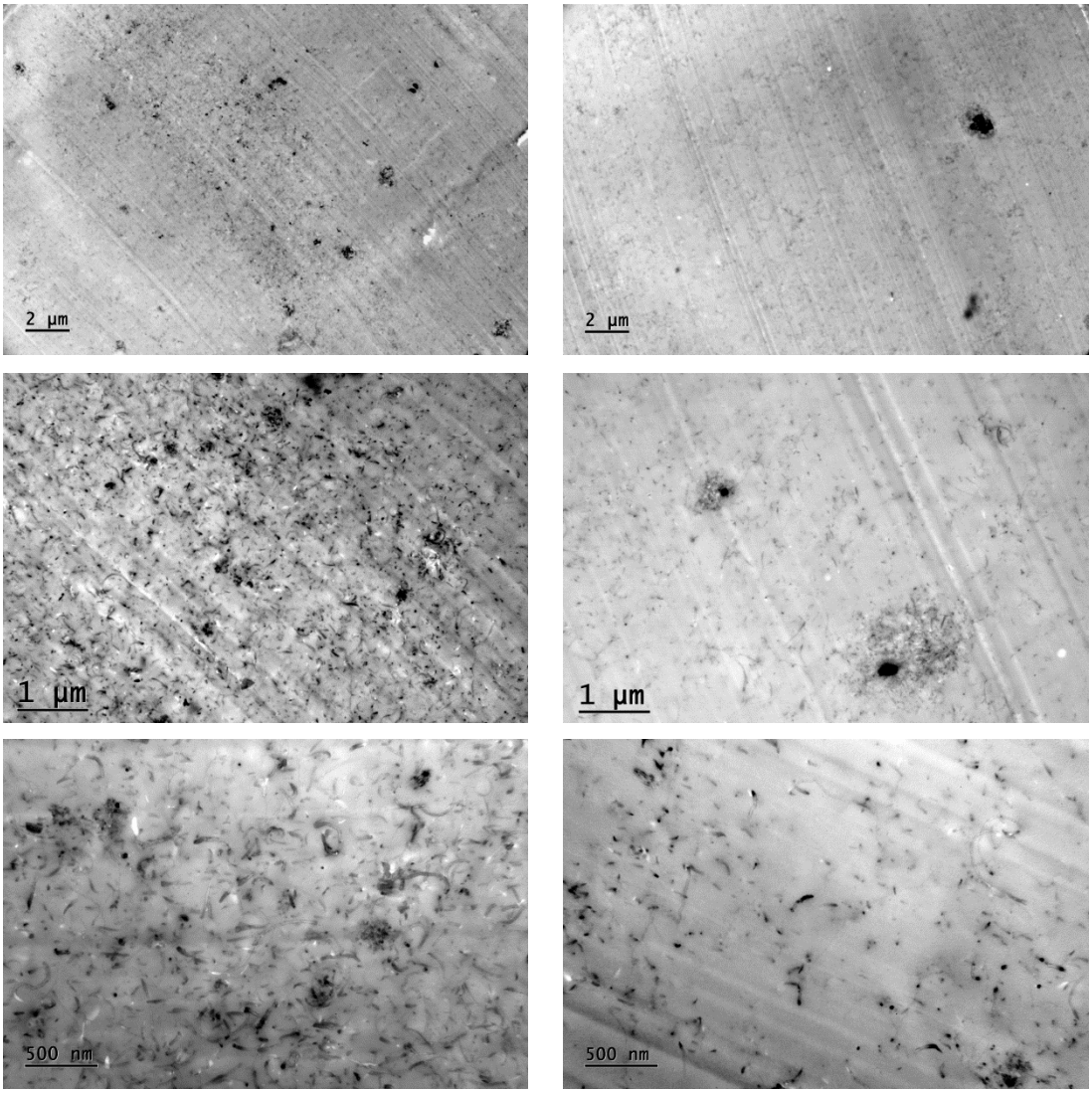

Figure 21. TEM images of composites containing 2.0 wt% SMW200 (purified - left column) and SMW210 (unpurified - right column).

For the present study, bulk material conductivity was used as an indirect metric to quantify dispersion state. **Error! Reference source not found.** illustrates the results of this comparison in which the conductivity of the composites formulated with SouthWest tubes are consistently one decade higher when compared above percolation threshold. We attribute this increase in bulk conductivity to the improved dispersion state brought on by the superior tube quality associated with the SouthWest tubes. For comparison sake, at

5.0 wt% loading the bulk conductivity of the Baytube sample was 0.06 S/cm compared to 0.35 S/cm for both the SMW200 and 210 samples. Although higher concentrations of tubes have not yet been investigated for the SouthWest tubes, the conductivity for Baytubes at 26wt% has been demonstrated as high as 0.84 S/cm and, providing the trend in comparative conductivities continues, it would be reasonable to expect SouthWest composites to approach the 5-10 S/cm range, which would be an exceptional result for this class of material.

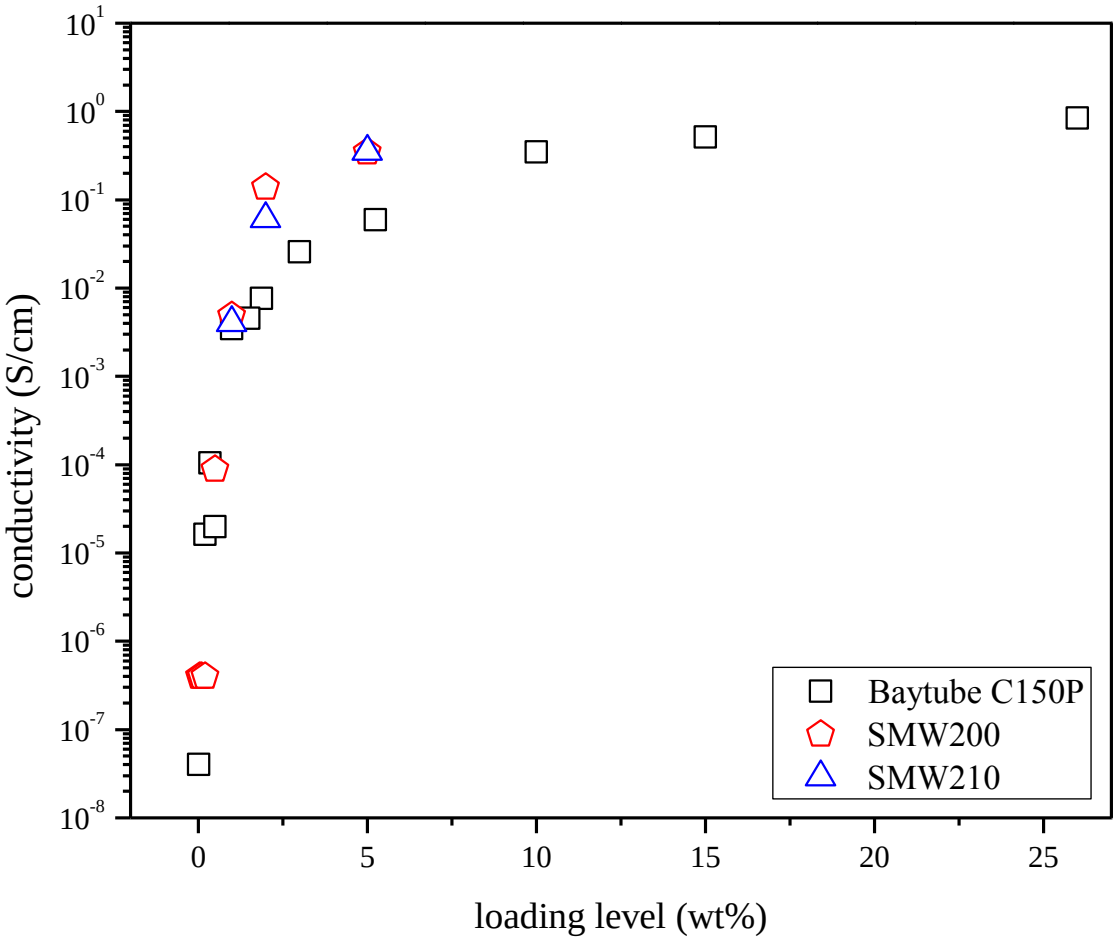

Figure 22. Four-point probe bulk conductivity measurements for cured MWCNT composites

Conclusion

TGDDM/MWCNT nanocomposite prepolymers were successfully prepared in a one-step high volume process using a continuous reactor method based on twin screw extrusion. The continuous reactor was modified to achieve two principle aims, the partial curing of epoxy at a high temperature to advance conversion, tack and room temperature viscosity, and the second for maximizing MWCNT dispersion and to aid in post processing stabilization of dispersion state through final cure.

Differential scanning calorimetry and rheological analyses provided information on the cure conversion, viscosities, and glass transition temperatures of the epoxy prepolymers and showed that the extent of B-staging can be controlled and targeted by hot zone temperature. Optical microscopy and transmission electron microscopy illustrated carbon nanotube dispersion obtained by this method can be greatly enhanced by increasing the processing viscosity and shear environment imposed on the nanotube agglomerates by decreasing the processing temperature within the cold zone. Additionally, the partially cured epoxy resin was found to help in stabilizing the nanotube dispersion by slowing the kinetics of secondary agglomeration during cure.

Beyond the differences in dispersion state observed between purified and un-purified tubes, as in the example of the SMW200 versus 210 tubes used here, it is important to note the dispersion differences between the SouthWest and the Baytube samples from above. Despite the on-paper similarities between the two brands of tubes relating to length, diameter, carbon content, *etc*. the dispersion state realized with the SouthWest tubes was found to be greatly improved when processed using identical conditions. This is an important note to consider when weighing methods of dispersion.

For one reason or another, not all nanotubes are created equal. This makes direct comparison of dispersion methods, for example calendaring or sonication to the TSE method proposed in the present work, difficult unless identical nanotubes have been used.

The significance of this work is the demonstration of a simple method to prepare epoxy/MWCNT prepolymers in large volumes using a continuous process. The expansion of continuous reactors in this field would lead to new avenues for mixing and blending of a broad array of co-reactants, blends, and nanoparticles. This advancement could be afforded, first off due to the benefits of increased production scale which provides economic feasibility to the process, and second due to the advantages associated with modular reactor designs which allow for increased control over matrix viscosity profiles and the ability to impose high yet controlled shear environments as a dispersive measure on otherwise onerously dispersed media.

CHAPTER IV – CURE PATH DEPENDENCE

Introduction

The tendency for nanotubes to agglomerate due to a drop in matrix viscosity, especially during cure, is widely acknowledged and well reported.[47, 91-93] Controlling agglomeration is considered one of the biggest challenges facing CNT nanocomposites today.[48] The experimentally observed property enhancements attributed to the incorporation of CNT reinforcement depend heavily on the aggregation state of the nanotubes. The process of CNT agglomeration and end material properties share a complex relationship.[94] For example, certain nanotube agglomeration states enhance the development of an electrically percolated network. [49] When maximization of electrical properties is desired, it is ideal to have an interconnected network of nanotubes which act to limit the extent of contact of the conductive pathway with the high resistance matrix. Consequently, agglomeration, or better stated, certain agglomeration states within a polymer matrix often leads to enhanced electrical properties as loosely packed secondary agglomerates formed out of well-dispersed materials develop into three dimensional conductive networks of nanotube bundles within the matrix.[49, 95] This agglomeration process, although favorable for gains in electronic properties, may be undesirable when mechanical properties are the aim. Large CNT agglomerates tend to act as stress concentrators rather than nano-scale reinforcement leaving the cured network with diminished material properties.[57, 82-84] For many CNT-modified epoxies strength and stiffness reach a maximum around 1 wt% CNT, with increased loadings abating these benefits as nanotube aggregates begin to dominate material properties.[40, 44]

Agglomerate morphology is often overlooked or goes unreported in literature. Uncommented on disparity between experiments in this specific attribute may hold the justification for why both improvements and degradation of mechanical properties in CNT filled nanocomposites have been reported. When dealing with nanocomposites it is important to consider that material properties depend not only upon the type and quality of reinforcement used, but also the size and morphology of agglomerates within the network, which is influenced by processing route. Within comparison of a single type and brand of nanotubes dispersion size-scale along with agglomerate morphology strongly influence bulk material properties.

It has been shown that agglomerate size and morphology can be manipulated by processing conditions in thermoplastic materials, specifically by adjusting shear conditions or annealing temperature.[49-52] In fact, conductivity gains approaching four orders of magnitude were reported by Alig and co-workers, within a single sample, as a percolated network type agglomerate morphology was developed upon annealing well above the melting temperature in a polypropylene/MWCNT composite.[50] Schueler and co-workers extended this work and observed they could control agglomerate morphology in a carbon black/epoxy composite by applying shear forces through mechanical stirring or through increasing the matrix ionic strength by the addition of copper chloride.[53, 54] In these cases the state of dispersion morphology was being investigated specifically emphasizing its roll with conductivity within the composite material.

Prior work within our group has established the relationship between epoxy network architecture, which develops and can be controlled through the manipulation of cure conditions, and chemical structure of the epoxy and amine chemistries.[96] Within the

current work we investigate the use of cure to drive CNT agglomerates, in a pre-gelation B-staged epoxy, to distinct morphologies in the vitrified state. Although the influence of agglomerate morphology on electrical properties is better understood, it is still unclear what may be the effect on mechanical and thermal properties. Understanding the role of agglomerate morphology with respect to these attributes will aid the scientific community in further development of multifunctional materials with truly exemplary properties. To understand which agglomerate morphologies correlate favorably and directly with certain physical, chemical, thermal, and electrical properties, we must first have an adequate understanding and method for targeting controlled dispersion states and agglomerate morphologies within these materials. The level of control over cured agglomerate morphology presented in this work will help to gain a fundamental understanding of CNT spatial contributions to nanocomposite performance. The result of this work will allow for the development of more optimized cure prescriptions to target specific agglomerate morphologies and therefore tailored properties.

Results and Discussion

Error! Reference source not found. depicts the viscosity evolution of aliquots of two identical nano-composite prepolymer material prepared with 0.2 wt% Baytubes cured using two selected thermal profiles. The 1S cure was designed to mimic a thermal cure profile common in industry for high T_g epoxies, such as the one used in this study. Viscosity of the 1S sample evolves as a parabolic well brought on first by rising temperatures and then by chemical gelation, which is common to crosslinking epoxies. The 2S thermal prescription was designed specifically to limit the drop in viscosity prior to gelation seen in the 1S method. Aliquots cured by this 2S thermal prescription

exhibited a constant increase in viscosity through to the point of chemical gelation. This stark difference in viscosity profile is important, as it is within the low viscosity "well" that nanotubes are known have the highest mobility and secondary agglomeration is accelerated. Previous work within our group has shown that, specifically in the 1S samples, during the ramp to cure, the drop in viscosity facilitates agglomeration of tubes until a percolated network of nanotubes forms. Analogous to a "log jam", this network morphology can cause a physical gelation that temporarily locks the morphology in place and arrests agglomeration. This physical gelation will either hold until chemical gelation ceases any further movement or be broken up by increasing matrix flow, which is a result of increasing thermal energy and a continued drop in matrix viscosity resulting in a second onset of macro-scale secondary agglomeration. For the 1S cure nanocomposite samples showcased in this study, agglomeration remained arrested in the network type morphology. This statement was supported and verified by a video taken of agglomeration within the matrix, collected during cure. It should be noted that differential scanning calorimetry (DSC), although not shown, was used to verify the one and two stage cures developed equivalent conversions within the matrix crosslinking reaction to remove this as a possible justification of any differences in material properties observed.

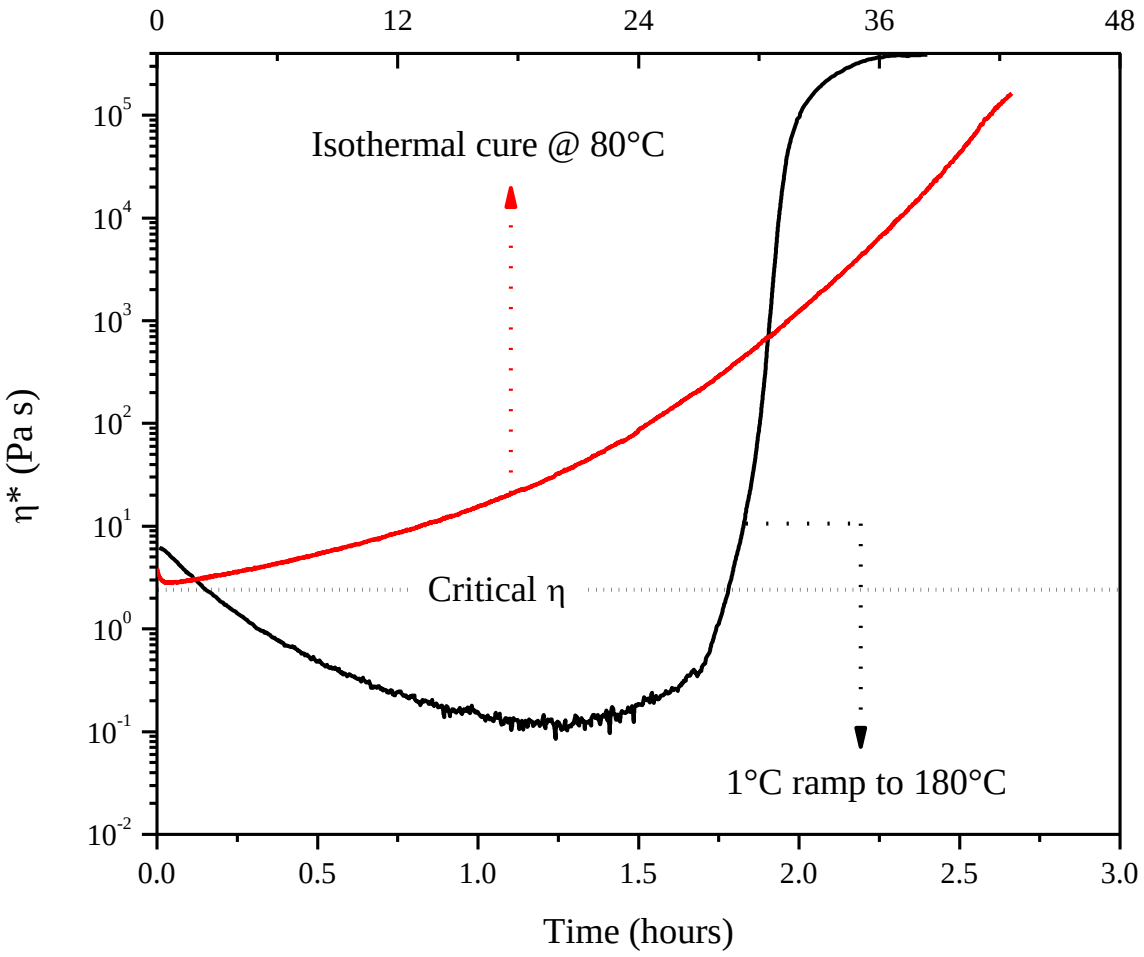

Figure 23. Viscosity evolution of 0.2 wt% Baytubes in 44-TGDDM pre-polymer cured using 1S (bottom range) and 2S (top range) temperature profiles.

Dispersion at the micro scale is often used as a representation of the overall dispersion state of a material. We chose to track the effect on agglomeration within these two cure prescriptions using optical microscopy, specifically because the overall sample size was much larger than the average nanotube agglomerate size. Because of this, it was possible to evaluate the development of agglomerate size and morphology developing during cure. **Error! Reference source not found.** shows OM images taken of 0.2 wt% Baytube loaded samples before and after cure of both 1S and 2S samples demonstrating their nanotube agglomerate morphologies. Although a wide range in MWCNT loading

level materials were prepared, for OM observation the 0.2 wt% loaded samples specifically were chosen for their more favorable optical clarity compared to higher loaded samples. Above 0.2 wt% loading, increasing nanotube concentration made resolution of individual agglomerates difficult, confounding observation or remarks on agglomerate size or morphology. These agglomerate size and morphology changes were tracked throughout cure as a time lapse capturing the entire agglomeration development. However due to the limitations of presenting this result in a paper, before and after cure images, in **Error! Reference source not found.**, were chosen to highlight the mentioned cure effect. The nanotube agglomerates in the 2S sample remained essentially stationary throughout cure, while the 1S sample developed a nanotube agglomerate morphology resembling a nanowire network. This percolated network type morphology has been reported by Alig, Yourdkhani, Martin, *etc.* in various systems, but not necessarily commented on.[91, 97, 98] In these cases demonstration of a controlled method for dictating morphology state in cured thermoset matrices was absent. Also unreported was a means to leave a maximally dispersed morphology state intact, as observed in the 2S samples of this study. To our knowledge the ability to adjust dispersion morphologies in the cured nanocomposites from aliquots of a single composition has never been reported and is a novel contribution to the field.

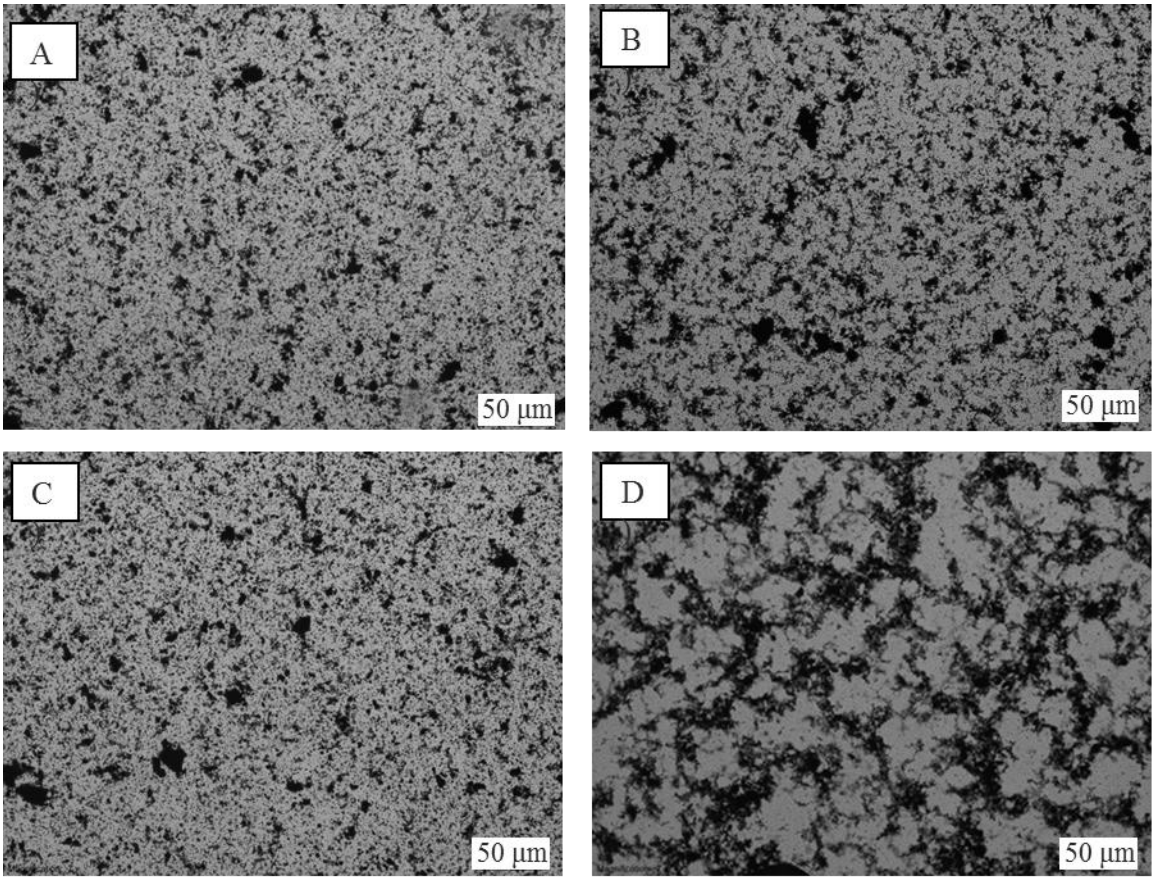

Figure 24. OM images showing nanotube dispersion states before and after cure for 2S and 1S samples, A and B and C and D respectfully.

Error! Reference source not found. presents the in-plane DC conductivity of samples cured under the two prescribed cure conditions and MWCNT contents ranging from 0.02 to 15 wt%. The 2S samples exhibited conductivities consistently an order of magnitude lower than the 1S samples at concentrations above percolation threshold. Also, the onset of percolation was shifted from 0.5 wt% to 0.1 wt% nanotubes when comparing the 2S to the 1S prescription which indicates the formation of a conductive network much sooner in the 1S samples. The decade shift in conductivity observed between the two cure cycles would suggest a more extensive or perfect percolated network structure being formed within the 1S cured samples, which is supported by OM

and consistent with findings of increased conductivity with increasing agglomeration observed by dielectric spectroscopy in polycarbonate/CNT blends. [56] It is also interesting to note that the trend of conductivity between the two cure protocols appears to be converging at high loading levels. This result agrees with the comparative degree of agglomeration reported by Rosca and coworkers and is rationalized by a viscosity argument.[99] At low loading levels the material viscosity is a matrix driven property and therefore temperature dependent. However, at high loading levels material viscosity becomes increasingly dependent on the dispersion state of the nanotubes and therefore less temperature dependence. This in turn leads to a lower mobility of nanotubes limiting the driving force behind gains in electrical conductivity.

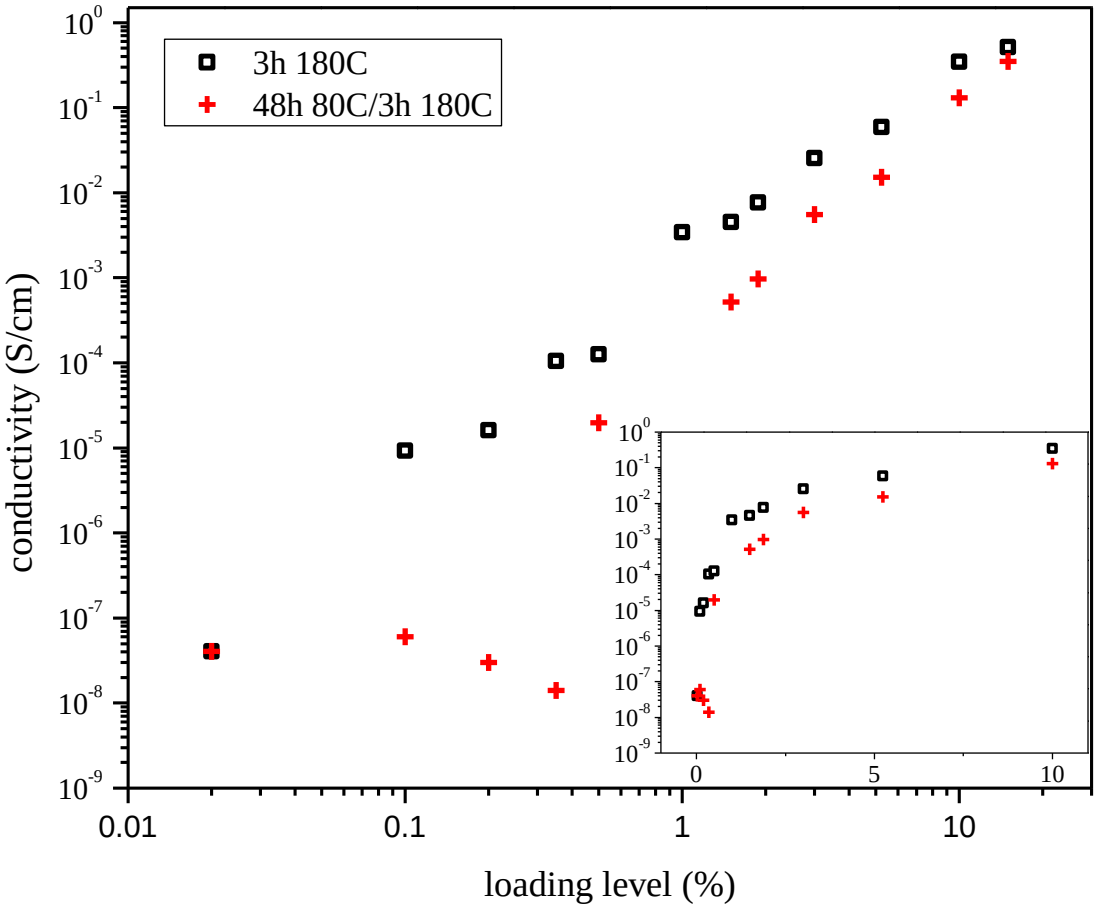

Figure 25. Four point probe conductivity measurements comparing single stage, 1S, samples with dual stage, 2S, nanocomposite samples

TEM images of 2S and 1S cured samples are presented in **Error! Reference source not found.** and are representative and consistent with all areas of these samples imaged and show typical agglomerate sizes observed at the sub-micron level. Similar to the trends observed in OM, altering the cure prescription appears to result in distinguishing agglomerate content and size-scale across all loading levels. The qualitative differences in the spacial arrangement of nanotubes favors the theory that agglomeration during cure is driven by viscosity which leads to the decade shift in bulk conductivity. At the highest loaded levels, namely the 5 and 10 wt%, samples begin to

appear nearly analogus which agrees with the trends observed in the bulk conductivity measurements previously discused.

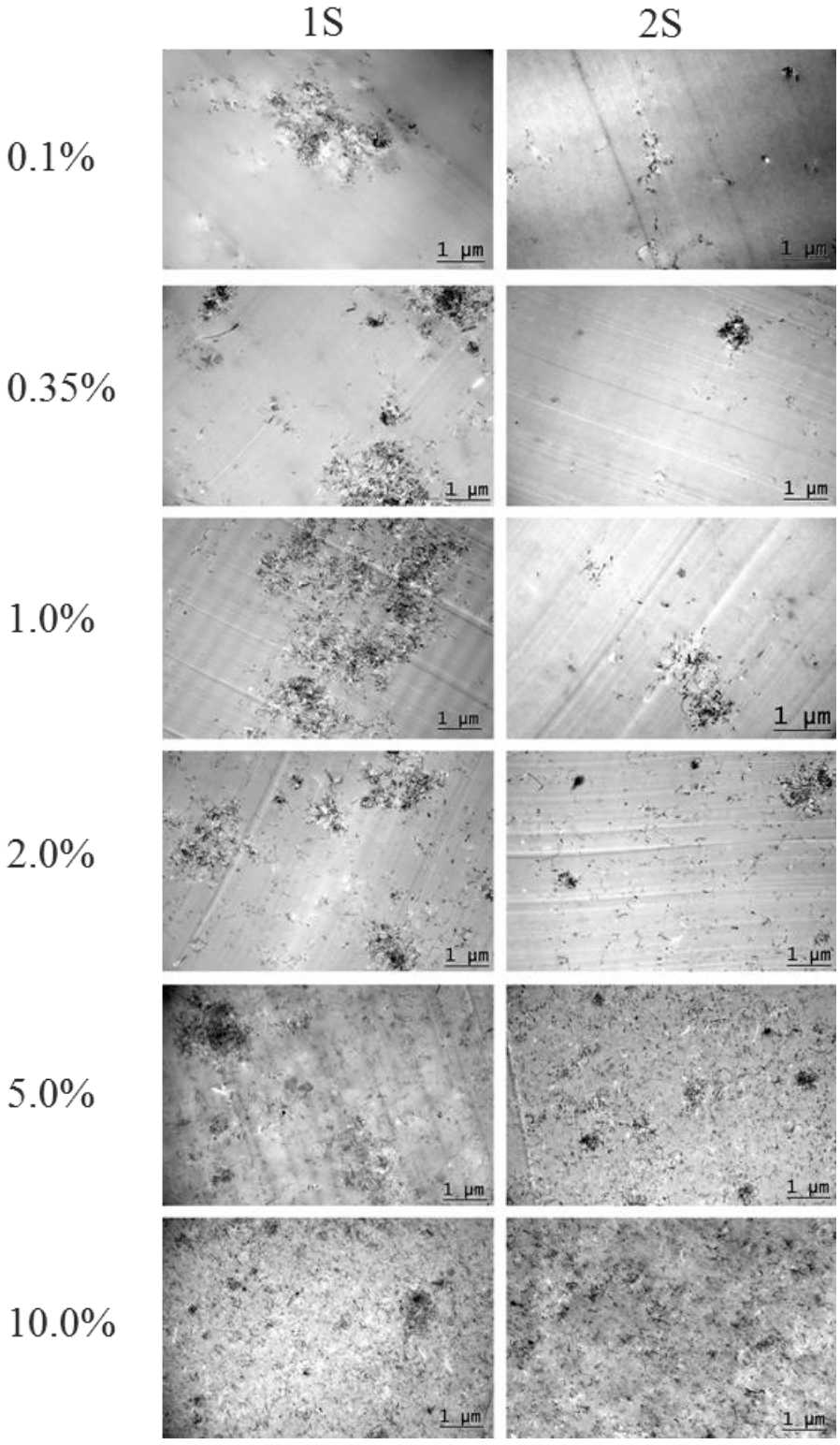

Figure 26. TEM images showing nanotube dispersion after cure for 2S and 1S samples at nanotube loadings between 0.1 and 10.0 wt%

Conclusion

The performance of nanotube reinforced structures is heavily dependent on agglomeration state and morphology. The effect, particularly of the agglomerate morphology and the role it plays, on the development and final properties of nanocomposites has remained unreported. The reason for this can be explained by two main issues; 1) The particular state of agglomerate morphology is seldom commented on in literature, and 2) a simple method for driving MWCNT nanocomposites to deliberate morphologies to use as a direct comparison has remained absent. We demonstrated a method for controlling nanotube secondary agglomerate morphology through the adjustment of cure prescription in an epoxy nanocomposite. We showcased two cure prescriptions for our system. One protocol is a single-step high temperature cure that favors nanotube agglomeration, and the second progresses reaction to gelation at a low temperature and maintains the "as processed" dispersion state through cure. The high temperature cure promoted the formation of a network of nanowire agglomerates during the parabolic well in matrix viscosity, which occurs during the ramp to elevated temperature prior to gelation. This type of morphology is attributed to the decade increase in conductivity and a decrease in percolation threshold observed when compared to identical samples cured in a way to maintain agglomerate size and morphology state.

Using the low temperature, 2S, cure protocol we were able to demonstrate the ability to arrest nanotube movement and maintain an as dispersed agglomerate state. This result has otherwise presented a significant challenge within the field of thermosetting nanocomposites. A dispersed cured morphology is detrimental to bulk electrical properties. However, a nanocomposite maintaining a higher dispersion state could

contribute positively to other material attributes such as mechanical or possibly thermal properties yet to be investigated.

In conclusion, the combined rheological and conductivity measurements coupled with OM and TEM imaging provide a new experimental protocol for driving agglomerations to intentional morphologies which will aid a better understanding of the role of agglomerate morphology on material properties in thermosetting matrices. This methodical approach to controlling secondary agglomeration through matrix viscosity can be extended to other nanofillers in thermosetting polymers as well. Work still remains to determine the effect of agglomerate morphology on other material properties of importance to applications in which carbon nanocomposites are used, namely mechanical and thermal in nature. For a more complete understanding of agglomerate development, it would be beneficial to track agglomerate evolution at the sub-micron length-scale throughout the curing process and conclude if the same trends in reagglomeration are apparent with what is observed at the upper micron scale. A fundamental understanding of these processes is key for the development of nanocomposites and future multifunctional materials.

CHAPTER V – AGGLOMERATION MONITORING

Introduction

The findings discussed in Chapter IV relating to the relationship between conductivity and agglomeration observed at length-scales relevant to OM made us interested in finding a method to further monitor the through-space relationships between nanotubes at decreasing length-scales as well as track the rate of conductivity building during cure.

AFM has proven sufficient to observe individual nanotubes both before and after cure for these materials. **Error! Reference source not found.** is a good example of this showing individual nanotubes in a 10 wt% cured 44DDS/TGDDM nanocomposite material. Height and phase representations of this material correlate well. Conductivity mapping, obtained using a C-AFM tip, shows aggregates that correspond to higher area on corresponding height images and is illustrated in **Error! Reference source not found.**. Smaller scans show that the aggregates appearing as large in wide scans are actually composed of many smaller conductive agglomerates. In all cases conductive areas still appear in the higher areas of the height image.

Once convinced that the current images correlated well with the height and phase images C-AFM was used to collect before and after cure images for many of the nanocomposite loaded samples. The results of the 10 and 15 wt% loaded samples are illustrated in **Error! Reference source not found.**. In these images the lighter the color the more conductive the local environment. It is interesting that, for all loading levels, the uncured material is essentially a non-conductive material. Upon cure by either protocol the conductivity is augmented by orders of magnitude. At length-scales observable by

OM for these materials agglomeration is essentially frozen out using the 2S protocol yet at the sub-micron length-scale CNT mobility still appears to be contributing. This result solidified the need for a method of agglomeration monitoring analogous to the hot stage OM method, described in the earlier chapters of this document, but at much shorter length-scales.

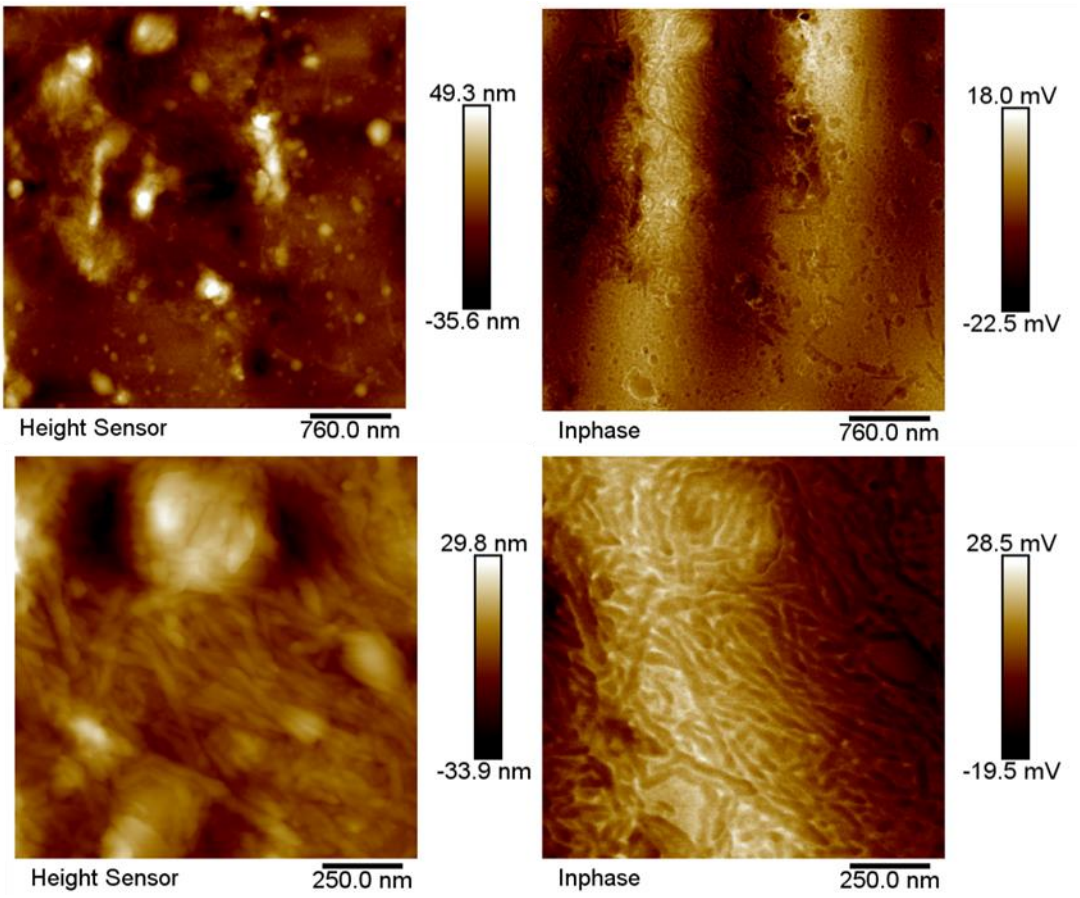

Figure 27. AFM height and phase images collected in tapping mode showing individual nanotubes in 10 wt% cured 44DDS/TGDDM nanocomposite

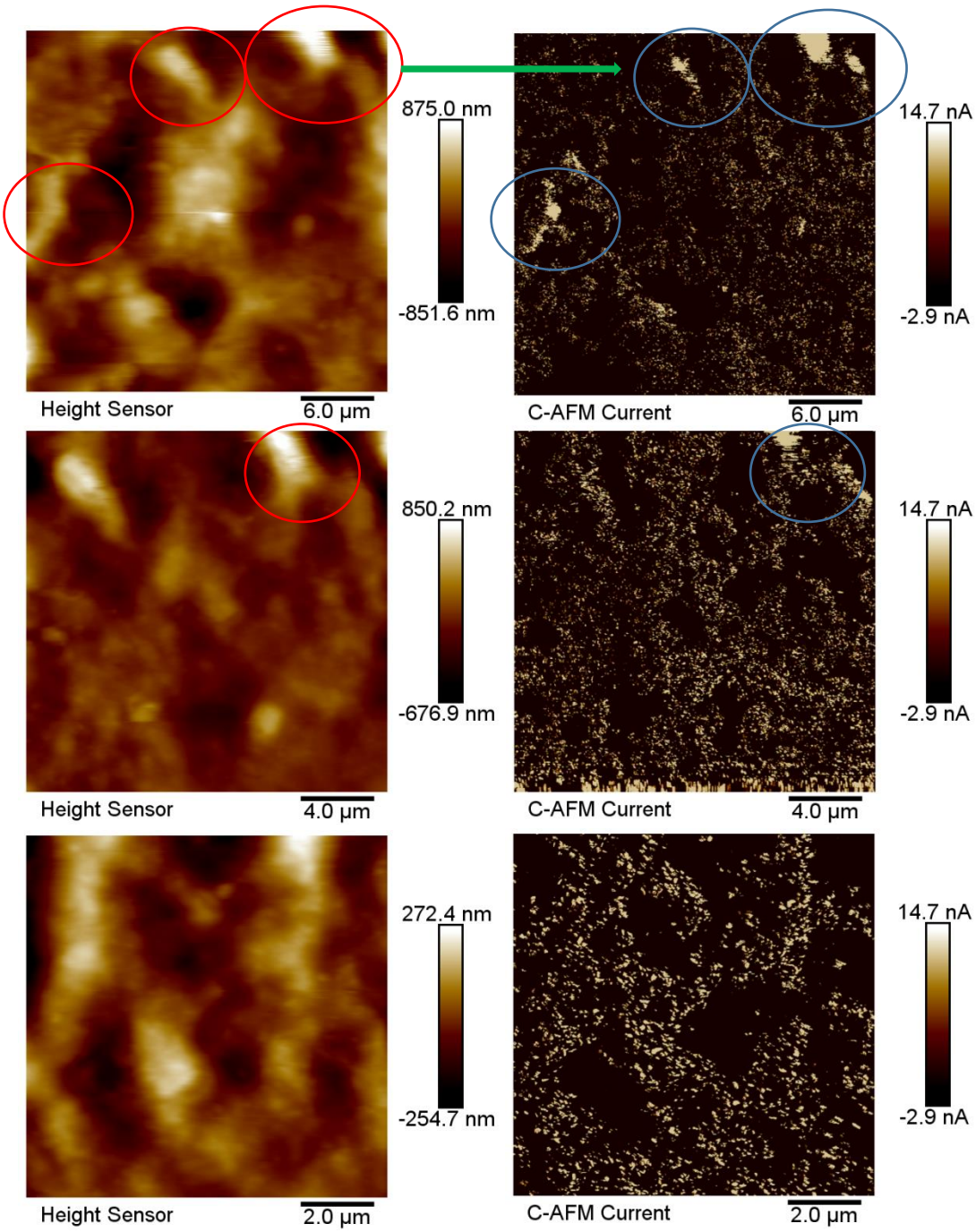

Figure 28. C-AFM height and current images collected in tapping mode for 10 wt% cured 44-DDS/TGDDM nanocomposite

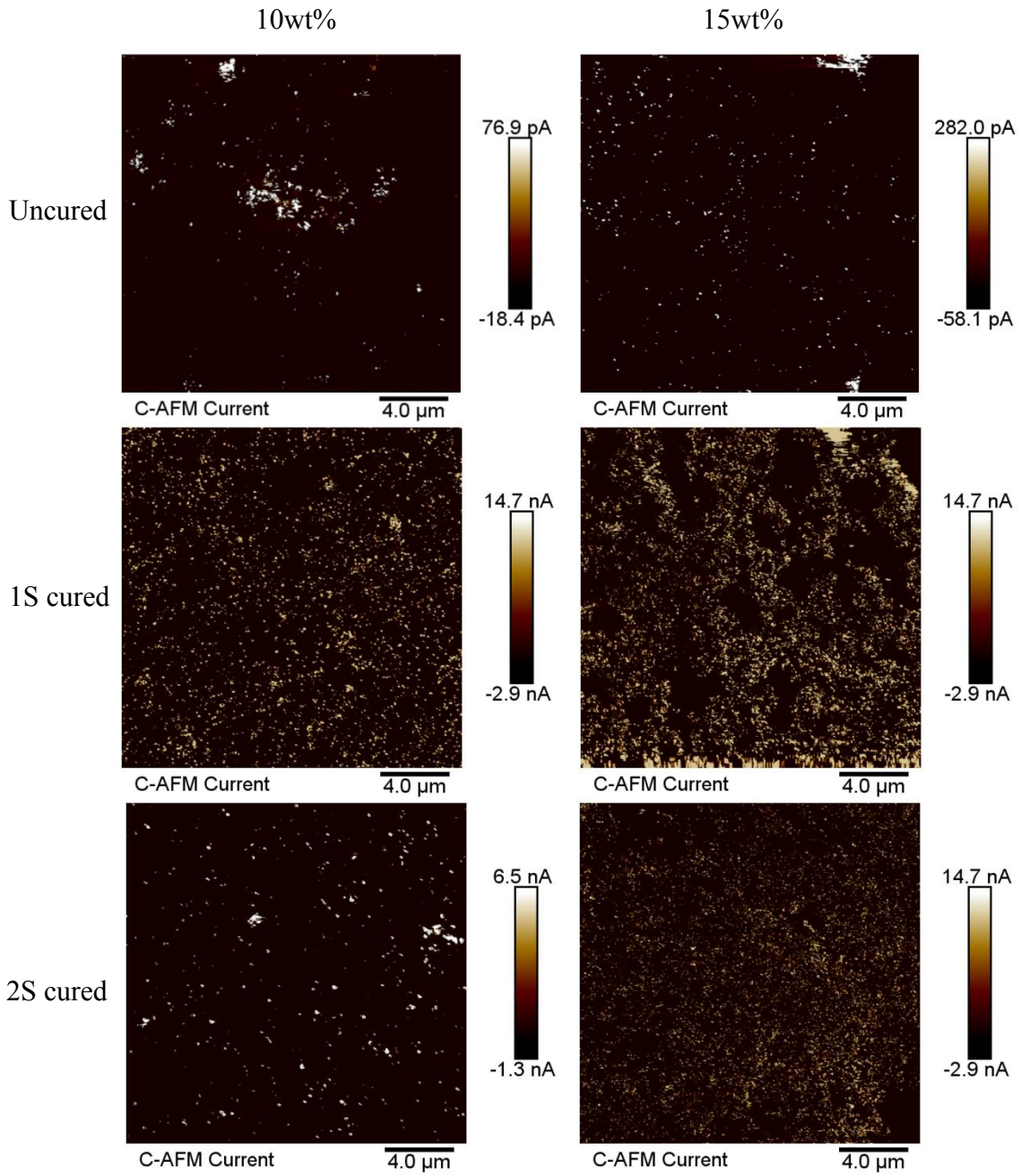

Figure 29. C-AFM images for 10 and 15 wt% nanotube loaded composite materials showing before and after cure for both the 1S and 2S prescriptions

Percolation threshold and conductivity growth can be easily tracked using BDS. Conductivity measurements were taken every 25 ˚C from 25-175 ˚C through the ramp portion of the cure and then every 20 minutes during the three hour isothermal soak at 180

˚C for the 1S samples with the only difference for the 2S sample being a scan taken every five hours durring the 80 ˚C isothermal portion of the cure. The conductivity traces for the 0.2wt% sw200 tubes cured under the 1S prescription is shown in **Error! Reference source not found.**. In these traces a trend in data with slope approaching zero is charasteristic of overwhelming DC conductivity which indicates that percolation threshold has been reaced at that frequency. The height along the vertical axes of these these pateau areas indicate the magnitude of conductivity, with increasing values being more conductive. It is apparent in **Error! Reference source not found.** that as the cure progresses, there is not only an increse or building of conductivity occuring with cure, but also an increase in the frequency range at which the material has reached the precolation threshold.

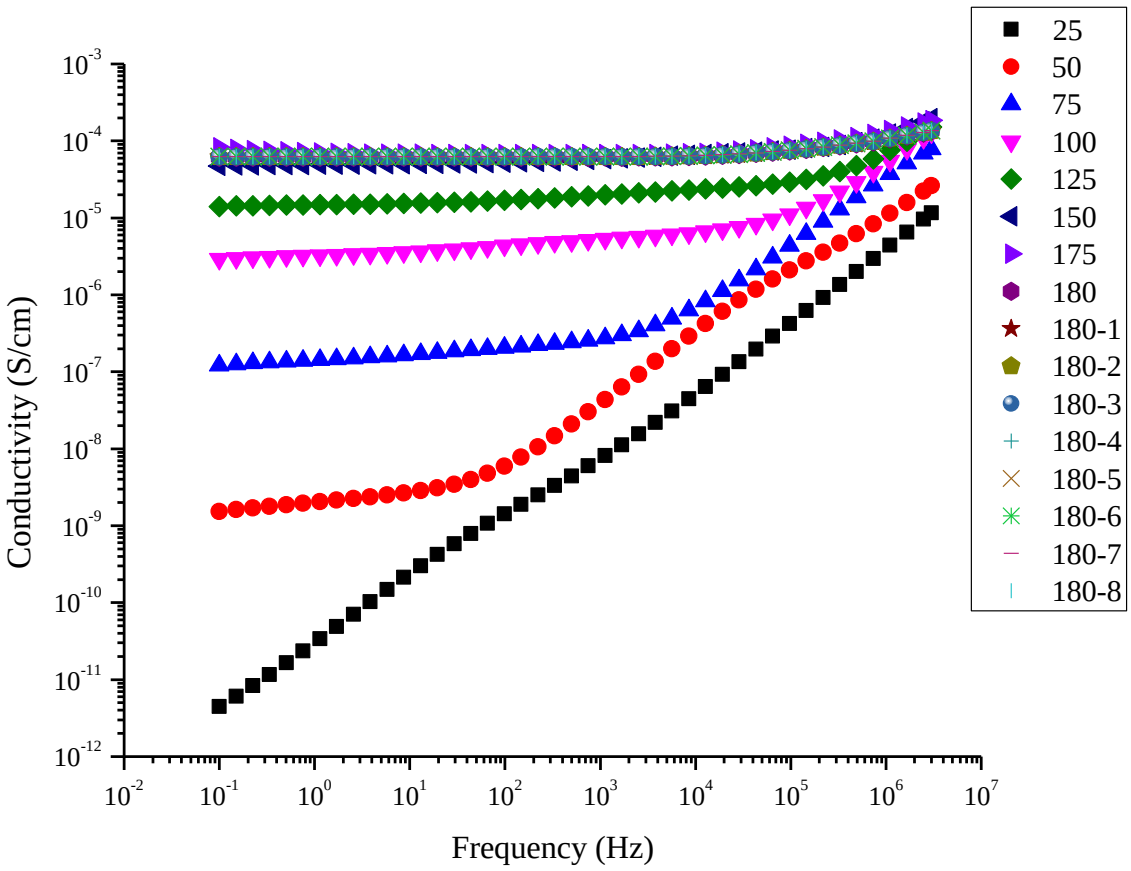

Figure 30. BDS in-situ cure conductivity trace for 0.2 wt% SW200 cured using 1S temperature profile

It has been shown elsewhere in literature that conductivity, specifically the DC conductivity measured through BDS, is temperature dependent. So in order to obtain meaningful results from the raw conductivity data, illustrated in **Error! Reference source not found.**, in a manner so that it is not confounded by differences in acquisition temperature, results were normalized to a standard curve which was constructed from an additional temperature sweep of the cured material. Conductivity was determined from 20-180 ˚C at incriments of 20 ˚C on the fully cured sample. These sweeps are illustrated in **Error! Reference source not found.**. A standard curve for the 1S sample was constructed by plotting temperature versus the conductivity throughout the temperature

sweep. Conductivity values were chosen as the height of the plateau region along the frequency versus conductivity plot. This standard curve can be found in **Error! Reference source not found.** along with the regression line that fit to an R^2 value of 0.99.

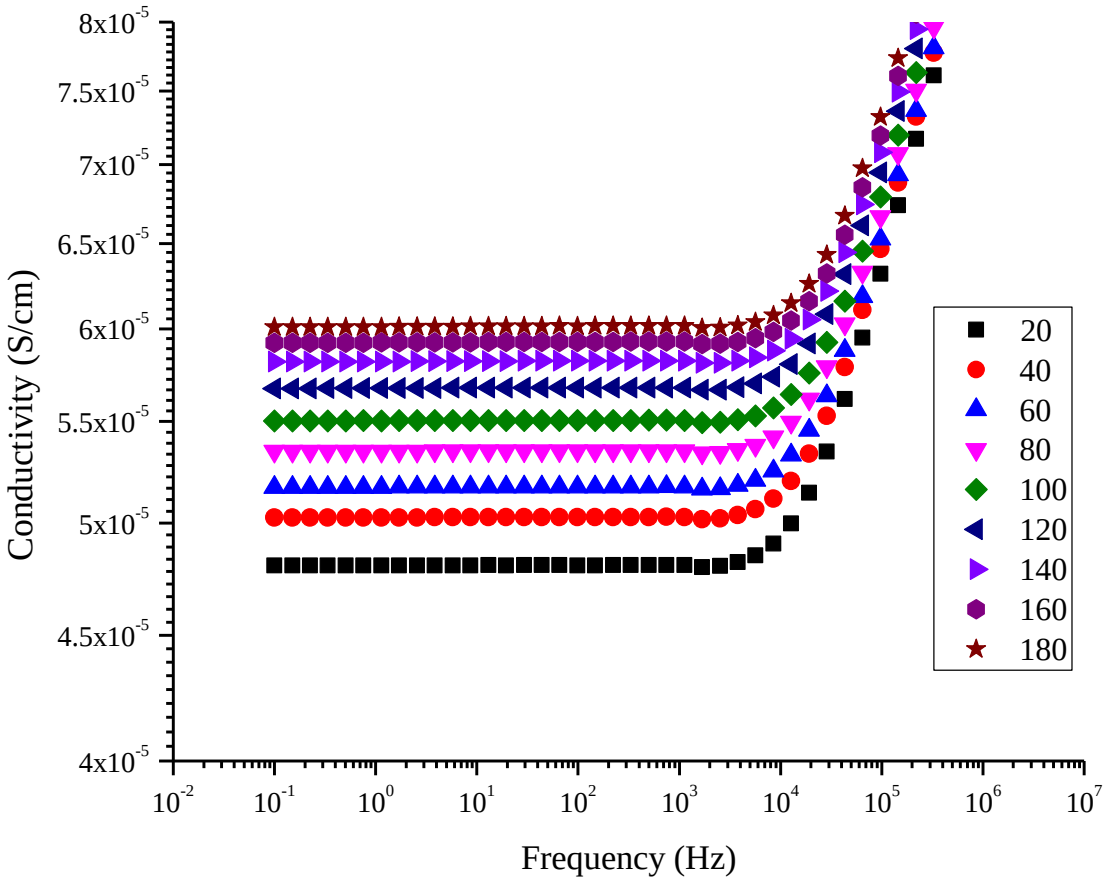

Figure 31. BDS post-cure temperature dependence sweep

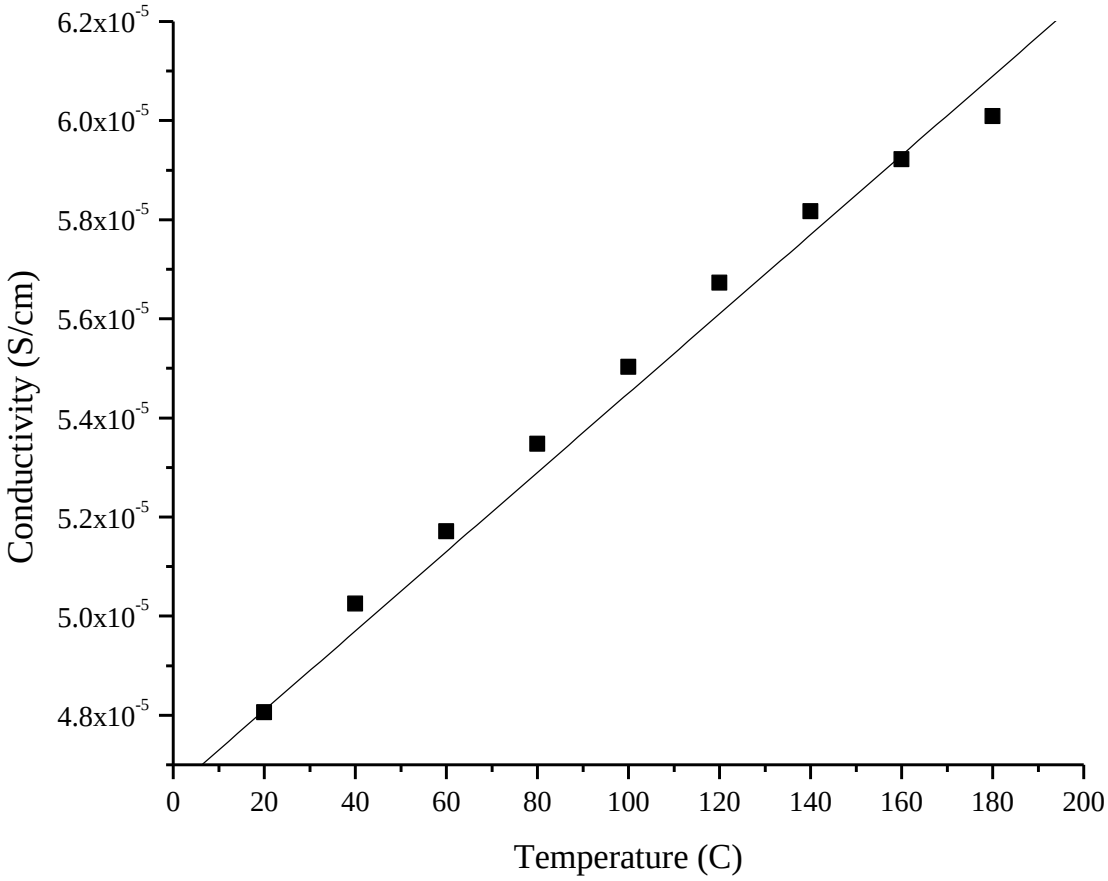

Figure 32. BDS temperature dependence standard curve

Error! Reference source not found. plots the conductivity of the plateau region of each temperature recorded durring the 1S and normalizes them to the regression line fit from **Error! Reference source not found.**. along with a line to remind the reader of the thermal environment at each particular point along the cure. There is a sharp rise in conductivity at ~2 hours into the ramp which correlates to approximately 100 ˚C. Conductivity peaks at 175 ˚C with a fall in conductivity beginning immediately upon entering the three hour soak at 180 ˚C. We attribute this drop in conductivity to the reaching of a vitrification point in the cure process where the materials' instintaneous T_g begins to excede the cure temperature.

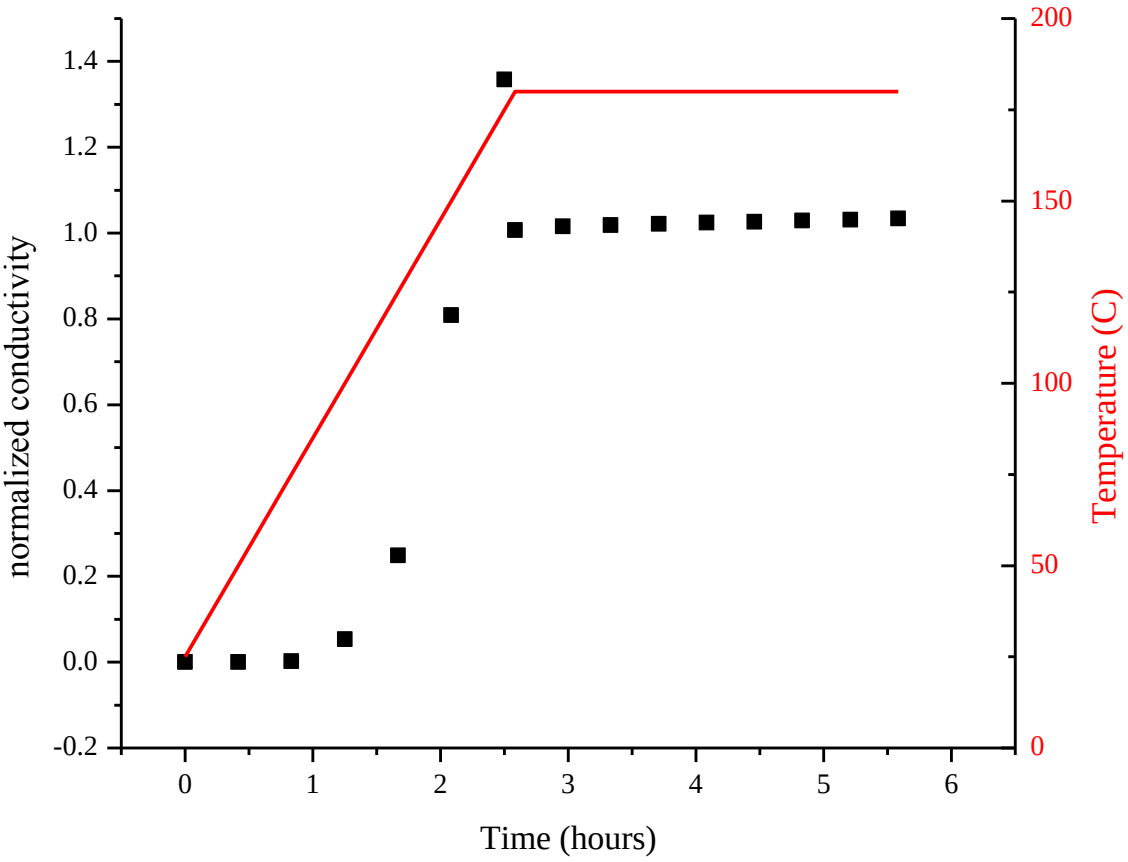

Figure 33. Normalized conductivity and cure profile for 0.2 wt% SW200 cured with 1S temperature profile

Since BDS had proved to be a sensitive and easy method for *in situ* conductivity monitoring our hypothesis was that it could be further utilized to track the threw-space relationships of mobile nanotubes agglomerating in curing matrix at the same length-scales observed previously using AFM. The following describes the investigation of a curing and agglomerating nanocomposite with respect to the Mauritz theory of disordered materials, the universal dynamic response, and how we hoped to use these theories to monitor this agglomeration.

Results and Discussion

Optical microscopic images of the nanocomposite morphology before (a) and after (b) cure are in **Error! Reference source not found.**. In these images the epoxy matrix is a light colored background while the MWCNT agglomerates are black. The before/after cure images illustrate the transition of morphology from that of small, dispersed bundles of tubes ranging in size from 50 μm to individually dispersed tubes (verified by TEM imaging), to a percolated network visible at the micron length-scale. This agglomeration is facilitated by a drop in matrix viscosity – which allows bundles to come in contact with each other - due to heating prior to gelation. Agglomerate morphology evolves in a continuous and progressive manner during cure. This percolated MWCNT network initially becomes apparent during the 1° C/min ramp between 25 and 50 ˚C, a process which can be observed with the OM with a hot stage which provides temperature control through cure. One can imagine conductive pathways along contacting MWCNT agglomerates that form throughout cure. This difference is most apparent in the images of 25 ˚C and 180 ˚C. The particular morphology observed in the cured state, apparent in the 180 ˚C image, is considered to be a network of MWCNT. It is this network formation that drives the increase in electrical conductivity observed as the emergence of a frequency independent conductivity plateau at 50 ˚C in the σ' vs. f plot and an extension of this plateau into higher and higher frequencies with increasing cure as illustrated in **Error! Reference source not found.**.

The curves show the same three distinct regimes that have been exhibited by other disordered conductive solids as depicted in **Error! Reference source not found.**: (1) a low frequency upturn at lower temperatures, (2) a plateau region, and (3) a ‘dispersion’

region at the highest tested frequencies. The frequency dependence of conductivity in the dispersion region for the epoxy-matrix nanocomposite, at various temperatures throughout cure, was compared against Equation 3.

There are frequency - independent plateau sections, **Error! Reference source not found.**, corresponding to a dc electrical conductivity, σ_{dc}, throughout cur.[100] The plateau region of σ′ vs. *f* curves widen with increasing temperature indicating increasing conductivity over a broad range of frequency. At higher frequencies there is a 'dispersion' region which might be interpreted as arising from a β relaxation within the polymer network as depicted in Figure 4.[101, 102] The β relaxation is assigned to local motions of dipoles, specifically the hydroxyl ether and amine functionalities formed during the crosslinking reaction.[103-105] This particular dispersion is most apparent in the σ′ and ε′′ traces of 25 and 75 ˚C in **Error! Reference source not found.** and **Error! Reference source not found.**.

This conductive behavior is in fact typical for disordered materials and is consistent with the Jonscher Universal Power law illustrated in Equation 3. Deviations in the data fittings to the low frequency end, in the σ′ vs. frequency spectra, might be attributed to sample/electrode interfacial polarization effects which are capacitive (current-limiting) in nature; this is a common artifact owing to the presence of ionic impurities, in dielectric spectra. [59-62, 101]. Traces of the NaOH catalyst used in the synthesis of TGDDM may contribute to conduction to some extent. [106] Sample/electrode interfacial polarization manifestation is more significant for temperatures up to 100 ˚C as the crosslinking reaction would be expected to be activated above 100 ˚C. Crosslinking would result in less segmental mobility which would restrict charge hopping causing, in

turn, a lower degree of fluctuating positive-negative charge polarization in the near-electrode regions.

The solid curves superimposed on σ′ vs. *f* data points are fits of Equation 3 using non-linear fitting Origin® software. These fits are rather good as indicated by high correlation coefficient (R^2) values listed in **Error! Reference source not found.**. Fitted σ_{dc}, *A*, and *n* values are listed in **Error! Reference source not found.**, as well. As cure progresses there is an increase in σ_{dc}. The parameter *n* decreases as conversion increases with temperature through cure. The general expectation in a non-dynamic (constant temperature) situation is that $n \rightarrow 1.0$ as $T \rightarrow 0$, but the complicating influence of evolving morphology must be factored in. The temperature dependence of *A* is not as well understood, but in the case of curing seen here, we observe it increasing directly with temperature and conversion.

Table 6

Parameters from fit of $\sigma'(\omega) = \sigma_{dc} + A\omega^n$ *to experimental data for 0.2 wt% nanotube loaded 44DDS-TGDDM nanocomposite during cure.*

Temperature	σ_{dc} [S/cm]	*n*	*A*	R^2
25˚C	4.46E-12	0.69	4.41E-15	0.946
50˚C	1.54E-09	0.60	1.89E-14	0.977
75˚C	2.28E-07	0.49	8.08E-12	0.973
100˚C	2.92E-06	0.32	1.76E-07	1.000
125˚C	1.41E-05	0.30	4.05E-07	0.999
150˚C	4.89E-05	0.27	7.19E-07	0.993
180˚C	6.14E-05	0.34	8.16E-08	0.978

As discussed in the Introduction, –log*A*/*n* is has been reported to be insensitive to material composition or structural transitions that occur on increase in temperature. For

the system reported here, –log*A*/*n* vs. temperature is seen in **Error! Reference source not found.** in which this ratio indeed remains essentially constant. This occurs despite the shifts in both *A* and *n* throughout the temperature ramp as seen in the inset of **Error! Reference source not found.**. The temperature ramp causes the material to go through a process of re-agglomeration starting as an array of largely disconnected small nanotube agglomerates seen in **Error! Reference source not found.**a and evolving to the percolated disordered network of tubes/bundles seen in **Error! Reference source not found.**b. This re-agglomeration process is well documented and is caused by a drop in viscosity during cure and more effective attractive forces between nanotubes.

If *n* were linked to particular details of the biphasic morphology there should be an obvious trend in it as influenced by phase morphology change. In particular, one would expect *n* to move closer to unity as the material exceeds a percolation threshold between 25 and 50 ˚C. However, *n* is seen to decrease with increase in temperature, excepting the value at 180° C.

The –log*A* vs. *n* plot in **Error! Reference source not found.** illustrates the direct tracking of these quantities, in that, the temperature evolution of log*A* is proportional to the temperature evolution of n. While a straight line ($R^2 = 0.9825$) has been fitted to the data points a sigmoidal curve might be considered but this would add another parameter which would complicate the analysis. Due to the fact that A and n show a linear correlation, agglomerate morphology would appear to be independent of trends or values of these two parameters. This result reinforces the idea that this response is likely just a general feature of the universal power law that is not linked to particular substructure or

changes within as stated by others.[71, 72] One obtains the same general relationship for a system that does not undergo structural evolution.

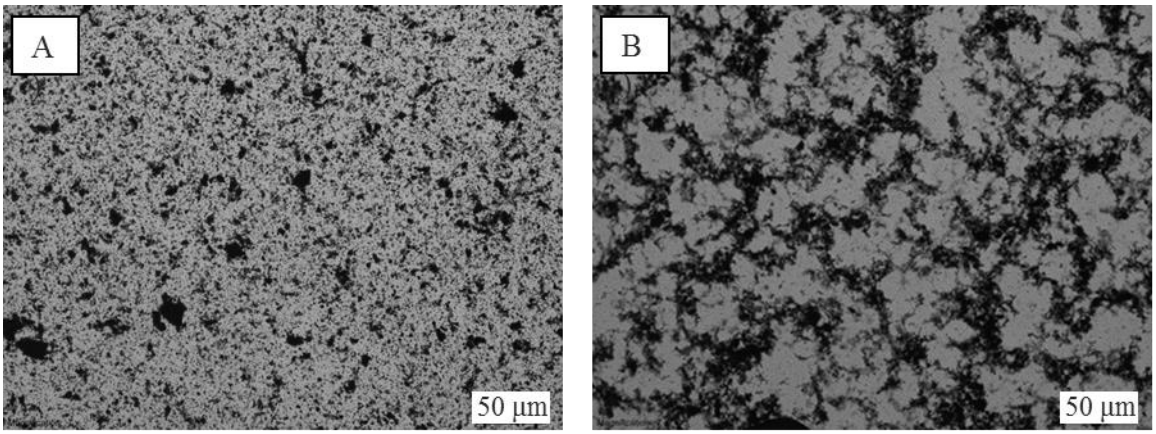

Figure 34. Optical microscope (OM) images illustrating nanotube dispersion states (a) before and (b) after cure for a 0.2 wt% 44DDS-TGDDM nanocomposite cured at 25-180 °C at 1 °C/min and 180 ˚C soak for 3 hrs.

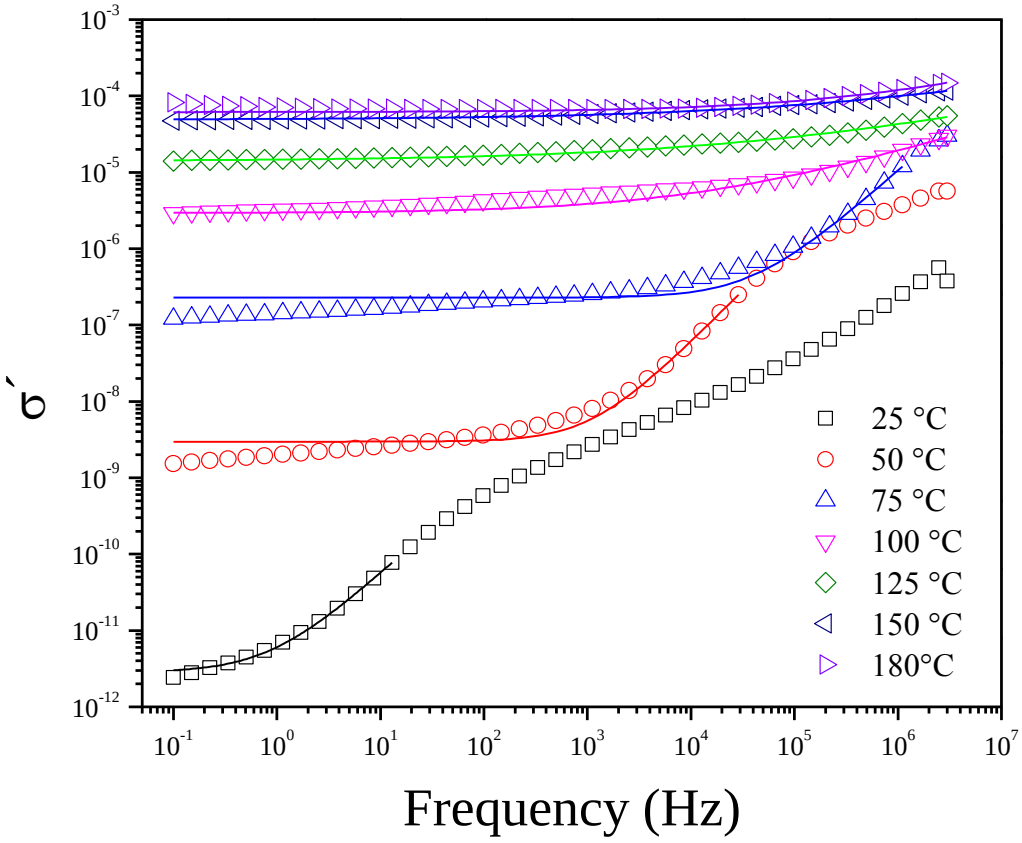

Figure 35. σ´, the real part of the complex conductivity (σ* = σ' +i σ"; i = √-1), vs. frequency through 1 °C/min ramp to 180 °C for nanocomposite epoxy.

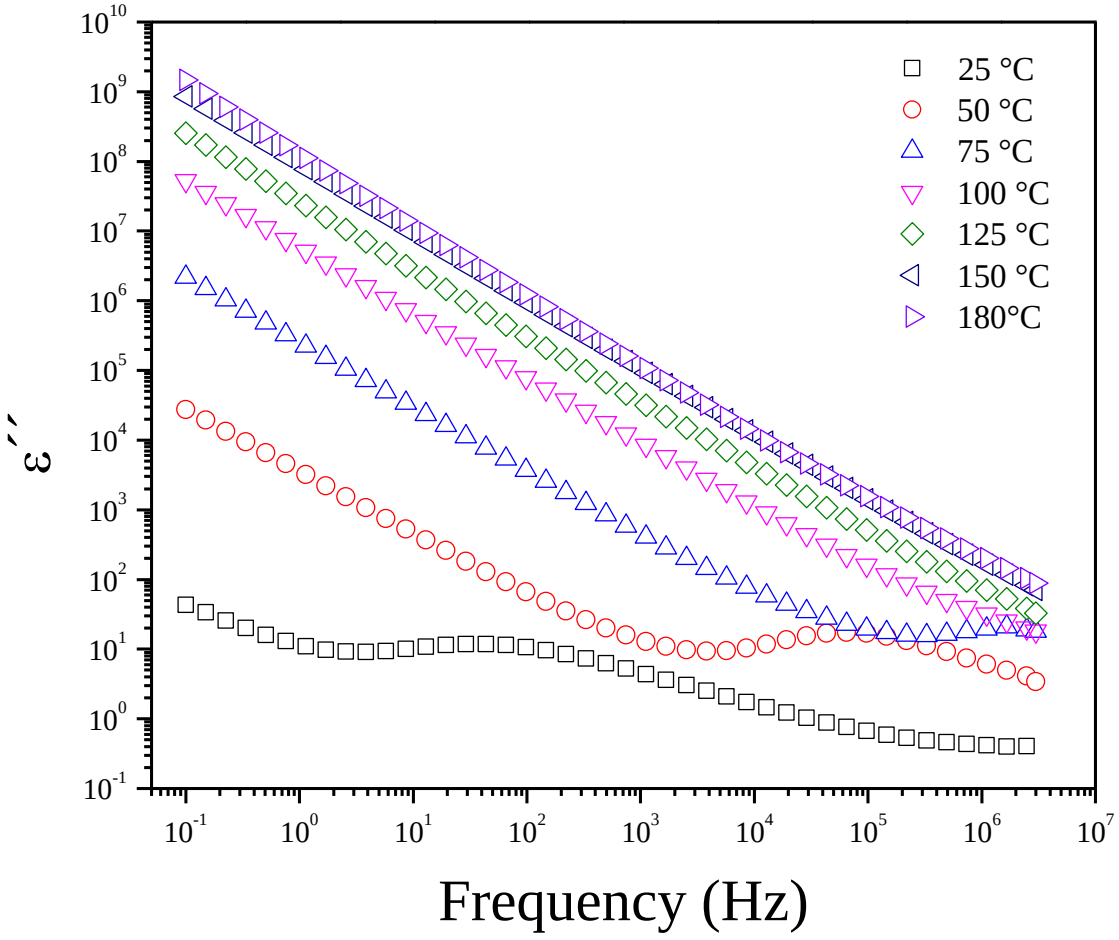

Figure 36. ε´´ versus frequency at different temperatures showing the β relaxation.

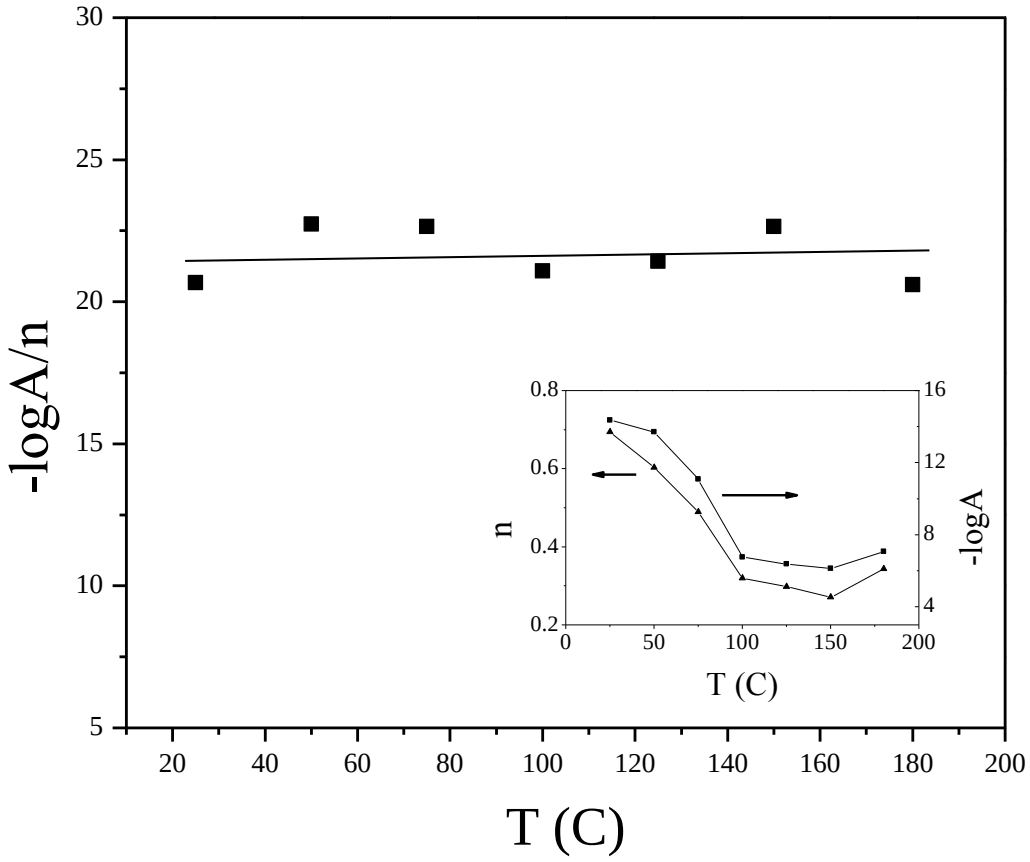

Figure 37. logA/n versus temperature for 0.2 wt% 44DDS-TGDDM nanocomposite cured at 25-180 °C at 1 °C min^{-1}, 180 ˚C soak for 3 hrs. Inset is -logA and n versus temperature.

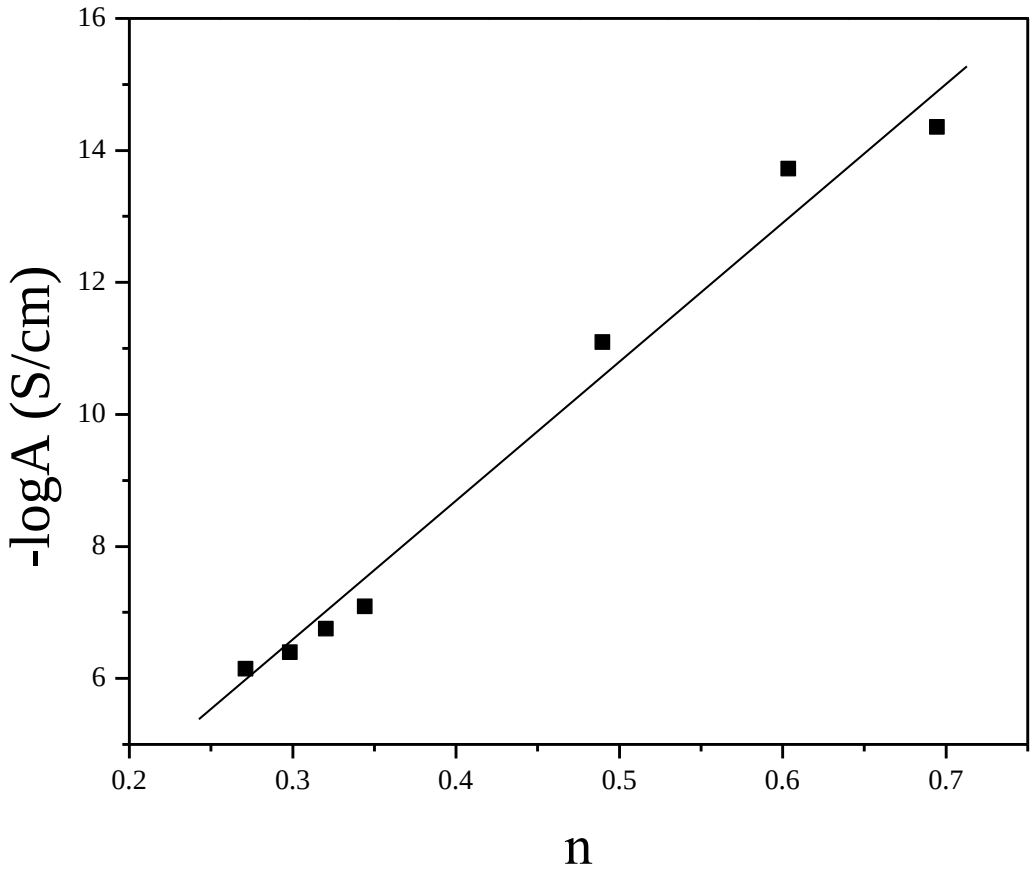

Figure 38. –log A versus n. Line was best-fit to experimental data points.

Conclusion

Utilizing C-AFM we observed mobility in nanotubes threw both the 1S and 2S cure prescriptions at the sub-micron length-scale. This result led us to the use of BDS for the *in situ* monitoring of secondary agglomeration during cure. This method did not yield the information on the through-space orientation of tubes like some previous some previous literature had hypothesized it would, instead we serendipitously contributed to the fundamental understanding of the power law also known as the universal dynamic response.

The direct relationship between parameters A and n held true through the progression from small agglomerates of nanotubes to a percolated network of nanowire type agglomerates during cure observed at the micron length-scale suggesting a relationship strictly empirical in nature. It is still an open question of what is the link between $\underline{A}$ and n with microscopic quantities and, if any, why power law applies to different materials and charge transport mechanisms.

CHAPTER VI – ROLE OF SLURRIES

Introduction

In this chapter a novel protocol to disperse and control dispersion states of MWCNT within an epoxy-amine prepolymer matrix through cure is described. Materials were evaluated regarding the effect of MWCNT dispersion on the glassy network development via dynamic mechanical analysis by comparing T_g. Rheological and microscopic evaluations confirmed that epoxy matrices processed as a slurry, undissolved 44DDS, afforded the highest matrix viscosity, or shear, to debundle primary MWCNT agglomerates with the highest quality of dispersion. Dispersion quality was stabilized through cure in a slurried matrices taking advantage of the simultaneous dissolution of 44DDS and reaction with TGDDM.

As a reminder from the introduction, the dispersion of MWCNT is inherently challenging due to their inert nature and propensity to agglomerate and entangle with neighboring tubes. There are several dispersion methods used to achieve effective primary agglomeration break-up be it mechanical agitation of some nature or chemical functionalization. Adjustment of cure profile, as described in chapter IV, was successfully utilized to control the secondary agglomeration known to occur in these materials.

It is well understood that increases in matrix viscosity contribute positively to the break-up of primary CNT agglomerates, and can act to stabilize dispersed states in un-cured or B-staged epoxy materials. We know that this high viscosity condition depreciates rapidly under the relatively fast high temperature cure cycles practical to industrial use. To build on this understanding, focus was set to rethinking the role of

matrix formulation in a manner to maximize primary agglomerate break-up and facilitate the stabilization of dispersion states through cure.

In the current study we hypothesized that the initial dispersion state could be augmented and through cure dispersion can be stabilized by increasing the solids content within our epoxy system. A common term to the prepreg industry, slurried matrices, are those containing a high solids content which occurs due to a large content of undissolved curative agent. Dispersion of MWCNT within a slurried matrix would afford the highest shear environment to disperse the primary agglomerates while also providing the highest matrix viscosity, prior to the dissolution temperature of the undissolved 44DDS crystals, to maintain a maximally dispersed state during post-processing cure.

Results and Discussion

Matrices at three MWCNT loading levels were prepared with solids content internally varied based on the extent of DDS solubilized into each respective system. The dissolution temperature of DDS in TGDDM is approximately 130 °C, therefore samples processed at or below this temperature create a condition called a slurry where and augmented solids content arises due to undissolved DDS crystals. Samples were named based upon the barrel temperature of the TSE at which they were processed. Therefore, a 60 °C sample have 100% of the crystalline DDS remaining in solution, the 120 °C samples, due to high shear and local heating has forced some amount of the curative into solution, and the 180 °C samples have the DDS homogenously dissolved and are partially reacted with the epoxy in solution. Comparatively, the 60, 120, and 180 °C samples can be considered high, intermediate, and low solids content materials respectively.

The complex viscosity, η*, profile was collected for all of the composite samples during the temperature ramp to cure. These profiles are illustrated in **Error! Reference source not found.**-41. For all nanotube loading levels, at all processing conditions tested, viscosity profiles trend analogous to that of the neat processed at the same TSE condition. It is well reported that a highly dispersed matrix will have an augmented viscosity profile, but trend similarly to that of the neat matrix.[107] Viscosity was seen to increase with increasing loading levels, and a consistent viscosity profile shape suggests that the modes of molecular relaxations were not significantly altered.

A typical viscosity response to secondary agglomeration can be observed in the viscosity profile of the non-slurried or low solids content samples processed at 180 °C and illustrated in **Error! Reference source not found.**. Here we see a drop in viscosity caused by heating and increased mobility of nanotubes. The following feature is closely tied to the specific nanotube loading level. A shoulder or even a temporary increase in viscosity was observed which was attributed to the physical gelation of the nanotubes. In the lowest loaded samples this physical gelation event is eventually overcome by continued drop in matrix viscosity which results in a massive migration of tubes and enlargement of agglomerates. In this case the viscosity further drops until continued chemical reaction drives an irreversible chemical gelation event. This was confirmed by comparison of the rheological profile to a time lapse taken by hot-stage OM imagery.

Physical gelation occurs when a network of physical bonds are formed between neighboring nanotubes.[107, 108] Said physical gelation is disrupted when the kinetic energy of the matrix moving around the "log-jammed" agglomerate bundles surpasses a threshold energy required to overcome this physical interaction.[46] In the highest loaded

sample of **Error! Reference source not found.** the viscosity profile trends practically linear prior to the chemical gelation event. In this instance, the increased concentration of nanotubes brought about a near instantaneous physically gelled state which was never overcome prior to chemical gelation. Again these are typical viscosity responses to secondary agglomeration within these types of materials for low and high concentration nanotube loadings.

The viscosity traces for the intermediate and high solids content slurries are illustrated in **Error! Reference source not found.** and 41 respectfully. The traces for these samples differ from the low solids analogs in a few ways. First, there is no observable physical gelation event, and second, the initial viscosities of the slurries are comparatively augmented by about one order of magnitude. This means the slurried materials not only afforded the highest shear environment for primary agglomerate break-up, but also provided the highest matrix viscosity to maintain dispersion during post-processing cure. Furthermore, the slopes in viscosity drop decrease with increasing solids content. This behavior is due to the simultaneous dissolution and conversion of undissolved 44DDS which acts to stabilize the dispersed states throughout cure, which was again confirmed through hot stage OM time lapse observation. A similar result was demonstrated by Young and coworkers who controlled the dispersion of covalently reacted reduced single-walled carbon nanotubes into epoxy matrices using slurried specimen.[109]

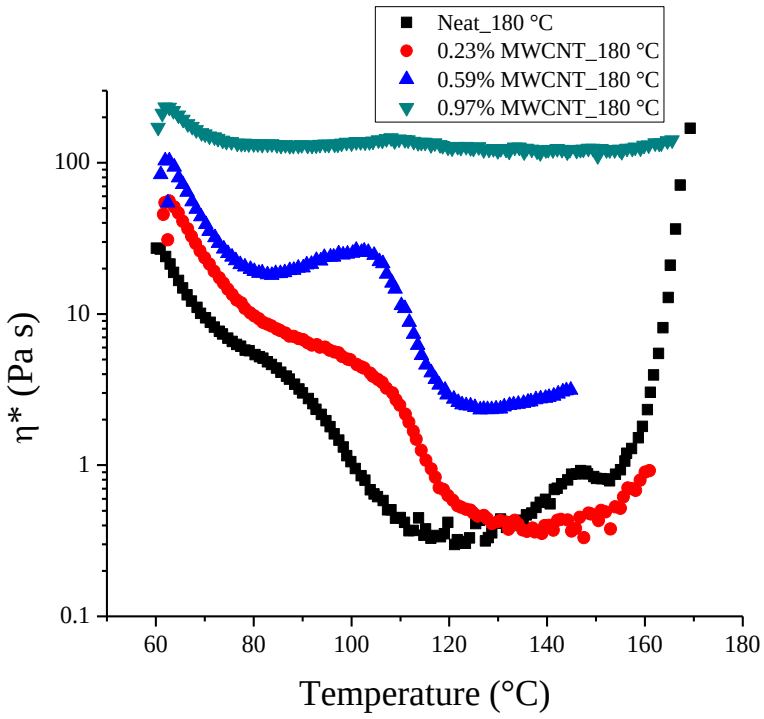

Figure 39. η* traces of low solid content material collected during cure (samples processed at 180°C)

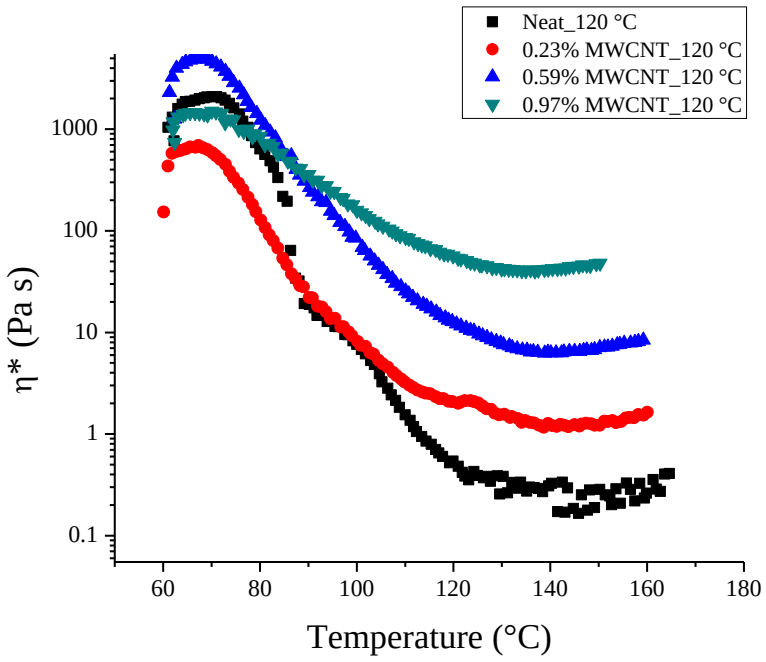

Figure 40. η* traces of intermediate solid content material collected during cure (samples processed at 120°C)

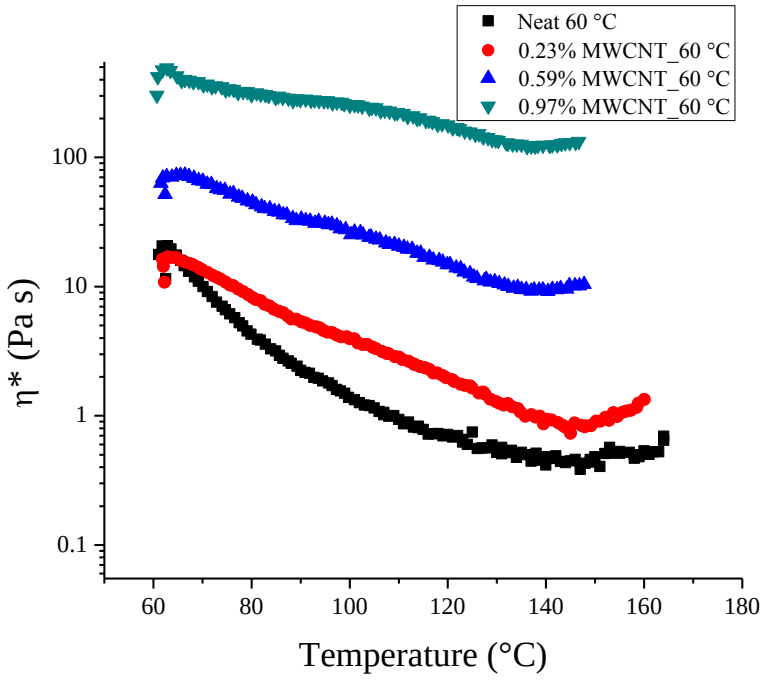

Figure 41. η* traces of high solid content material collected during cure (samples processed at 60°C)

Error! Reference source not found. provides a visual representation of the multi-scale effect of varied solids content on cured dispersion quality. In the OM images nanotube agglomerates can be identified as black while matrix appears white. These images show that the samples with initially the highest solids content maintained the best dispersion quality through cure. This result is reinforced by TEM observation where nano-scale agglomerate size is reduced with increasing DDS solids content. Real-time hot stage cure monitoring shows inactivity in secondary agglomeration up to 130 °C, at which point the curative crystals melt hence eliminating the DDS from contributing to the solids content in the matrix. In the cured form, matrix rich holes in the cloud of dispersed nanotubes are often left retaining the original shape of the DDS crystal that originally resided there. In this way a maximally dispersed state can be obtained and maintained with a cure protocol 48 hours faster than the cure induced method described in Chapter IV.

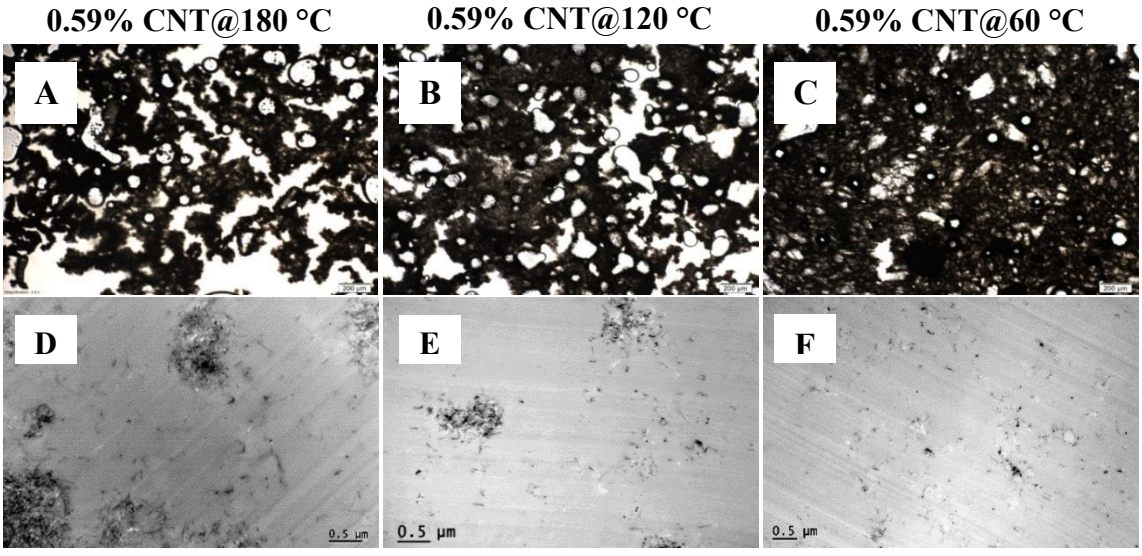

Figure 42. OM images (A-C, scale bar = 200 µm) of cured samples containing 0.59 wt% MWCNT processed at 180, 120, and 60 °C, respectively. TEM images (D-F, scale bar =

0.5 µm) of cured samples containing 0.59 wt% MWCNT processed at 180, 120, 60 °C, respectively

There was an initial concern that the simultaneous dissolution and reaction of DDS into the network might affect network properties or architecture. We also wanted to determine the effect of MWCNT loading on network development of the matrix. T_g and crosslink density were chosen as simple metrics for characterizing network development and were determined by DMA analysis. These findings have been tabulated in **Error! Reference source not found.** and show insignificant variations in both properties suggesting the presence of undissolved curative in the initial stages of cure has little to no effect on final matrix properties.

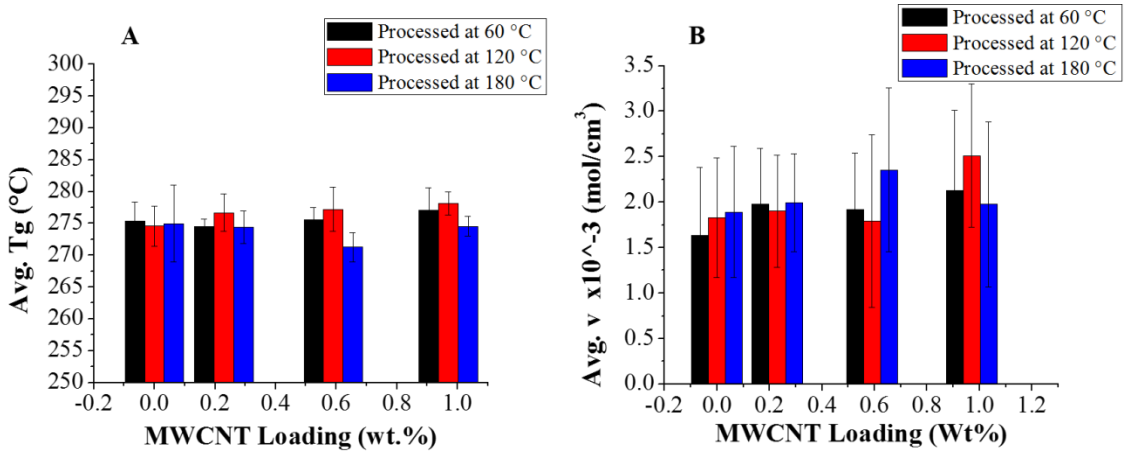

Figure 43. (A) T_g and (B) crosslink density obtained from DMA results of cured samples containing zero, 0.23, 0.59, and 0.97 wt% MWCNT loadings and processed at 60, 120, and 180 °C

A one-way ANOVA statistical analysis of the DMA data at a 95% confidence level further showed that there was no statistically significance difference between the T_g and crosslink density as a result of MWCNT loading or curative solids content. The results of this statistical manipulation of data are illustrated in **Error! Reference source not found.**.

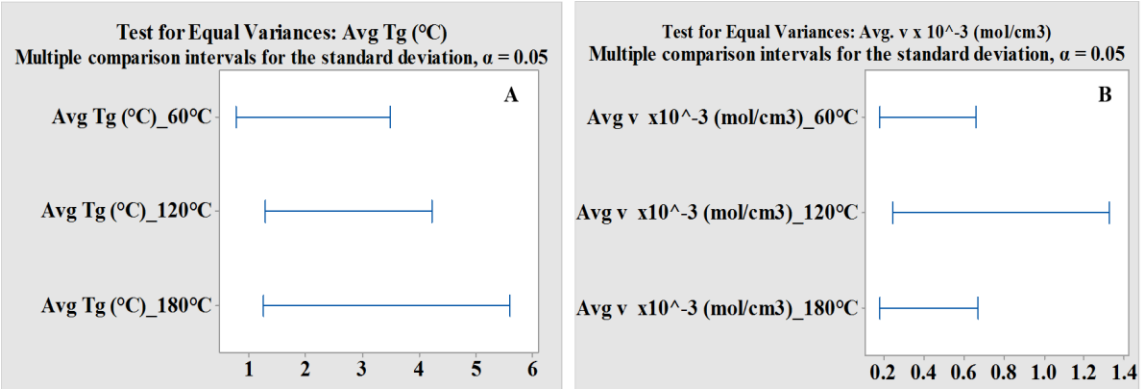

Figure 44. One-way ANOVA statistical analysis at $p < 0.05$ level of the (A) T_g and (B) crosslink density data

Conclusion

In this chapter, a method of processing where unreacted and undissolved solid curative dispersed in an epoxy diluent, as a slurry, was shown to provide additional gains in CNT dispersion as well as stabilization of dispersion states through cure. The mode of this stabilization effect is attributed to the increased viscosity due to an augmented solids content in the early, otherwise low viscosity, stages of cure which limit the migration of nanotubes prior to gelation. Statistical analysis of crosslink density and glass transition temperature show that this processing method had no detectable effect on matrix properties despite the difference in cure kinetics. Also, this slurry method provides an avenue for obtaining a maximally dispersed nanocomposite material but 48 hours faster than the method described in Chapter IV.

REFERENCES

1. Rana, S.; Alagirusamy, R.; Joshi, M., A review on carbon epoxy nanocomposites. *Journal of Reinforced Plastics and Composites* **2008**.

2. Coleman, J. N.; Khan, U.; Gun'ko, Y. K., Mechanical reinforcement of polymers using carbon nanotubes. *Advanced Materials* **2006,** *18* (6), 689-706.

3. Garcia, E. J.; Wardle, B. L.; John Hart, A., Joining prepreg composite interfaces with aligned carbon nanotubes. *Composites Part A: Applied Science and Manufacturing* **2008,** *39* (6), 1065-1070.

4. Qian, H.; Greenhalgh, E. S.; Shaffer, M. S.; Bismarck, A., Carbon nanotube-based hierarchical composites: a review. *Journal of Materials Chemistry* **2010,** *20* (23), 4751-4762.

5. Winey, K. I.; Vaia, R. A., Polymer nanocomposites. *MRS bulletin* **2007,** *32* (04), 314-322.

6. Sandler, J.; Shaffer, M.; Prasse, T.; Bauhofer, W.; Schulte, K.; Windle, A., Development of a dispersion process for carbon nanotubes in an epoxy matrix and the resulting electrical properties. *Polymer* **1999,** *40* (21), 5967-5971.

7. Bryning, M. B.; Islam, M. F.; Kikkawa, J. M.; Yodh, A. G., Very Low Conductivity Threshold in Bulk Isotropic Single- Walled Carbon Nanotube–Epoxy Composites. *Advanced Materials* **2005,** *17* (9), 1186-1191.

8. Zaragoza-Contreras, E.; Lozano-Rodríguez, E.; Román-Aguirre, M.; Antunez-Flores, W.; Hernández-Escobar, C.; Flores-Gallardo, S. G.; Aguilar-Elguezabal, A., Evidence of multi-walled carbon nanotube fragmentation induced by sonication during

nanotube encapsulation via bulk-suspension polymerization. *Micron* **2009,** *40* (5), 621-627.

9. Chang, L.; Friedrich, K.; Ye, L.; Toro, P., Evaluation and visualization of the percolating networks in multi-wall carbon nanotube/epoxy composites. *J Mater Sci* **2009,** *44* (15), 4003-4012.

10. Gojny, F. H.; Schulte, K., Functionalisation effect on the thermo-mechanical behaviour of multi-wall carbon nanotube/epoxy-composites. *Composites Science and Technology* **2004,** *64* (15), 2303-2308.

11. Gojny, F. H.; Wichmann, M. H.; Fiedler, B.; Kinloch, I. A.; Bauhofer, W.; Windle, A. H.; Schulte, K., Evaluation and identification of electrical and thermal conduction mechanisms in carbon nanotube/epoxy composites. *Polymer* **2006,** *47* (6), 2036-2045.

12. Thostenson, E. T.; Chou, T.-W., Processing-structure-multi-functional property relationship in carbon nanotube/epoxy composites. *Carbon* **2006,** *44* (14), 3022-3029.

13. Wichmann, M. H.; Sumfleth, J.; Gojny, F. H.; Quaresimin, M.; Fiedler, B.; Schulte, K., Glass-fibre-reinforced composites with enhanced mechanical and electrical properties–benefits and limitations of a nanoparticle modified matrix. *Engineering Fracture Mechanics* **2006,** *73* (16), 2346-2359.

14. Karippal, J.; Narasimha Murthy, H.; Rai, K.; Krishna, M.; Sreejith, M., Electrical and Thermal Properties of Twin-Screw Extruded Multiwalled Carbon Nanotube/Epoxy Composites. *Journal of Materials Engineering and Performance* **2010,** *19* (8), 1143-1149.

15. Karippal, J. J.; Murthy, H. N. N.; Rai, K. S.; Krishna, M.; Sreejith, M., The Processing and Characterization of MWCNT/Epoxy and CB/Epoxy Nanocomposites Using Twin Screw Extrusion. *Polymer-Plastics Technology and Engineering* **2010,** *49* (12), 1207-1213.

16. Prat, L.; N'Diaye, S.; Rigal, L.; Gourdon, C., Solid–liquid transport in a modified co-rotating twin-screw extruder—dynamic simulator and experimental validations. *Chemical Engineering and Processing: Process Intensification* **2004,** *43* (7), 881-886.

17. Finnigan, B.; Martin, D.; Halley, P.; Truss, R.; Campbell, K., Morphology and properties of thermoplastic polyurethane nanocomposites incorporating hydrophilic layered silicates. *Polymer* **2004,** *45* (7), 2249-2260.

18. Cai, C.; Shi, Q.; Li, L.; Zhu, L.; Yin, J., Grafting acrylic acid onto polypropylene by reactive extrusion with pre-irradiated PP as initiator. *Radiation Physics and Chemistry* **2008,** *77* (3), 370-372.

19. Shokoohi, S.; Arefazar, A.; Naderi, G., Compatibilized Polypropylene/Ethylene–Propylene–Diene-Monomer/Polyamide6 ternary blends: Effect of twin screw extruder processing parameters. *Materials & Design* **2011,** *32* (3), 1697-1703.

20. Mark, H. F.; Bikales, N.; Overberger, C. G.; Menges, G.; Kroschwitz, J. I., Encyclopedia of polymer science and engineering, Vol. 10: Nonwoven fabrics to photopolymerization. **1987**.

21. Xanthos, M., *Reactive Extrusion: Principles and Practice*. Hanser Publishers: 1992.

22. Moad, G., The synthesis of polyolefin graft copolymers by reactive extrusion. *Progress in polymer Science* **1999,** *24* (1), 81-142.

23. Karippal, J. J.; Murthy, H. N.; Rai, K.; Krishna, M.; Sreejith, M., The processing and characterization of MWCNT/epoxy and CB/epoxy nanocomposites using twin screw extrusion. *Polymer-Plastics Technology and Engineering* **2010,** *49* (12), 1207-1213.

24. Karippal, J. J.; Murthy, H. N.; Rai, K.; Krishna, M.; Sreejith, M., Electrical and thermal properties of twin-screw extruded multiwalled carbon nanotube/epoxy composites. *Journal of materials engineering and performance* **2010,** *19* (8), 1143-1149.

25. Rauwendaal, C.; Osswald, T.; Tellez, G.; Gramann, P., Flow analysis in screw extruders-Effect of kinematic conditions. *International Polymer Processing* **1998,** *13* (4), 327-333.

26. Rauwendaal, C. J., Analysis and experimental evaluation of twin screw extruders. *Polymer Engineering & Science* **1981,** *21* (16), 1092-1100.

27. Kasaliwal, G. R.; Pegel, S.; Göldel, A.; Pötschke, P.; Heinrich, G., Analysis of agglomerate dispersion mechanisms of multiwalled carbon nanotubes during melt mixing in polycarbonate. *Polymer* **2010,** *51* (12), 2708-2720.

28. Villmow, T.; Kretzschmar, B.; Pötschke, P., Influence of screw configuration, residence time, and specific mechanical energy in twin-screw extrusion of polycaprolactone/multi-walled carbon nanotube composites. *Composites Science and Technology* **2010,** *70* (14), 2045-2055.

29. Seyhan, A. T.; Gojny, F. H.; Tanoğlu, M.; Schulte, K., Critical aspects related to processing of carbon nanotube/unsaturated thermoset polyester nanocomposites. *European polymer journal* **2007,** *43* (2), 374-379.

30. Noll, A.; Burkhart, T., Morphological characterization and modelling of electrical conductivity of multi-walled carbon nanotube/poly (p-phenylene sulfide) nanocomposites

obtained by twin screw extrusion. *Composites Science and Technology* **2011,** *71* (4), 499-505.

31. Schulz, S.; Faiella, G.; Buschhorn, S.; Prado, L.; Giordano, M.; Schulte, K.; Bauhofer, W., Combined electrical and rheological properties of shear induced multiwall carbon nanotube agglomerates in epoxy suspensions. *European polymer journal* **2011,** *47* (11), 2069-2077.

32. Isayev, A.; Kumar, R.; Lewis, T. M., Ultrasound assisted twin screw extrusion of polymer–nanocomposites containing carbon nanotubes. *Polymer* **2009,** *50* (1), 250-260.

33. Fornes, T.; Yoon, P.; Keskkula, H.; Paul, D., Nylon 6 nanocomposites: the effect of matrix molecular weight. *Polymer* **2001,** *42* (25), 09929-09940.

34. Chu, D., The effect of matrix molecular weight on the dispersion of nanoclay in unmodified high density polyethylene. **2006**.

35. Cheng, X.; Wiggins, J. S., Continuous reactor preparation of thermoplastic modified epoxy- amine prepolymers. *Polymer International* **2014,** *63* (10), 1777-1784.

36. Liu, H.; Wang, P.; Zhang, X.; Shen, F.; Gogos, C. G., Effects of extrusion process parameters on the dissolution behavior of indomethacin in Eudragit® E PO solid dispersions. *International journal of pharmaceutics* **2010,** *383* (1), 161-169.

37. Wen, M.; Sun, X.; Su, L.; Shen, J.; Li, J.; Guo, S., The electrical conductivity of carbon nanotube/carbon black/polypropylene composites prepared through multistage stretching extrusion. *Polymer* **2012,** *53* (7), 1602-1610.

38. Ma, P.-C.; Mo, S.-Y.; Tang, B.-Z.; Kim, J.-K., Dispersion, interfacial interaction and re-agglomeration of functionalized carbon nanotubes in epoxy composites. *Carbon* **2010,** *48* (6), 1824-1834.

39. Yang, K.; Gu, M.; Guo, Y.; Pan, X.; Mu, G., Effects of carbon nanotube functionalization on the mechanical and thermal properties of epoxy composites. *Carbon* **2009,** *47* (7), 1723-1737.

40. Yaping, Z.; Aibo, Z.; Qinghua, C.; Jiaoxia, Z.; Rongchang, N., Functionalized effect on carbon nanotube/epoxy nano-composites. *Materials Science and Engineering: A* **2006,** *435*, 145-149.

41. Moniruzzaman, M.; Du, F.; Romero, N.; Winey, K. I., Increased flexural modulus and strength in SWNT/epoxy composites by a new fabrication method. *Polymer* **2006,** *47* (1), 293-298.

42. Cui, S.; Canet, R.; Derre, A.; Couzi, M.; Delhaes, P., Characterization of multiwall carbon nanotubes and influence of surfactant in the nanocomposite processing. *Carbon* **2003,** *41* (4), 797-809.

43. Geng, Y.; Liu, M. Y.; Li, J.; Shi, X. M.; Kim, J. K., Effects of surfactant treatment on mechanical and electrical properties of CNT/epoxy nanocomposites. *Composites Part A: Applied Science and Manufacturing* **2008,** *39* (12), 1876-1883.

44. Cho, J.; Daniel, I.; Dikin, D., Effects of block copolymer dispersant and nanotube length on reinforcement of carbon/epoxy composites. *Composites Part A: Applied Science and Manufacturing* **2008,** *39* (12), 1844-1850.

45. Luan, J.; Zhang, A.; Zheng, Y.; Sun, L., Effect of pyrene-modified multiwalled carbon nanotubes on the properties of epoxy composites. *Composites Part A: Applied Science and Manufacturing* **2012,** *43* (7), 1032-1037.

46. Martin, C. A.; Sandler, J. K. W.; Shaffer, M. S. P.; Schwarz, M. K.; Bauhofer, W.; Schulte, K.; Windle, A. H., Formation of percolating networks in multi-wall carbon-

nanotube–epoxy composites. *Composites Science and Technology* **2004,** *64* (15), 2309-2316.

47. Sandler, J. K. W.; Kirk, J. E.; Kinloch, I. A.; Shaffer, M. S. P.; Windle, A. H., Ultra-low electrical percolation threshold in carbon-nanotube-epoxy composites. *Polymer* **2003,** *44* (19), 5893-5899.

48. Velasco-Santos, C.; Martinez-Hernandez, A.; Castano, V., Carbon nanotube-polymer nanocomposites: The role of interfaces. *Composite Interfaces* **2005,** *11* (8-9), 567-586.

49. Pegel, S.; Pötschke, P.; Petzold, G.; Alig, I.; Dudkin, S. M.; Lellinger, D., Dispersion, agglomeration, and network formation of multiwalled carbon nanotubes in polycarbonate melts. *Polymer* **2008,** *49* (4), 974-984.

50. Alig, I.; Potschke, P.; Pegel, S.; Dudkin, S.; Lellinger, D., Composites of thermoplastic polymers and carbon nanotubes. *GUMMI FASERN KUNSTSTOFFE* **2007,** *60* (5), 280.

51. Zhang, C.; Wang, P.; Ma, C.-a.; Wu, G.; Sumita, M., Temperature and time dependence of conductive network formation: dynamic percolation and percolation time. *Polymer* **2006,** *47* (1), 466-473.

52. Villmow, T.; Pötschke, P.; Pegel, S.; Häussler, L.; Kretzschmar, B., Influence of twin-screw extrusion conditions on the dispersion of multi-walled carbon nanotubes in a poly (lactic acid) matrix. *Polymer* **2008,** *49* (16), 3500-3509.

53. Schueler, R.; Petermann, J.; Schulte, K.; Wentzel, H. P., Agglomeration and electrical percolation behavior of carbon black dispersed in epoxy resin. *Journal of Applied Polymer Science* **1997,** *63* (13), 1741-1746.

54. Schueler, R.; Petermann, J.; Schulte, K.; Wentzel, H. P. In *Percolation in carbon black filled epoxy resin*, Macromolecular Symposia, Wiley Online Library: 1996; pp 261-268.

55. Mitchell, C. A.; Bahr, J. L.; Arepalli, S.; Tour, J. M.; Krishnamoorti, R., Dispersion of functionalized carbon nanotubes in polystyrene. *Macromolecules* **2002,** *35* (23), 8825-8830.

56. Pötschke, P.; Dudkin, S. M.; Alig, I., Dielectric spectroscopy on melt processed polycarbonate—multiwalled carbon nanotube composites. *Polymer* **2003,** *44* (17), 5023-5030.

57. Coleman, J. N.; Khan, U.; Blau, W. J.; Gun'ko, Y. K., Small but strong: A review of the mechanical properties of carbon nanotube–polymer composites. *Carbon* **2006,** *44* (9), 1624-1652.

58. Gojny, F. H.; Wichmann, M. H.; Fiedler, B.; Schulte, K., Influence of different carbon nanotubes on the mechanical properties of epoxy matrix composites–a comparative study. *Composites Science and Technology* **2005,** *65* (15), 2300-2313.

59. Stefanithis, I.; Mauritz, K. A., Microstructural evolution of a silicon oxide phase in a perfluorosulfonic acid ionomer by an in situ sol-gel reaction. 3. Thermal analysis studies. *Macromolecules* **1990,** *23* (8), 2397-2402.

60. Chen, H.; Hassan, M. K.; Peddini, S. K.; Mauritz, K. A., Macromolecular dynamics of sulfonated poly (styrene-b-ethylene-ran-butylene-b-styrene) block copolymers by broadband dielectric spectroscopy. *European polymer journal* **2011,** *47* (10), 1936-1948.

61. Klein, R. J.; Zhang, S.; Dou, S.; Jones, B. H.; Colby, R. H.; Runt, J., Modeling electrode polarization in dielectric spectroscopy: ion mobility and mobile ion concentration of single-ion polymer electrolytes. *Journal of Chemical Physics* **2006,** *124* (14), 144903-144903.

62. Atorngitjawat, P.; Runt, J., Dynamics of sulfonated polystyrene ionomers using broadband dielectric spectroscopy. *Macromolecules* **2007,** *40* (4), 991-996.

63. Hench, L. L.; West, J. K., *Principles of electronic ceramics*. Wiley: 1990.

64. Joncher, A., Phys. *Thin films* **1980,** *11*, 232.

65. Jonscher, A. K., A new understanding of the dielectric relaxation of solids. *J Mater Sci* **1981,** *16* (8), 2037-2060.

66. Ingram, M. D., Ionic conductivity in glass. *Physics and Chemistry of glasses* **1987,** *28* (6), 215-234.

67. Jonscher, A. K., Theuniversal'dielectric response. *Nature* **1977,** *267*, 673-679.

68. Dyre, J. C.; Schrøder, T. B., Universality of ac conduction in disordered solids. *Reviews of Modern Physics* **2000,** *72* (3), 873.

69. Mauritz, K. A., Dielectric relaxation studies of ion motions in electrolyte-containing perfluorosulfonate ionomers. 4. Long-range ion transport. *Macromolecules* **1989,** *22* (12), 4483-4488.

70. Papathanassiou, A., Novel feature of the universal power law dispersion of the ac conductivity in disordered matter. *Journal of Non-Crystalline Solids* **2006,** *352* (50), 5444-5445.

71. Cramer, C.; Brunklaus, S.; Ratai, E.; Gao, Y., New mixed alkali effect in the ac conductivity of ion-conducting glasses. *Physical review letters* **2003,** *91* (26), 266601.

72. Papathanassiou, A., On the power-law behavior of the AC conductivity of the mixed crystal (NH 4) 3 H (SO 4) 1.42 (SeO 4) 0.58. *Journal of Physics and Chemistry of Solids* **2005,** *66* (10), 1849-1850.

73. Almond, D. P.; Bowen, C., Anomalous power law dispersions in ac conductivity and permittivity shown to be characteristics of microstructural electrical networks. *Physical review letters* **2004,** *92* (15), 157601.

74. Bayer Material Science Material Data Safety Sheet Baytubes C 150 P.

75. Bayer Material Science Product Information Brouchure Baytubes C 150 P.

76. Cheng, X.; Wiggins, J. S., Continuous reactor preparation of thermoplastic modified epoxy-amine prepolymers. *Polymer International* **2014,** *63* (10), 1777-1784.

77. Cheng, X. Cure kinetics, morphologies, and mechanical properties of thermoplastic/MWCNT modified multifunctional glassy epoxies prepared via continuous reaction methods. Ph.D., The University of Southern Mississippi, Ann Arbor, 2015.

78. Greenhoe, B. M. X. C. S., Amit; Wiggins, Jeffrey S. , High Loading, Dispersion and Stabilization of MWCNT in Epoxy Prepolymers from Continuous High Shear Reactor Processing. *Carbon* **2016**.

79. Kasaliwal, G. R.; Göldel, A.; Pötschke, P.; Heinrich, G., Influences of polymer matrix melt viscosity and molecular weight on MWCNT agglomerate dispersion. *Polymer* **2011,** *52* (4), 1027-1036.

80. Shaffer, M. S. P.; Windle, A. H., Fabrication and Characterization of Carbon Nanotube/Poly(vinyl alcohol) Composites. *Advanced Materials* **1999,** *11* (11), 937-941.

81. Brian M Greenhoe, X. C., Amit Sharma, Jeffrey S. Wiggins High Loading, Dispersion and Stabilization of MWCNT in Epoxy Prepolymers from Continuous High Shear Reactor Processing. *Submitted to Carbon* **2016**.

82. Rahmat, M.; Hubert, P., Carbon nanotube–polymer interactions in nanocomposites: a review. *Composites Science and Technology* **2011,** *72* (1), 72-84.

83. Spitalsky, Z.; Tasis, D.; Papagelis, K.; Galiotis, C., Carbon nanotube–polymer composites: chemistry, processing, mechanical and electrical properties. *Progress in polymer Science* **2010,** *35* (3), 357-401.

84. Ma, P.-C.; Siddiqui, N. A.; Marom, G.; Kim, J.-K., Dispersion and functionalization of carbon nanotubes for polymer-based nanocomposites: a review. *Composites Part A: Applied Science and Manufacturing* **2010,** *41* (10), 1345-1367.

85. Gojny, F. H.; Wichmann, M.; Köpke, U.; Fiedler, B.; Schulte, K., Carbon nanotube-reinforced epoxy-composites: enhanced stiffness and fracture toughness at low nanotube content. *Composites Science and Technology* **2004,** *64* (15), 2363-2371.

86. Ma, P. C.; Kim, J.-K.; Tang, B. Z., Effects of silane functionalization on the properties of carbon nanotube/epoxy nanocomposites. *Composites Science and Technology* **2007,** *67* (14), 2965-2972.

87. Li, Q.; Zaiser, M.; Koutsos, V., Carbon nanotube/epoxy resin composites using a block copolymer as a dispersing agent. *physica status solidi (a)* **2004,** *201* (13), R89-R91.

88. Battisti, A.; Skordos, A. A.; Partridge, I. K., Dielectric monitoring of carbon nanotube network formation in curing thermosetting nanocomposites. *Journal of physics D: Applied physics* **2009,** *42* (15), 155402.

89. Kasaliwal, G.; Göldel, A.; Pötschke, P., Influence of processing conditions in small- scale melt mixing and compression molding on the resistivity and morphology of polycarbonate–MWNT composites. *Journal of Applied Polymer Science* **2009,** *112* (6), 3494-3509.

90. Pötschke, P.; Villmow, T.; Krause, B., Melt mixed PCL/MWCNT composites prepared at different rotation speeds: Characterization of rheological, thermal, and electrical properties, molecular weight, MWCNT macrodispersion, and MWCNT length distribution. *Polymer* **2013,** *54* (12), 3071-3078.

91. Martin, C.; Sandler, J.; Shaffer, M.; Schwarz, M.-K.; Bauhofer, W.; Schulte, K.; Windle, A., Formation of percolating networks in multi-wall carbon-nanotube–epoxy composites. *Composites Science and Technology* **2004,** *64* (15), 2309-2316.

92. Godara, A.; Mezzo, L.; Luizi, F.; Warrier, A.; Lomov, S. V.; Van Vuure, A.; Gorbatikh, L.; Moldenaers, P.; Verpoest, I., Influence of carbon nanotube reinforcement on the processing and the mechanical behaviour of carbon fiber/epoxy composites. *Carbon* **2009,** *47* (12), 2914-2923.

93. Chakraborty, A. K.; Plyhm, T.; Barbezat, M.; Necola, A.; Terrasi, G. P., Carbon nanotube (CNT)–epoxy nanocomposites: a systematic investigation of CNT dispersion. *Journal of Nanoparticle Research* **2011,** *13* (12), 6493-6506.

94. Martin, C.; Sandler, J.; Windle, A.; Schwarz, M.-K.; Bauhofer, W.; Schulte, K.; Shaffer, M., Electric field-induced aligned multi-wall carbon nanotube networks in epoxy composites. *Polymer* **2005,** *46* (3), 877-886.

95. Lin, B.; Sundararaj, U.; Pötschke, P., Melt Mixing of Polycarbonate with Multi-Walled Carbon Nanotubes in Miniature Mixers. *Macromolecular Materials and Engineering* **2006,** *291* (3), 227-238.

96. Jackson, M.; Kaushik, M.; Nazarenko, S.; Ward, S.; Maskell, R.; Wiggins, J., Effect of free volume hole-size on fluid ingress of glassy epoxy networks. *Polymer* **2011,** *52* (20), 4528-4535.

97. Alig, I.; Skipa, T.; Lellinger, D.; Pötschke, P., Destruction and formation of a carbon nanotube network in polymer melts: rheology and conductivity spectroscopy. *Polymer* **2008,** *49* (16), 3524-3532.

98. M. Yourdkhani, P. H., reagglomeration of carbon nanotubes during processing of epoxy nanocomposites. In *The 19th International Conference on Composite Materials* 2013.

99. Rosca, I. D.; Hoa, S. V., Highly conductive multiwall carbon nanotube and epoxy composites produced by three-roll milling. *Carbon* **2009,** *47* (8), 1958-1968.

100. Lee, W.; Lim, B.; Liu, J.; Nowick, A., ac conductivity in ionically conducting crystals and glasses. *Solid state ionics* **1992,** *53*, 831-836.

101. Hassan, M. K.; Tucker, S. J.; Abukmail, A.; Wiggins, J. S.; Mauritz, K. A., Polymer chain dynamics in epoxy based composites as investigated by broadband dielectric spectroscopy. *Arabian Journal of Chemistry*.

102. Childers, C. H.; Hassan, M. K.; Mauritz, K. A.; Wiggins, J. S., Molecular scale cure rate dependence of thermoset matrix polymers. *Arabian Journal of Chemistry*.

103. Ochi, M.; Iesako, H.; Shimbo, M., Relaxation mechanism of epoxide resin cured with acid anhydrides. III. Effect of alkyl side chains on mechanical and dielectric β

relaxations. *Journal of Polymer Science Part B: Polymer Physics* **1986,** *24* (6), 1271-1282.

104. Shimbo, M.; Ochi, M.; Iesako, H., Mechanical relaxation mechanism of epoxide resins cured with acid anhydrides. *Journal of Polymer Science: Polymer Physics Edition* **1984,** *22* (8), 1461-1470.

105. Mangion, M.; Johari, G., Relaxations of thermosets. IV. A dielectric study of crosslinking of diglycidyl ether of bisphenol- a by two curing agents. *Journal of Polymer Science Part B: Polymer Physics* **1990,** *28* (9), 1621-1639.

106. F, M., *Handbook of Polymer Synthesis: Part B*. CRC Press: Boca Raton, 1991.

107. Zhang, Q.; Fang, F.; Zhao, X.; Li, Y.; Zhu, M.; Chen, D., Use of Dynamic Rheological Behavior to Estimate the Dispersion of Carbon Nanotubes in Carbon Nanotube/Polymer Composites. *The Journal of Physical Chemistry B* **2008,** *112* (40), 12606-12611.

108. Chapartegui, M.; Markaide, N.; Florez, S.; Elizetxea, C.; Fernandez, M.; Santamaria, A., Curing of epoxy/carbon nanotubes physical networks. *Polymer Engineering & Science* **2012,** *52* (3), 663-670.

109. Martinez-Rubi, Y.; Ashrafi, B.; Guan, J.; Kingston, C.; Johnston, A.; Simard, B.; Mirjalili, V.; Hubert, P.; Deng, L.; Young, R. J., Toughening of Epoxy Matrices with Reduced Single-Walled Carbon Nanotubes. *ACS Applied Materials & Interfaces* **2011,** *3* (7), 2309-2317.